RESTING STATE FUNCTIONAL CONNECTIVITY MRI IN THE RODENT BRAIN:

APPLICATIONS TO HUMAN DISEASE

By

Brian D. Mills

A DISSERTATION

Presented to the Department of Behavioral Neuroscience and the

Oregon Health & Science University School of Medicine

In partial fulfillment of the requirements for the degree of

Doctor of Philosophy

March 2018

School of Medicine

Oregon Health & Science University

_____

CERTIFICATE OF APPROVAL

_____

This is to certify that the PhD Dissertation of

Brian D. Mills

Has been approved

_____

Damien Fair, Mentor/Advisor

_____

Chris Kroenke, Oral Exam Committee Chair

_____

Elinor Sullivan, Member

_____

Kim Neve, Member

i

Table of Contents

Figures

Tables

Abbreviations

FC – Functional connectivity

rs-fcMRI – resting state functional connectivity magnetic resonance imaging

fMRI – Functional magnetic resonance imaging

BOLD – Blood oxygen level dependent

ROI – Region of interest

CGE – Correlated gene expression

AMBCA – Allen Mouse Brain Connectivity Atlas

ABI – Allen Brain Institute

ISH – In-situ hybridization

IHC - immunohistochemistry

G - Communicability

M – Matching index

FD – Frame displacement

ORA – Over representation analysis

FDR – False discovery rate

ASD – Autism spectrum disorders

EPI – Echo planar imaging

FOV – Field of view

IL-6 – Interleukin-6

MIA – Maternal immune activation

PolyI:C – Polycytidylic acid

LPS – Lipopolysaccharide

PND – Postnatal day

PBS – Phosphate buffered saline

Acknowledgements

Science is truly a collaborative endeavor and this research would not be possible without the help and guidance of a number of people I have been lucky enough to cross paths with. First, thank you Damien, for all the opportunities you have provided me. I am lucky to have learned so much from such an outstanding scientist. A number of others have contributed to the work detailed in the thesis. Chapter two was a joint effort with David Grayson, whose contributions were invaluable to this project; thank you for all work on this project with me. Work from the Allen Brain Institute was used extensively throughout this dissertation and I am indebted to all those who developed such valuable datasets. Chapter three would not have been possible without the help of Anand Shunmugavel, particularly for his help on animal surgeries, tissue extractions, and experimental guidance. I am also indebted to Alina Goncharova for her efforts in collecting and analyzing animal behavior, as well as assistance on many aspects of this project. This was truly a team effort between us on 'rodent team' and I thank you both for all your help over the years. Chapter four was in collaboration with efforts led by Ben Jarrett and James Stafford for the mouse imaging projects, and Oscar Miranda-Dominguez on the comparisons of the macaque connectome. Further, the programming expertise of Eric Earl was invaluable for pipeline development and problem solving. I appreciate your patience and guidance in tackling these tricky and complex problems. Thank you Oscar and Eric Feczko for your guidance throughout the years. I consider you mentors through my graduate school and thank you for all you have taught me. Thank you to all those in the Fair Lab, across OHSU, and academia more broadly, who I have crossed paths during my time at OHSU. I am grateful to have learned from everyone I have met. Finally, thank you so much to all my friends who made this experience so memorable and enjoyable. I have made lifelong friendships here in graduate school and I am so lucky to have met all of you. There are too many to name but you know who you are. Finally,

thank you Haley for all of your love and support, and for making my life so much better (and more colorful). Thank you to Robbie, Mom, and Dad for all you have done for me over the years. I couldn't imagine my life without you and I love you all so much!

Abstract

Resting state functional connectivity Magnetic Resonance Imaging (rs-fcMRI) is a non-invasive technique that can be used to investigate the brain's functional network organization in both healthy individuals and patients with psychiatric disorders. A crucial discovery that has emerged from the past decade of cognitive neuroscience is that using a network characterization of synchronized functional activity with rs-fcMRI can be leveraged to identify complex and reproducible topological systems-level organization of the brain. We have also begun to identify how this organization is altered in psychiatric and neurological disease. However, despite these advances, our understanding of what drives this organization in both health and disease has seen limited progress. This reality is, in part, because the molecular substrates that shape functional network organization remain poorly understood and require the integration of data across various scales of investigation (i.e. data at the cellular and molecular level). Another reason for our lack of progress is that the measurements used in clinical investigation of psychiatric disorders (e.g. non-invasive measures such as fMRI) are often distinct from measurements used in preclinical animal models (e.g. single-unit electrophysiology, histology/histochemistry, etc), which are uniquely helpful in elucidating the causal mechanisms and biological underpinnings associated with various mental health issues. In order to progress on these fronts, the current work is separated into two projects which, 1) validate the use of rs-fcMRI in preclinical models and investigate how functional connectivity (FC) is shaped by its cellular and molecular substrates, and 2) apply these validated techniques to a preclinical animal model that can be then be compared to humans using the same non-invasive rs-fcMRI measurements.

Accordingly, project 1 presents a novel linear model to explain functional connectivity in the mouse brain by integrating systematically obtained measurements on axonal connectivity,

gene expression, and rs-fcMRI. The model suggests that functional connectivity emerges from additive and interactive combinations of white matter connectivity and inter-areal similarities in gene expression. By estimating these contributions, anatomical modules are identified in which correlated gene expression and anatomical connectivity cooperatively, versus distinctly, support functional connectivity. We also provide evidence that not all genes contribute equally to functional connectivity and highlight candidate gene clusters, which may contribute most to the signal. This project validates functional connectivity as a viable method that can be applied to preclinical animal models, and establishes new insights on the biological underpinnings of synchronized brain activity.

The second project applies rs-fcMRI to a preclinical animal model characterizing the effects of prenatal exposure to chronic inflammation, an important risk factor for developmental disorders. Gestational inflammation is characterized by elevated levels of pro-inflammatory cytokines, including interleukin 6 (IL-6). IL-6 has been shown to contribute to developmental disorders, and has been associated with various risk factors for mental health issues including prenatal exposure to stress, high fat diet, and viral infection. To investigate the role of elevated prenatal IL-6 on offspring brain and behavioral development, dams were administered chronic increases in systemic IL-6 though an osmotic mini pump throughout their gestational period. Offspring were then longitudinally tracked on component behaviors associated with developmental mental health disorders. Rs-fcMRI network structure in IL-6 exposed offspring is assessed in early (PND 30) and late (PND 55) development. Relative to controls, offspring from IL-6 administered dams show subtle differences in social behavior and locomotion, but exhibit more persistent anxiety-like behavior into early adulthood. IL-6 offspring also show an altered developmental trajectory of functional connectivity in the amygdala as well as the subcortical

network, and parietal and frontal cortex networks more broadly. This altered developmental trajectory was characterized by relative under-connectivity during early development, but over-connectivity late in development. Further, amygdala connectivity also relates to anxiety-like behavior such that increased anxiety is related to increased amygdala connectivity to cortical and subcortical structures. Overall, this study highlights the association between behavioral and functional connectivity alterations resulting from the prenatal exposure to IL-6. Importantly, these methods also enable us to compare these causal IL-6-induced changes to correlational studies done in infants and children who underwent gestational exposure to elevated inflammatory cytokines, as well as children and adolescents with developmental disorders. Through the use of non-invasive rs-fcMRI measurements in preclinical animal models, we can progress in our understanding of how functional connectivity relates to the underlying biology, and how that relationship may unfold in human disease. Insights obtained from such efforts will undoubtedly be crucial in the development of more targeted treatments and interventions for neuropsychiatric disorders.

Chapter 1: Introduction

Section 1: Bridging the gap between human and animal models using functional connectivity across species

In the United States alone, an estimated 44 million adults suffer from mental illness and 55 million people suffer from neurological conditions (Alzheimer's Association, 2014; WHO, 2014). Despite decades of effort, progress with regard to treatment has been limited. This is in part because the field of neuroscience is extremely broad, and complex, spanning multiple spatial scales of inquiry. Churchland and Senjnowski's famous diagram provides an illustration of these levels (Churchland & Sejnowski, 1992) (see Figure 1 for a modified version of this figure). To date, a great deal of research has been conducted to characterize brain functioning at the lowest, i.e. the cellular and molecular level. This level includes the study of ion-channels, receptors, and transmitter dynamics, as well as the influence of gene expression on protein production critical for cellular function. Insights at this lower level are critical to our understanding of the brain, but alone cannot explain complex behavioral and cognitive phenomena.

Figure 1.1. Modified from Churchland & Sejnowski's (1992) diagram of the levels of organization across the central nervous system. The nervous system is organized on multiple spatial scales. These scales range from the molecular and cellular level, to intermediate levels dealing with local circuits, to the level of functional network organization between regions. An understanding of how these levels of inquiry relate to one another, and are impacted in disease states, is a critical for progress in neuroscience and medicine.

At the next level, neuroscience examines the structure and function of cellular subunits such as axons, synapses, and dendritic spines. The formation and modification of synaptic connections, cellular proliferation, and cell death all contribute to the patterning of the nervous system. We also know that neurons are organized into local circuits, columns, and topographic maps underlying sensorimotor and perceptual functions. Understanding these intermediary levels is critical, but likely still inadequate to explain fully complex cognitive and behavioral processes.

4

Technologies such as Magnetic Resonance Imaging (MRI) have allowed us to study regional patterns of brain activity, interactions between regions and functional systems, as well as large scale network organization across the brain at the highest level (Figure 1.1). These technologies have allowed us to gain insights into the ways in which large brain organization relate to complex behaviors, and critically, how these measures are affected in human disease. That being said, alone, none of these scales of inquiry is sufficient to explain the complexities of the brain. We are only beginning to understand the inter-relationships among these scales of inquiry and the way in which each affects behavior in health and disease.

Accordingly, part of the reason for our relative lack of progress in treating brain related disease is due to an incomplete understanding of the convergence between these levels of inquiry. For instance, neuroscientific investigations at the top, systems level, of brain function, are typically done with non-invasive brain imaging techniques such as functional MRI (fMRI). Traditionally, this level of inquiry has been reserved for studying human brain function. Conversely, the cellular and molecular level has generally been investigated using animal models. In the following thesis, we begin to highlight how using non-invasive imaging such as MRI in preclinical animal models can begin to fill this gap between research done in humans and basic science research that is often done in preclinical animal models. Using these measurements, we identify relationships between levels of inquiry and further our knowledge of the biological bases of non-invasive measures, in particular fMRI. Next, we apply these measurements to preclinical animal models to both test the causal mechanisms underlying changes to network topology (measured with fMRI), and importantly, could be used to compare between these measurements obtained in both human and animal models of disease.

Preclinical models of disease are essential for neuroscience

Preclinical translational animal models provide a powerful way to understand the pathobiological mechanisms underlying disease states, and for testing therapeutic interventions in a controlled environment. However, one problem with these models is that their relevance and overlap with human disease is often unknown. This is, in part, because we typically use a separate set of measurements in animal models vs. humans. This fact leads to a major gap between basic and translational science. This gap results in a lack of understanding in how brain function relates between humans and animal models, and how cellular and molecular mechanisms influence the measurements we use in humans.

Focusing on measurements that can be collected in both humans and animal models allows us to work towards the following goals. First, the use of these non-invasive measurements in animal models allow us to understand their biology by linking these measurements to their cellular and molecular underpinnings. Further, as stated earlier, the degree to which the animal model is representative of the disorder being studied is often unclear. By understanding how atypical brain function in human disease overlaps with the same measurements in animal models of the disorders, we can gain a sense of their shared and distinct biological presentations. Finally, the use of animal models allows for causal manipulation to evaluate and describe risk factors for human developmental neuropsychiatric disorders and assess whether they are indeed a source of atypical brain function seen in human studies that typically assess correlational relationships.

Resting state functional connectivity as a bridge measurement between species

An ideal measurement to bridge this gap between human and animal research is resting state functional connectivity MRI (rs-fcMRI). Rs-fcMRI is a powerful tool for investigating functional brain organization across diseases states including developmental disorders. The technique relies on the temporal correlation of spontaneous blood oxygen level dependent (BOLD) signals

6

between spatially distributed brain regions when a subject is not performing an explicit task. The BOLD signal is used to estimate brain activity. However, BOLD measurements are indirect, and rely on the ability to measure the magnetic properties of hemoglobin and the fact that blood flow increases more than the rate of oxygen metabolism when local neuronal activity increases (Scott A. Huettel; Allen W. Song; Gregory McCarthy et al., 2004). More specifically, when hemoglobin loses an oxygen to become deoxyhemoglobin, its iron becomes paramagnetic, and influences the magnetic field experienced by protons in surrounding water molecules (Attwell & Iadecola, 2002; Ogawa, Lee, Kay, & Tank, 1990). T2*-sensitive MRI sequences, the sequences used to measure the BOLD signal, take advantage the fact that quicker signal loss (transverse magnetization decay) occurs in the presence of deoxyhemoglobin (Chavhan, Babyn, Thomas, Shroff, & Haacke, 2009). During neuronal activity, an increase of oxygen usage is followed within a few seconds by a larger fractional increase in blood flow and an increase in blood volume, resulting in a net decrease of the amount of deoxygenated hemoglobin present (Malonek et al., 1997).

Local field potentials (LFP) are an electrophysiological signal that measures neuronal activity by summing the electric potentials recorded in the extracellular space in brain tissue. LFPs are an invasive method for studying brain activity so are only performed while under open brain surgery in humans or in preclinical animal models. Simultaneous fMRI/LFP studies have shown that fMRI responses are tightly linked to neural activity, and particularly synaptic activity thought to be reflected in the gamma band of the LFP signal (Logothetis, Pauls, Augath, Trinath, & Oeltermann, 2001; Scholvinck, Maier, Ye, Duyn, & Leopold, 2010). Together, mounting evidence using new techniques for studying and controlling neuronal activation, including

7

simultaneous fMRI and optogenetics studies (Lee et al., 2010; Palmer, 2010), further conclude that the BOLD signal is driven by changes in neuronal signaling.

A measure derived from the BOLD signal is functional connectivity (FC), which describes the relationship between BOLD activation patterns of anatomically separated brain regions and reflects the level of functional communication between regions. More detail on these methods are provided in the sections below and figure 1.2 provides an overview of this technique.

FC is an ideal measure to compare human and animal physiology for a number of reasons. The first reason is that it is a non-invasive measure that can be reliably and easily assessed in both humans and animals. Further, FC evaluates regional interactions that spontaneously occur in the absence of a task. This makes FC an ideal measurement for populations who have difficulty performing tasks, such as developmentally delayed or cognitively impaired populations, and for animal models, in which task related brain measures can be difficult to administer. Finally, FC is an ideal measure because it has been widely used to elucidate abnormal connectivity patterns in a variety of neurological and psychiatric conditions (M. Greicius, 2008), and has been shown to relate to clinically meaningful outcomes, cognition, and behavior (Craddock, Hu, Mayberg, & Holtzheimer, 2009; M. Greicius, 2008; Raichle, 2015).

Section 2: Using resting state functional connectivity in rodents

Rodent models allow the assessment of the cellular and molecular mechanisms that underlie non-invasive imaging measures (i.e. rs-fcMRI), which are used to assess human disease. They also allow us to probe causal mechanisms of disease related phenotypes observed with non-invasive imaging. They offer advantages in terms of experimental and environmental control, two critical foundations of the scientific method. Multiple groups have taken initial steps towards

8

using resting state connectivity as a bridge between humans and preclinical animal models. The ways in which these studies are performed will be briefly outlined in the following section.

Defining regions of interest

Prior to examining connectivity patterns, first, one must be able to define meaningfully delineated brain regions. These delineations can be derived from anatomical or physiological observations. However, regions used for analyses, particularly in preclinical animal models, are generally derived by parcellating cortical and subcortical gray matter regions according to areal borders (Markov et al., 2014; Oh et al., 2014). One advantage of rodent models is that these delineations have been well studied and histologically validated in rats and mice (Paxinos & Franklin, 2007; Schwarz et al., 2006). Once areal definitions have been defined, structural or functional relationships between regions can be estimated, either through histological techniques (e.g. anatomical tracing, gene expression, or MRI imaging).

Seed-based connectivity and connectivity matrices

Seed-based connectivity is a method for assessing a regions FC (i.e. temporal correlation in BOLD activity) to other regions in a given areal atlas. Pairwise relationships between all nodes (i.e. multiple regions/seeds) can also calculated to obtain connection matrices that describe connectivity patterns between all regions in the brain. Connection matrices can then be averaged across multiple scans or subjects. These matrices are often thresholded to remove inconsistent or weak connections (Sporns, 2013). FC between individual connections or between larger anatomical divisions (frontal cortex, subcortical, limbic, sensory cortex, etc.) can then be compared between subject groups or as they change through development. The functional

connectome refers to the organization of FC between all region pairs, and has been the focus of a

great deal of research in recent years (Sporns, 2011).
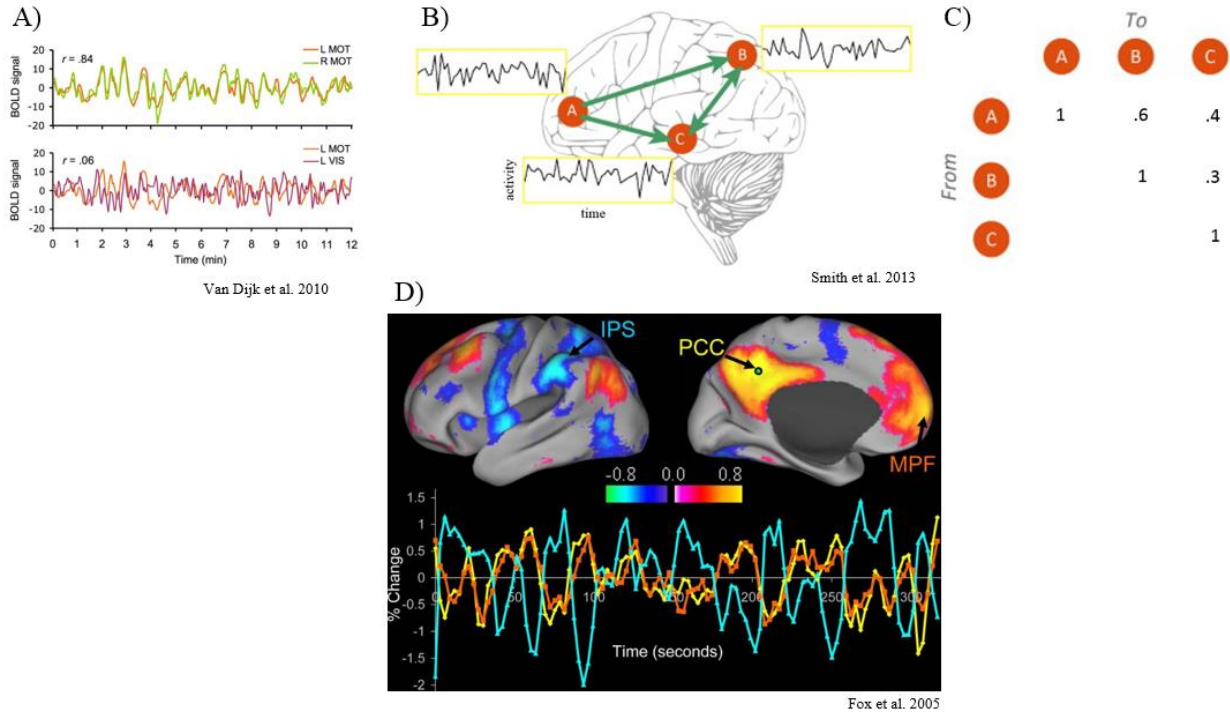
Figure 1.2 Overview of resting state functional connectivity. FC measures the temporal

correlation of brain activity between brain regions. A) Brain activity, measured by the BOLD

signal (y axis) is measured for a particular brain region across time (x axis). The temporal

correlation between two regions is then assessed. Regions with highly similar patterns of FC, in

this example the left and right motor cortex, and correspondingly high correlation (r) is shown in

the top panel of section A. The bottom panel shows regions with dissimilar patterns of

connectivity, in this example between the motor and visual cortex, and low correlation (Figure

adapted from (Van Dijk et al., 2010)). B) These comparisons can be done between multiple

regions, as in this hypothetical example using three regions. Here one can compare timeseries

between region pairs to construct a C) correlation matrix, which quantifies this similarity in

BOLD signal activity across time. Note that some pairs of regions (i.e. connections) will show higher correlation than others, but that the diagonal represents correlations between the same regions (and are not used for analyses). D) By comparing these relationships across the brain, maps can indicate regions with similar connectivity. For instance, correlations between the posterior cingulate (PCC) seed region and all other brain regions reveals areas with both highly similar functional connectivity patterns (in red), for instance the medial prefrontal cortex (MPF). In blue are regions that negatively correlated patterns of connectivity to the PCC (Fox et al., 2005). Understanding the organization of these relationships in health and disease is a major goal in neuroscience.

Functional Connectivity in rodents

As in humans (Cohen et al., 2008; Cole, Pathak, & Schneider, 2010; Gordon et al., 2014), resting state networks in preclinical animal models generally reflect anatomical divisions and functional modules, in both the rat (Becerra, Pendse, Chang, Bishop, & Borsook, 2011; B. B. Biswal & Kannurpatti, 2009; Hutchison, Mirsattari, Jones, Gati, & Leung, 2010; Jonckers, Van Audekerke, De Visscher, Van der Linden, & Verhoye, 2011; Majeed et al., 2011; Pawela et al., 2008; Zhao, Zhao, Zhou, Wu, & Hu, 2008) and mouse (Mills et al., 2016; Sforazzini, Schwarz, Galbusera, Bifone, & Gozzi, 2014; Stafford et al., 2014). These connectivity patterns often follow a symmetric structure (i.e., similar FC patterns on left and right hemispheres), including strong bilateral connectivity between somatosensory, motor, and visual cortex, hippocampus and subcortical areas, such as the caudate putamen, thalamus, superior colliculus, and hypothalamus (Chuang & Nasrallah, 2017).

Rodents also display large scale-cross modular connectivity patterns. An example of a large scale FC network is the default mode network (DMN). The DMN is comprised of a set of

regions that consistently show strong FC between the constituent nodes in the resting state. One way to identify the DMN is by using the retrosplenial or medial prefrontal cortex as the seed region and generating a timeseries correlation-based FC map between that seed region and the rest of the brain. Multiple groups have identified DMN-like connectivity patterns in rats (Chuang & Nasrallah, 2017; Lu et al., 2012) and mice (Stafford et al., 2014). Similarities between the rodent and human DMN is particularly robust between more well-conserved regions between species, such as the anterior cingulate, and retrosplenial, parietal, prelimbic, and auditory/temporal association cortical areas, and dorsal hippocampus (Lu et al., 2012; Upadhyay et al., 2011). A more detailed discussion on how the DMN and other networks compare between humans and animal models is presented in Chapter 4 section 3.

In short, comparative studies suggest that aspects of the functional connectome are shared between preclinical animal models and humans. Given the wide use of FC for characterizing human disease (Di Martino et al., 2014; M. Greicius, 2008), resting state networks may be able to serve as a translatable method for examining relationships between preclinical animal models and the human disorders they are meant to elucidate. However, the use of preclinical animal research requires one to consider additional factors compared to human research; for instance the use of anesthesia during scanning.

Additional considerations: Anesthesia

Rodent models often require anesthesia, while humans do not. Although it is possible to acclimate rodents to restraints while inside the MRI without anesthesia (Henckens et al., 2015), this presents significant complications. For instance, constantly receiving strong sensory inputs from the MRI environment and the increased motion artifact during the awake condition often results in poor data quality compared to the sedated state. Given the increased stress, potential

reaction to the loud environment, significant motion, and the requirement for habituation to the MRI, it is difficult to ascertain whether the awake condition is truly advantageous over the well documented effects of the low anesthesia state.

Although anesthesia is known to elicit complicated effects on neural, metabolic and hemodynamic responses (Gao et al., 2017; Masamoto & Kanno, 2012), studies have demonstrated that resting state networks are highly reproducible and consistent across different anesthesia regimens at optimal dose (Chuang & Nasrallah, 2017). That being said, the choice of anesthesia should be carefully considered. The following section will briefly discuss two anesthetic agents commonly used in preclinical animal FC research and discuss their limitations and advantages.

Isoflurane has been used extensively in rodents (Chuang & Nasrallah, 2017; Guilfoyle et al., 2013). As isoflurane is a quick, easy, and safe way to anesthetize animals and ensure good recovery post scan, it has been an attractive and commonly used choice in preclinical research. At a low dose, such as 1–1.5%, a strong focal and distributed network connectivity patterns can be obtained (Hutchison et al., 2010; Nasrallah, Tay, & Chuang, 2014; Stafford et al., 2014). Isoflurane is also an attractive choice because its gaseous nature allows for the maintenance of anesthesia levels to adjust for changes in respiration. This is not the case for injected anesthetic agents such as medetomidine.

Low level of isoflurane (<0.5%) together with a low dose of medetomidine infusion is also a robust anesthesia protocol for detecting strong bilateral FC and human-like FC networks such as the DMN (Grandjean, Schroeter, Batata, & Rudin, 2014; Lu et al., 2012). A problem with medetomidine is the restrictive sedative duration and complications due to the critical nature of the route and timing of delivery (Hutchison et al., 2010; Liang, King, & Zhang, 2011).

For example, using a single bolus injection rather than continuous delivery of medotomindine could lead to a variable depth of anesthesia, physiological state, and could result in variable FC throughout the scan. For these reasons, the current report opted to use low dose isoflurane. Other anesthesia regimes or awake imaging protocols could be potentially beneficial for future research.

Conclusion to rodent imaging section

In summary, there is an emerging body of literature investigating the organization of the rodent functional connectome. The literature described shows that rodent FC organization follows known anatomical and functional networks (e.g. somato-motor and default networks), is often bilateral in organization, and has identified specific functional networks (the default and motor networks for example), which are similar to those seen in humans (Lu et al., 2012; Stafford et al., 2014).

A major advantage of animal models is the ability to gain additional insights into the cellular and molecular mechanisms of the brain. Although our understanding of how biology influences FC is still in its infancy, advancement on these aims can be obtained through integrating these preclinical FC studies with data from detailed histological tracing studies and post mortem markers of genetic expression. Through this level of detailed investigation, we can further validate and expand understanding of the FC signal in a way that remains elusive in humans.

Section 3. Goals of project 1 (validation) and project 2 (applications)

The use of animal models allows investigation of questions we would not be able to probe in humans. This gives us the capability to contribute to our understanding of the mechanisms behind measurements we use in humans and to answer questions about the

underlying influences on FC patterns related to human disease. This document is separated into two projects. The first project validates and explores the underpinnings of rs-fcMRI and the second applies FC methods to a translational model of human disease.

The aim of the first project is to use rodent imaging to validate rs-fcMRI and to further understand the FC signal via integration with detailed molecular and cellular information. As such, project 1 explores the following open questions about the nature of FC. 1) It has been demonstrated that FC is to some degree guided by the underlying anatomical wiring. However, the details of these anatomical influences are unclear. Here we assess the degree that FC overlaps with direct (monosynaptic) and indirect (polysynaptic) anatomical pathways. 2) Recent evidence has suggested that FC is also influenced by the similarity in genetic expression between regions. To investigate this influence, we assess the overlap between FC and genetic similarity between regions, also referred to as correlated gene expression between region pairs. We then employ a novel method to identify which genes are most likely to relate to the emergence of FC between regions. 3) Finally, we assess the degree that gene expression and mono and polysynaptic axonal connectivity interact with one another and are spatially distributed in their influence on FC. Overall, project 1 helps to validate rodent FC, further our understanding of their mechanisms underlying FC, and identify potential genetic targets to later investigate as potential causal influences that give rise to FC.

Using animal models, we can investigate more causal changes to FC in ways we could not in humans. For example, correlational studies in humans have identified prenatal exposure to inflammatory cytokines, namely IL-6. IL-6 may be a key mediator for risk factors including prenatal stress, high fat diet, and increased risk for developmental disorders (Ashwood et al., 2011b; Wei, Alberts, & Li, 2013; Wu, Hsiao, Yan, Mazmanian, & Patterson, 2017). Although

15

these domains have been explored using FC in humans, and it has been theorized that IL-6 is a key factor mediating FC changes, the causal influence of FC change resulting from exposure to IL-6 is unknown.

Under this context, project 2 aimed to understand how exposure to IL-6 affects offspring FC development and alters component behaviors associated with developmental disorders. To accomplish these goals dams were exposed to chronic elevations in IL-6 throughout gestation through the use of a surgically implanted osmotic mini-pump. Offspring were then longitudinally tracked on both behavior and FC network change during early and late development. We hypothesized that FC would change both within targeted networks and more broadly across the brain. Specifically, we hypothesized that prenatal IL-6 would alter amygdala FC, a key structure implicated in developmental disorders, stress, and anxiety (Monk, 2008; Roy et al., 2009). A targeted analyses of the amygdala also offers the benefit of allowing for comparison to similar studies done in humans prenatally exposed to IL-6 (Graham et al., 2017), infants exposed to stress (Graham et al., 2015; Qiu et al., 2015; Scheinost et al., 2016), and the wide literature implicating the amygdala in autism (Nordahl et al., 2012; Verhoeven, De Cock, Lagae, & Sunaert, 2010). In addition to focusing on the amygdala, this project examined large scale network reorganization to discover brain wide changes which may result from prenatal IL-6 exposure. Finally, associations between FC and behavior were examined, with the hope of identifying critical circuits supporting component behaviors associated with developmental disorders.

Overall, this project highlights behavioral and functional connectivity alterations resulting from prenatal exposure to IL-6. This project offers the ability to compare changes in preclinical animal models to what is observed in infants and children who were prenatally

exposed to inflammatory cytokines, as well as to children and adolescents with developmental disorders, for whom maternal cytokine exposure may also play a role. Accumulated insights from the current study and others like it will further our understanding of the causal influences on FC patterns associated with these disorders, and ultimately increase our ability to develop better ways of treating them.

Chapter 2: Project 1. Correlated gene expression and anatomical communication support

synchronized brain activity in the mouse functional connectome

Introduction

    The brain is organized into a network of synchronized activity that has a complex and

reproducible topological structure (Bullmore & Sporns, 2009; D. Wang et al., 2015). Resting

state functional connectivity (FC) MRI, a technique which measures inter-areal correlations in

spontaneous brain activity, has been particularly useful for studying functional network

organization in both health and disease. Local and global features of this functional network are

carefully calibrated to support healthy cognition (Petersen & Sporns, 2015) and network

dysfunction is seen in numerous neurodevelopmental (Grayson & Fair, 2017; Vértes &

Bullmore, 2015) and neurodegenerative diseases (Fornito, Zalesky, & Breakspear, 2015; Seeley,

Crawford, Zhou, Miller, & Greicius, 2009). Therefore, identifying the substrates that shape

functional network organization is critical in linking molecular (e.g. gene transcription) and

behavioral (e.g. psychometric) markers of disease to brain function.

    Despite an abundance of prior work examining the correspondence of large-scale

functional and anatomical connectivity, the precise substrates that shape functional network

organization remain unknown. Modeling approaches to predict FC networks based on macro- or

meso-scale anatomical connectivity networks commonly simulate mass neuronal activity by

optimizing parameters that describe local population dynamics as well as the contribution of

inter-areal connectivity (Honey et al., 2009; Messé, Rudrauf, Benali, Marrelec, & Honey, 2014;

Sanz-Leon, Knock, Spiegler, & Jirsa, 2015). These approaches allow for detailed theoretical

exploration regarding the relative contributions of local dynamics vs global coupling, but are

limited by a lack of empirical data regarding true areal differences in function. Furthermore,

analytic measures of anatomical communication appear to predict FC at comparable values (Abdelnour, Voss, & Raj, 2014; Goñi et al., 2014), suggesting an upper limit to the predictive validity of models based on anatomical connectivity alone.

The integration of diverse data from different scales of investigation in such models may enhance our understanding of how functional networks are shaped. Although the idea is intuitive to most that FC may be guided by a combination of factors above and beyond anatomical wiring, studies investigating how the molecular properties of a given tissue influence these functional dynamics have historically been difficult to study and remain incompletely understood. There is work emerging suggesting that gene expression and areal chemoarchitecture influence spontaneous functional brain activity. For instance, associations have been found between areal densities of excitatory receptors and strength of functional connections (Turk, Scholtens, & van den Heuvel, 2016; van den Heuvel et al., 2016). Others have found that correlated gene expression, a measure of transcriptional similarity between regions, is greater within than between functional networks, and that the genes driving these relationships are involved in ion channel activity and synaptic function (Richiardi et al., 2015). With that said, questions remain regarding the degree to which these relationships can be explained and might interact. Previous studies in this realm have been limited in their sparsity of regions and networks investigated and a detailed understanding of the brain's complex network structure requires that gene expression data be comprehensively mapped onto corresponding whole-brain parcellations of structural and functional data. Furthermore, it remains unknown whether transcriptional similarities and anatomical connectivity modulate FC cooperatively, competitively, or overlap with FC uniquely depending on the connection.

Here we present a model of inter-regional FC in the mouse brain by integrating comprehensively and systematically obtained measurements of axonal connectivity (Oh et al., 2014) and gene expression data (Lein et al., 2007) from the Allen Institute for Brain Health. We investigated whether anatomical communication capacity and correlated gene expression (CGE) contribute uniquely or cooperatively to functional network architecture. We also examined whether these relationships are homogeneously expressed across the brain or whether these dependencies change according to cortical or subcortical subdivisions. Finally, in order to examine the molecular bases of the FC signal, we examined if specific clusters of genes disproportionately support these FC patterns.

Materials and Methods:

Subjects

In total, 23 C57BL/6J adult male mice ranging from 18-22g in body weight were used in the experiments. Mice were maintained on a 12-h light/dark cycle (lights on at 0600 h) at room temperature of 21 °C ± 1 °C and allowed food and water ad libitum. All experiments were performed during the animal's light cycle. Protocols were approved by Institutional Animal Use and Care Committees of the Oregon Health & Science University and the VA Portland HCS and conducted in accordance with National Institutes of Health Principles of Laboratory Animal Care.

Animal Preparation

Imaging in rodents generally requires the use of anesthesia to limit movement of the animals in the scanner. Here, anesthesia was induced by 3–4% isoflurane and maintained with 1–1.5% isoflurane. The selection of anesthesia may influence FC (Grandjean et al., 2014). Of

various anesthetic regimens, we selected low dose isoflurane for the present study based on the following previous findings: 1) Functional connectivity following 1% isoflurane is preserved and comparable to that of awake mice and rats (Jonckers et al., 2014; Mills et al., 2016; Shah et al., 2013; Stafford et al., 2014; K. Wang et al., 2011). 2) c-Fos activation (an immediate early gene) can be observed in isoflurane-anesthetized mice and rats (Kufahl, Peartree, Heintzelman, Chung, & Neisewander, 2015; Kufahl, Pentkowski, Heintzelman, & Neisewander, 2009; M. Smith, Li, Cote, & Ryabinin, 2016). That being said, acclimated awake animals or other anesthesia regimens, such as a combination of dexmedetomidine and lower dose isoflurane (.5-.75%) (Ash et al., 2016; Brynildsen et al., 2017), may be an alternative.

During scanning the head set stationary in a custom-built head holder designed to fit in the radiofrequency (RF) coil, as well as restrict any motion during the scan. Respiration (80–100 bpm) and animal temperature (maintained at 37 °C) were monitored and controlled by a small animal monitoring system (Model 1030 Monitoring and Gating System; SA Instruments).

Imaging acquisition

The imaging protocol is as described in our previous publication with slight modifications (Stafford et al., 2014). Imaging was performed during a single session for each animal on an 11.75T Bruker BioSpec scanner equipped with a Resonance Research, Inc. high-bandwidth shim power supply. A 20 mm ID RF quadrature volume coil (M2M, Cleveland, OH) was used for all studies. All scans were performed with Paravision 5. Using MAPSHIM, a 3D Fieldmap phase image was acquired; TR = 20 ms, TE1 = 2 ms, inter echo time = 4.003 ms, FA= 20∘, FOV= 40 mm × 18 mm × 25 mm, matrix = 80 × 90 × 125 (voxel size of $0.5 \times 0.2 \times 0.2$ mm^3, matching the EPI voxel size). This was followed by a T2-weighted structural image (RARE, TR = 4590 ms, effective TE = 32 ms, RARE factor = 8, 30 contiguous slices (0.5 mm

thick) with interleaved acquisition, FOV= 18 × 18 mm, matrix = 150 × 150, voxel size 0.12 ×

0.12 × 0.5 mm³, 2 repetitions). Global (volume) and local (brain voxel) shimming with

MAPSHIM were performed to calculate first and second order shims prior to the functional MRI

scan. The resting state fMRI consisted of a single shot gradient echo-planar imaging (EPI)

sequence with the following parameters: 360 repetitions (total scan time = 15 min), TR = 2500

ms, TE = 10 ms, FA= 60◦, 30 contiguous slices (0.5 mm thick) with interleaved acquisition,

FOV= 25.6 × 16 mm, matrix = 128 × 80, voxel size 0.2 × 0.2 × 0.5 mm³. An identical EPI

sequence with 20 repetitions was acquired in the reverse phase encoding direction for topup

distortion correction.

General fMRI BOLD preprocessing

Functional images were pre-processed to reduce artifact. These steps include: the removal

of a central spike caused by MR signal offset by discarding the first 10 EPI frames, slice timing

correction using FSL's slicetimer tool, correction of field inhomogeneities by applying topup

field map correction. This required that data was collected with reversed phase-encode blips,

resulting in pairs of images with distortions going in opposite directions. From these pairs the

susceptibility-induced off-resonance field was estimated using a method similar to that described

in (Andersson, Skare, & Ashburner, 2003) as implemented in FSL (S. M. Smith et al., 2004) and

the two images were combined into a single corrected one, and within run intensity

normalization to a whole brain mode value of 1000. Via the T2 scan, each scans functional data

was transformed to an anatomical rodent atlas supplied by the caret software (map 015 atlas) (D

C Van Essen et al., 2001; David C. Van Essen, 2012). We chose to map data to the caret atlas,

because it is MRI-based, free of the distortion from histological preparation, and allows for 3D

surface based visualization (Caret, map_015; available at sumsdb.wustl.edu/sums/

mousemore.do). Each run then was resampled in atlas space on an isotropic 0.2 mm grid combining atlas transformation in one interpolation (Lancaster et al., 1995).

Rs-fcMRI pre-processing

FC pre-processed was performed as previously described with the exception of small modifications (Stafford et al., 2014). Several additional preprocessing steps were used to reduce spurious variance unlikely to reflect neuronal activity (e.g. heart rate and respiration). These steps included the regression of the whole brain signal and the first order derivative of the whole brain signal, followed by a temporal band-pass filter ($f < 0.1$ Hz).

Regions of interest (ROIs)

One hundred-sixty cortical predefined areas based on the connectional and architectonic subdivisions in the mouse were used. These areas were obtained from the atlas as provided by the Allen Mouse Brain Connectivity Atlas at the Allen Institute for Brain Health (Oh et al., 2014). Regions are freely available online (Allen Brain Atlas Data Portal; connectivity.brain-map.org). To directly compare the Allen data with the functional MRI data, the Allen ROIs were registered to the caret, map_015 atlas using a six-parameter rigid body transformation. ROIs within the cerebrum were used which comprise both cerebral cortical areas and cerebral nuclei. Areas defined as brain stem and cerebellum by the allen brain institute and olfactory bulb regions were not included in this analyses due to potential differences in EPI data quality. All regions included in these analyses and their anatomical module assignments (Oh et al., 2014) can be found in supplementary table 2.1. Their anatomical projections can be visualized via the Allen Mouse Brain Connectivity Atlas at the Allen Brain atlas data portal.

Extraction and computation of regionwise resting state correlations

For each animal, 15 min of resting state BOLD time series data was collected. For each ROI, a resting time series was extracted post-processing and pearsons correlations were calculated for every region pair for each animal. Finally, ROI-ROI correlation, Fisher Z transformed r-values, were averaged across all subjects and used for analysis.

Allen anatomical projection acquisition methods

Structural data were obtained from the Allen Institute for Brain Science (Oh et al., 2014). Briefly, structural data on 400 adult male C57Bl/6J mice were obtained by performing stereotaxic tracer injection (recombinant adeno-associated virus expressing EGFP anterograde tracer mapping of axonal projections), image acquisition of tracer migration (serial two-photon tomography), and data processing to make structural connection matrices. Mutual connections among 426 regions (213 ipsilateral and 213 contralateral regions) were calculated, and of these 426 regions, 160 cortical regions were used for comparison with the functional data (80 ipsilateral/right hemisphere regions and 80 contralateral/left hemisphere regions). The best fit model for connections resulted from a bounded optimization followed by a linear regression to determine connection coefficients, which assigned statistical confidence (P value) to each connection in the matrix. Structural connectivity matrices were obtained by calculating the ratio of connection density to connection strength for each ROI-ROI pair and then normalizing the ratio by the volume of the target region (ROI). More specifically, as described in full in Oh et. al. 2014, a signal detection approach was used to separate GFP signal (from the viral tracer) from the backgrounds null signal. After segmentation and registration, quantitative values from segmented signals in each voxels contained within each brain were obtained. The projection signal strength between each source (injection region) and target was defined as the total volume of segmented pixels in the target (summed across all voxels within each target), normalized by

the injection site volume (total segmented pixels within the manually drawn injection area). The

segmented projection volume in an area was computed by integrating the per-voxel projection

density PD (fraction of segmented pixels) across all voxels. The normalized connection strength

described the amount of segmented signal activated in the target region by infecting one voxel in

the source region. In this sense, it can be thought of as proportional to the average out-degree of

neurons projecting from the source to the target. An extrinsic notion of connection strength can

be obtained by multiplying the normalized connection strength value by the size of the source

population; we call this the connection strength, and can be interpreted as proportional to the

total number of axonal fibers projecting from one area to the other. Conversely, an intrinsic

notion of connection density can be obtained through division by the size of the target

population, approximating the fraction of pixels in a voxel of the target region segmented

resulting from infection of all neurons in a single voxel of the source region (and thus less than 1;

normalized connection density). Combining these two operations results in a quantity analogous

to the fan-in of the source region to the target region, termed connection density; this can be

interpreted as the fraction of pixels segmented in a target voxel resulting from infecting the entire

source region (Oh et al., 2014).

Unlike the functional data that were undirected, the structural data contain directionality

(e.g., efferent vs. afferent pathways between two nodes/ROIs). We found that this directed

matrix required a very lenient threshold ($P < 0.75$) in order for the matrix to maintain

connectedness (the ability to traverse from one node to any other node via one or more network

links; a key property for making inferences regarding functional connectivity of each ROI pair).

To minimize the possibility of including spurious connections, an undirected matrix was

obtained, allowing us to reduce the threshold to $P < 0.05$. This threshold was applied first on the

directional matrix (i.e. each directional edge was thresholded based on its p-value). Then,

symmetry was imposed by taking the average of the directed matrix and its transpose. Using this

same procedure for generating undirected matrices, higher thresholds were also tested (P < 0.25)

and did not alter any variance estimates by more than 1%. Relationships between FC and

anatomical connectivity were assessed using both monosynaptic connectivity strength and using

a metric called communicability (G), which describes the ease of communication between

regions via mono- and polysynaptic connections. For instance, communicability between two

nodes will be stronger if there are multiple, or strong alternate paths connecting the two regions.

For communicability (Crofts & Higham, 2009) in a weighted matrix W, we begin by normalizing

each connection weight and defining a new matrix W', such that $W'_{ij} = W_{ij}/\sqrt{S_i \cdot S_j}$, where Si

and Sj are the strengths of node i and j. Communicability between i and j is defined as:

$$G_{ij} = \sum_{k=0}^{\infty} \frac{(W'^k)_{ij}}{k!} = (e^{W'})_{ij}$$

G is based on the notion of total communication capacity via parallel pathways, and is

computed by assigning exponentially decaying coefficients to the weight of pathways as the

walk length increases. Our previous work in macaques suggested that these coefficients may be

roughly optimal for predicting FC, resulting in superior results relative to other communication-

based models including SC weight or path length (Grayson et al., 2016). Therefore, we also

chose to examine the matching index (Hilgetag, Burns, O'Neill, Scannell, & Young, 2000),

which captures a conceptually different way in which functional connectivity could arise. Rather

than relying predominantly on the strength of communication paths, the matching index captures

the similarity of the connectivity patterns between two nodes. This accounts for third-party

contributors that may simultaneously influence activity patterns of both nodes through emergent

network effects but may not necessarily mediate communication (Adachi et al., 2012).

For weighted undirected networks, the matching index quantifies the similarity of

connections between two nodes excluding their mutual connection, as follows where $\Theta(W_{ik}) = 1$

if $W_{ik} > 0$ and 0 otherwise. A simplified depiction of these metrics are visualized in figure 2.1.

$$M_{ij} = \frac{\sum_{k \neq i,j}(W_{ik} + W_{jk})\,\Theta\,(W_{ik})\,\Theta\left(W_{jk}\right)}{\sum_{k \neq j} W_{ik} + \sum_{k \neq i} W_{jk}},$$
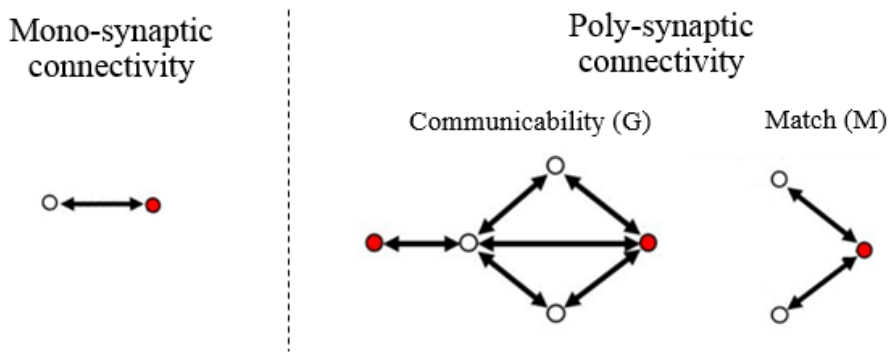
Figure 2.1. Structural connectivity metrics. Derived from the Allen mouse brain connectivity

viral tracing studies, structural connectivity can be computed to reflect either mono or

polysynaptic connectivity between regions pairs. Monosynaptic connectivity is based on direct

connectivity strength between regions. Polysynaptic connectivity metrics used are

communicability (G) and the matching index (M). Communicablity (G) takes the weighted sum

of all the paths between two regions, giving highest weights to shortest paths between regions.

Matching index (M) takes into account parallel communication via their common projections;

quantifying the similarity of the connectivity patterns between two nodes.

Allen gene expression data

Gene expression data measured using in situ hybridization (ISH) from the adult

C57BL/6J male mouse at age P56 were obtained from the Allen Mouse Brain Atlas (Lein et al.,

2007). Expression levels of mouse in situ hybridization data from the Allen Mouse Brain Atlas

were quantified using "expression energy" (fraction of stained volume * average intensity of

stain), as described previously (Lein et al., 2007). Because ISH data was only available for one

hemisphere, we retrieved expression energies for the same set of 80 functional ROIs used in our

analyses. Because of potential differences in data quality between coronal and sagittal methods

of ISH data collection (Fulcher & Fornito, 2016) we used only the higher quality coronal data.

To obtain this list we queried the Allen API (api.brain-map.org/api/v2/data) to obtain gene

expression energy for each region in the coronal plane called using the following API query:

api.brain-

map.org/api/v2/data/query.json?criteria=model::StructureUnionize,rma::criteria,section_data_set

[id$eqXXX],structure[id$eqYYY]. This resulted in 3318 genes, of these a final set of 3079 genes

had expression energy data available for each of the 80 ROIs, which was the set used for the

analyses. Gene expression energies were then normalized (z-scored) across brain regions, and

pearsons correlations were computed between brain regions to assess transcriptional similarity

between ROIs.

Statistical methods

Visualization of functional networks

Modular partitions of the network were obtained using the "Louvain" community

detection algorithm (Blondel, Guillaume, Lambiotte, & Lefebvre, 2008) adapted for full,

unthresholded networks with positive and negative weights (Rubinov & Sporns, 2011). This

algorithm identifies groups of nodes (communities, or modules) through optimization of the modularity index, or the fraction of edge weights within module partitions.

We found that the resulting partitions were stable for the current dataset at the default resolution parameter (gamma = 1). Across 1000 iterations of the algorithm with the default settings, 96.0% returned exactly 3 modules and only 4.0% returned 2 modules, and the Variation of Information (Meila, 2007; Rubinov & Sporns, 2011) from one iteration to the next was on average only 0.049 (SD: 0.055). Therefore we selected the result of one iteration at random, which was representative nonetheless.

The Q score for this partitioning was 0.36. Across different iterations of the Louvain algorithm, the mean was 0.36 (SD: 0.0014). This was significantly greater than comparable null models that were rewired to preserve weight and strength distributions (Rubinov & Sporns, 2011) ($p < 0.001$, 1000 null permutations), which had a mean Q score of 0.244 (SD: 0.21). Across the 1000 null networks, 64.3% resulted in 2 modules, 34.3% had 3 modules, and 1.4% had 4 modules.

We also tested the agreement between the Louvain decomposition and another conceptually very different partitioning approach known as Infomap (Rosvall & Bergstrom, 2008). Infomap is another widely used algorithm for functional connectivity data, which requires thresholding (setting weights below a certain value to 0). We used a previously described approach for generating a consensus partition across thresholds (Eggebrecht et al., 2017; Power et al., 2011), and apply it here on network sparsities of 10-50%. We again obtained a 3-network partition that was qualitatively not discernibly different from the Louvain results. Likewise, we found extremely low Variation of Information between the Infomap partition and the Louvain

results (mean VoI = 0.057). These data suggest that the modules ultimately displayed (see Figure 4) are quite robust with well-vetted approaches such as Louvain and Infomap.

The network was visualized using a force-directed graph layout where connections serve as attractive forces between nodes such that well connected groups of nodes are pulled closer together (Fruchterman & Reingold, 1991). Although no thresholding of the FC matrix was used in generating modular partitions, these types of spring-embedded diagrams require that some threshold is used to illustrate graphically the strongest links in the network. When this threshold is set too low, it is difficult to stably embed the low-degree nodes as they disconnect from the rest of the graph. When it is too high, nodes become 'latticized' and the edges are so densely populated that they become imperceptible. Again, this threshold affects none of the quantitative analyses or number of modules identified, and is purely for visualization purposes. We chose a threshold corresponding to a 20% network density (the top 20% of network edges are illustrated), as it provided a very reasonable tradeoff, although reasonable results could be obtained within a range of densities from 10-30%.

Modeling structure-function across both hemispheres

For making FC predictions across both hemispheres, only the structural network was used since the ABI gene expression data for each region is only available as an average of both hemispheres. We employed a general linear model of FC using communicability and the matching index as the two sole predictors. FC was then plotted as a function of the predicted values from the dual-variable model. ROI pairs were plotted as separate colors depending on ipsilateral, heterotopic, or homotopic, and the presence of a monosynaptic connection.

Modeling the transcriptional and anatomical contributions to the FC signal

Because the ABI gene expression data was only available as an average across hemispheres, the following analyses were conducted after averaging the FC networks across hemispheres as well. A series of linear regression models were assessed in order to examine the relationship between FC and transcriptional similarity, metrics derived from anatomical connectivity, and anatomical distance (computed as the log transformed Euclidian distance between the center of each ROI). See figure 2.2 for the full equation for each linear model.

As identified by previous work (Fulcher & Fornito, 2016), as well as our own (figure 3), Euclidian distance follows not only a distance dependent relationship but a logarithmic relationship with CGE. That is connectivity is better explained by the exponential than linear fit of distance on functional connectivity (Fulcher & Fornito, 2016). Spatial adjacency, a binary measure indicating whether two regions are touching, was also included in distance dependent models. Together log transformed Euclidian distance and spatial adjacency are referred to as spatial topography.

For the sake of brevity, we also refer to 'structure' as a predictor signifying the weighted combination of the two metrics derived from anatomical connectivity (i.e. G and M).

Anatomical, CGE, and FC matrices were converted to z-scores before being fit in each linear model. For these analysis all matrices (distance, anatomy, CGE, and FC) were unthresholded. Variance in FC explained was assessed after the inclusion of each term, as well as after the inclusion of the anatomy by CGE interaction (see all models in Figure 2.2). All linear models were calculated using the 'fitlm' function in Matlab (version 2014a). Goodness of fit for each model was assessed via Akaike information criterion (AIC). To compare model fits, the difference between models AIC were used to generate a chi-squared statistic and a Bonferroni adjusted p-value to account for multiple comparisons (based on five models comparisons

described next). Model AICs were compared to assess independent effects (did structure and CGE explain more variance than spatial topology), additive effects (did the combination of CGE + Structure explain more variance than either factor alone), and interactive effects (did the interaction between CGE and structure explain more variance then their additive effects).

A) $FC = \beta_0 + \beta_1 G + \varepsilon$

B) $FC = \beta_0 + \beta_1 G + \beta_2 M + \varepsilon$

C) $FC = \beta_0 + \beta_1 CGE + \varepsilon$

D) $FC = \beta_0 + \beta_1 G + \beta_2 M + \beta_3 CGE + \varepsilon$

E) $FC = \beta_0 + \beta_1 G + \beta_2 M + \beta_3 CGE + \beta_4 G \times CGE + \varepsilon$

F) $FC = \beta_0 + \beta_1 Euclidian\ distance + \beta_2 Spatial\ Adjacency + \varepsilon$

G) $FC = \beta_0 + \beta_1 Euclidian\ distance + \beta_2 Spatial\ Adjacency + \beta_3 G + \beta_4 M + \varepsilon$

H) $FC = \beta_0 + \beta_1 Euclidian\ distance + \beta_2 Spatial\ Adjacency + \beta_3 CGE + \varepsilon$

I) $FC = \beta_0 + \beta_1 Euclidian\ distance + \beta_2 Spatial\ Adjacency + \beta_3 CGE + \beta_4 G + \beta_5 M + \varepsilon$

J) $FC = \beta_0 + \beta_1 Euclidian\ distance + \beta_2 Spatial\ Adjacency + \beta_3 CGE + \beta_4 G + \beta_5 M + \beta_6 CGE * G + \varepsilon$

Figure 2.2. Models used to assess the relationships between functional connectivity *(FC)*, and measures of anatomical structure, communicability *(G)* and matching index *(M)*, correlated gene expression *(CGE)*, Euclidian distance between region pairs, and spatial adjacency, a binary measure of whether two regions are touching. Models A-J correspond to models used in scatters plots on Figure 2.2 and models described in Table 2.1.
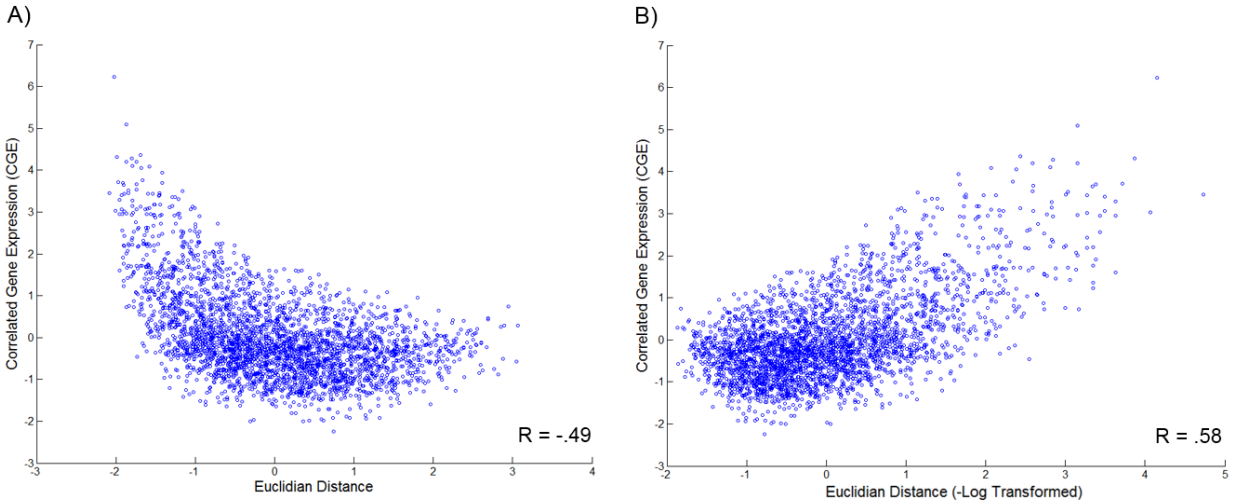
Figure 2.3. The relationship between Euclidian distance and correlated gene expression (CGE) is exponential, therefore, Euclidian distance was –log transformed before applied to all models throughout the manuscript. A) CGE by Euclidian distance (without transforming the distance matrix) shows an exponential relationship. B) The –log of Euclidean distance better fits the relationship between distance and CGE.

Shared connection patterns with FC

In order to assess the overlap between each connection type the following analyses were conducted. First, the FC, G, and CGE matrices (z-scored matrices) were thresholded and binarized in 1% increments from 10%-30% connection densities. Next, connections which survived a given threshold for all three matrices were given a value of 1. Similarly, connections which survived a threshold for FC and CGE, and FC and G, were given a value of 1. For each category, 1) overlap between all three matrices, 2) overlap between FC and G, and 3) overlap between FC and CGE, binary matrices were averaged across each connection density. Resulting matrices for each category were then binarized if their average value was greater than .5, indicating an overlap for that category across at least 50% of connection densities. Finally, in

order to assess the significance of these overlapping patterns we took a network level approach

to see if particular anatomical clusters (defined anatomically by the ABI) were overrepresented

for each category. This was implemented with a χ^2 approach. Briefly, the χ^2 test compares the

observed number of binary connections within a network pair with what would be expected if the

overall number of connections were evenly distributed across all network pairs. The resulting

statistic is large when there are more connections than expected by chance. An empirical p-value

is calculated by a permutation test, which is non-parametric and does not make assumptions

about the population distribution (Backes et al., 2014; Eggebrecht et al., 2017). Here, 10,000

permutations were performed, each time randomly shuffling the binary values for each

overlapping category (see above) and the reported p-values for each network reflect the observed

chi-square statistic compared to the permuted chi-square statistics obtained from the given

network-network pair. Significant networks for each category (p<.05, FDR corrected) are

highlighted in figure 2.6. In order to examine whether overlapping effects were driven by spatial

topology, an identical analyses was performed on residual matrices after each variable (FC,

CGE, and G) were adjusted for spatial topology.

Peak Analyses

In order to examine which genes were most critical for supporting the relationship

between FC and CGE the following analyses were performed. First, we computed the FC-CGE

relationship (i.e., with the inclusion of the full set of 3079 genes in the CGE matrix). We then

incrementally removed one gene before calculating the CGE matrix, and re-computed the FC-

CGE relationship. Then, we subtracted the FC-CGE relationship from the FC-CGE relationship

with one gene removed. Next, we rank ordered each gene according to how much the

relationship dropped after the removal of the gene. Finally, after rank ordering each gene we

incrementally re-introduced each gene (in rank order) into the CGE matrix and re-fit of the statistical models testing the relationship between FC and each predictor. We then identified the number of genes included in the CGE matrix that resulted in the highest amount of variance explained. Two analyses were performed, one which assessed the FC-CGE relationship in a linear model correcting for distance, an identical analyses was performed without correcting for Euclidian distance between region pairs.

Over-representation analysis

ErmineJ software, version 3.0.2 (Gillis, Mistry, & Pavlidis, 2010) was used to for over-representation analyses (ORA) comparing our target gene set corresponding to genes most related to FC (Peaks with and without covarying Euclidian distance in the gene rank list) to the background list of all coronal genes (3079 genes). Gene annotations were assigned from GO (Ashburner et al., 2000) using an annotation file from GEMMA (Zoubarev et al., 2012): Generic_mouse_ ncbiIds_noParents.an was downloaded from http://www.chibi.ubc.ca/microannots/ on December 6, 2016. From the 3079 genes in our set the annotations matched 3076 genes, the final list of genes included in our ORA analyses. Over-represented biological processes, molecular processes, and cellular components were tested. We used a maximum and minimum gene set size of 100 and 20 genes, respectively, used the best scoring replicate, and for scoring we weighted each gene within the peak as 1 and the remaining background genes as -1.

Results

Resting state functional connectivity of the mouse connectome

C57BL/6J mice (n = 23) were maintained under light anesthesia (1-1.5% isoflurane) and scanned in an 11.75T MRI. We computed FC (z-transformed correlations) between 160 bilateral regions of interest (ROIs) defined by Allen Mouse Brain Connectivity Atlas (AMBCA) (Oh et al., 2014) and detailed in previous work (Stafford et al., 2014). ROIs excluding regions labeled as brain stem and cerebellum by the AMBCA were chosen (see methods and supplementary table S2.1 for a complete list of regions). Figure 2.4 shows qualitative clustering of the mouse functional connectome, where brain regions (nodes) are pulled together if they share strong functional connections (edges) and weak functional connections are further apart in graphical distance. Regions are colored by functional module (figure 2.4A) as well as anatomical assignment based on the ABI region set (figure 2.4B). The mouse functional connectome appears to cluster by both functional as well anatomical subdivisions; the degree to which anatomical and transcriptional similarly between regions guides this organization is a major goal of this work.

Relationships between structural and functional connectivity

Measurements of anatomical connectivity, as assessed by viral tracing, were derived from the from the AMBCA (Oh et al., 2014). Anatomical communication capacity between the 160 ROIs used in the functional analyses was then computed on the weighted structural connectivity measurements. This communication capacity metric is termed, communicability (denoted $\underline{G}$), and is a weighted measure which describes the ease of communication between two regions (Crofts & Higham, 2009; Estrada & Hatano, 2008). It takes into account all possible routes between nodes (both mono and polysynaptic), but weights shorter pathways (those with fewer steps) exponentially higher. We chose this measurement of structural connectivity due to our recent work which highlights its improved capacity to model functional connectivity over simple mono-synaptic connectivity (Grayson et al., 2016). We also use the matching index (denoted *M*)

(Hilgetag et al., 2000), an index which quantifies the similarity of connections between two nodes excluding their mutual connection. Matching index captures additional small contributions to FC driven by interregional similarities in connectivity patterns, as demonstrated previously (Adachi et al., 2012).

Assessing the relationship between FC (unthresholded FC matrix using the bilateral 160x160 ROI set), the linear combination of G and M explained 22.1% of the variance in FC (Figure 2.4C) and was driven mostly by *G* (β=0.504 vs β=0.154 for *M*). Ipsilateral and heterotopic region pairs conformed closely to the overall regression line. However, homotopic region pairs showed consistently higher FC than expected by the overall regression line. This suggests an effect of functional areal similarity that is not explainable by network effects of anatomical connectivity alone.
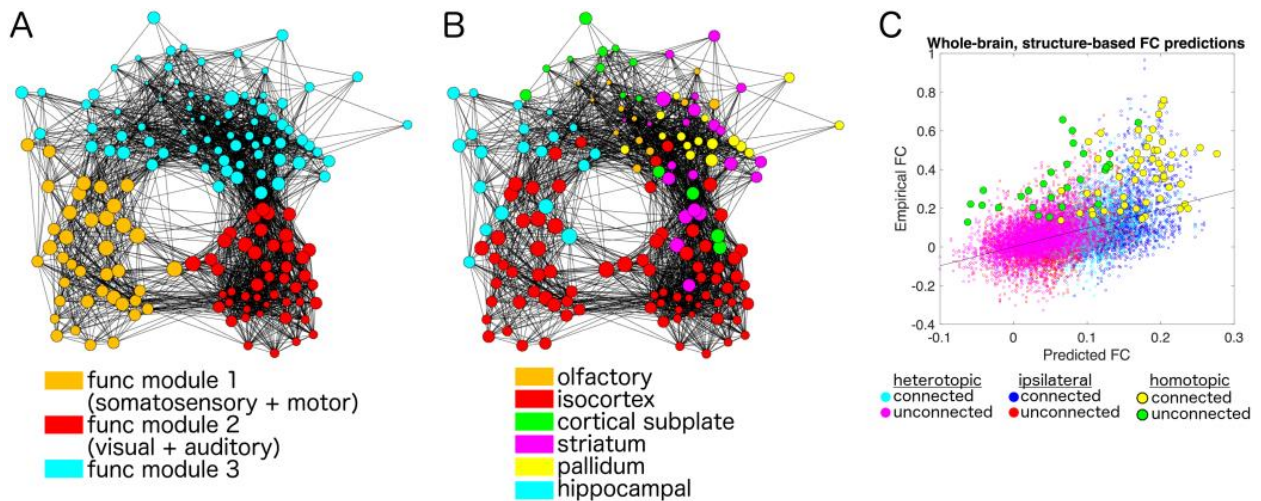
Figure 2.4. Clustering of the mouse functional connectome. Each brain region (node) shares a functional connectivity (FC) value (edge) with other nodes. Regions with strong FC are pulled more closely together and regions pairs with weak FC are moved further apart. Nodes are colored by functional (A) modularity assignment and (B) anatomical assignment. Nodes are

sized by their connectivity strength (i.e., the sum of all connectivity weights to that region). C) Empirical FC values across all region pairs, illustrated as a function of anatomical connectivity network-based (i.e. structure-based) predictions of FC. Each dot represents a unique region pair, colored according to whether it is heterotopic, ipsilateral, or homotopic, and whether the region pair possesses a direct anatomical link or not. Homotopic region pairs exhibit markedly higher FC than what is predicted by structure.

Inter-regional CGE, anatomical communication capacity, and spatial topology explain functional connectivity

In order to explain additional factors that contribute to the mouse functional connectome, we investigated the contribution of inter-regional CGE on resting state FC. For CGE we obtained measurements from the ABI mouse brain in-situ hybridization (ISH) data (Lein et al., 2007), which offers finely sampled whole-genome expression data within each of the allen ROIs. Due to potential differences in data quality between coronally and saggitally collected ISH data (Fulcher & Fornito, 2016), we used coronally obtained genes in order to ensure the highest data quality and to avoid mixing measures from both data sets. Genetic expression of all 3188 coronally obtained ISH probes were obtained for each ROI and for each gene. Expression intensities for all genes were z-scored within each ROI and fishers z-transformed pearson correlations were computed between each anatomical region pair across genes, yielding an 80x80 matrix of inter-regional CGE. The ABI gene expression data is provided as an average of both hemispheres, thus, for all subsequent measurements G and FC were averaged across left and right hemispheres yielding comparable 80x80 matrices.

Among ipsilateral region pairs connected via monosynaptic projections, we found FC to be significantly correlated with the weighted measure of monosynaptic anatomical connectivity

($r=0.33$, $p=10^{-6}$), but more so with communicability among monosynaptically connected ROI pairs (G; $r=0.40$, $p=10^{-6}$), in accordance with previous work (Grayson et al., 2016). FC and G were also correlated among region pairs with no monosynaptic connectivity ($r=0.35$, $p=10^{-6}$), which is also in line with our previous work (Grayson et al., 2016). FC and G were most strongly related when considering all connections (G; $r=.48$, $p=10^{-6}$).

Scatter plots shown in figure 2.5 correspond to models and their corresponding letters detailed in Figure 2.2. We found a strong relationship between G and FC among all region pairs (FC is unthresholded in all models, Figure 5A, $R^2=.227$, $\beta=.479$). CGE was also strongly correlated with FC (Figure 5C, $R^2=.412$, $\beta=0.642$). Models including the linear combination of both CGE and communicability (Figure 2.5D, $R^2=.452$) and the addition of the interaction between CGE and G increased the variance in FC explained (Figure 2.5E; $R^2=.488$, all individual terms except for M, are significant at $p<10^{-6}$).

Importantly, FC, CGE, and G all are distance dependent in real and biological meaningful ways. For instance, gene expression is more similar between similar structures which are also closer in proximity, white matter connectivity is stronger between regions which are closer from their source area, and FC is stronger between similar regions which are closer in proximity. That being said, Euclidian distance may also be partially driven by artefact, for instance, from virus spreading to nearby areas in anatomical viral tracing studies, and in FC where various artefacts can induce higher correlations between neighboring voxels. This has led to some controversy regarding the nature the overlap between CGE and FC (Pantazatos & Li, 2017; Richiardi, Altmann, & Greicius, 2017). For these reasons all analyses were analyzed including both Euclidian distance and spatial adjacency, a binary measure of whether two connections are touching, included as regressors in each linear model.

As expected, spatial topology explain a large amount of variance in the FC signal (Figure 2.5F, R^2=.549). Critically, the addition of each variable explains more variance than spatial topology alone, with the addition of structure (Figure 2.5G, R^2=.584), CGE (Figure 2.5H, R^2=.601), their linear combination (Figure 2.5I, R^2=.601), and interaction (Figure 2.2J, R^2=.624) explaining a total amount of variance of 62.4% of the FC matrix.

We also computed distance adjusted relationships between FC and G, and FC and CGE. Here, residuals for each matrix (FC, G, and CGE) were computed after the effects of spatial topology (spatial adjacency + Euclidean distance) were accounted for in a linear model. Residuals were then correlated. Scatter plots for FC and G (Figure 5K, $r = .269, p < 10^{-6}$) and FC and CGE (Figure 5L, $r = .337, p < 10^{-6}$) can be seen in figure 2.5.

Direct Model Comparisons

Importantly, direct comparisons of model fits based on their AIC and resulting chi-squared distributions, confirmed the independent, additive, and interactive effects (see Table 2.1 section 3). Independent effects were demonstrated by model comparisons showing that both structure ($\chi^2(2) = 379.96$, p = 7.27^{-54}) and CGE ($\chi^2(1) = 247.93$, p = 6.33^{-84}) explain more variance than spatial topology alone. The linear effects combination of CGE, structure, and spatial topology explained more variance than structure and spatial topology ($\chi^2(1) = 240.66$, p = 1.41^{-53}) or CGE and spatial topology ($\chi^2(2) = 108.63$, p = 1.29^{-23}). Finally, the interactive effect of CGE and structure explained more variance the linear combination of structure and CGE alone (all models including spatial topology, $\chi^2(1) = 80.19$, p = 9.76^{-25}). Overall, we show that transcriptional similarity and network effects of axonal connectivity cooperatively, but also uniquely, support FC beyond what can be explained by Euclidian distance and spatial adjacency between regions pairs.
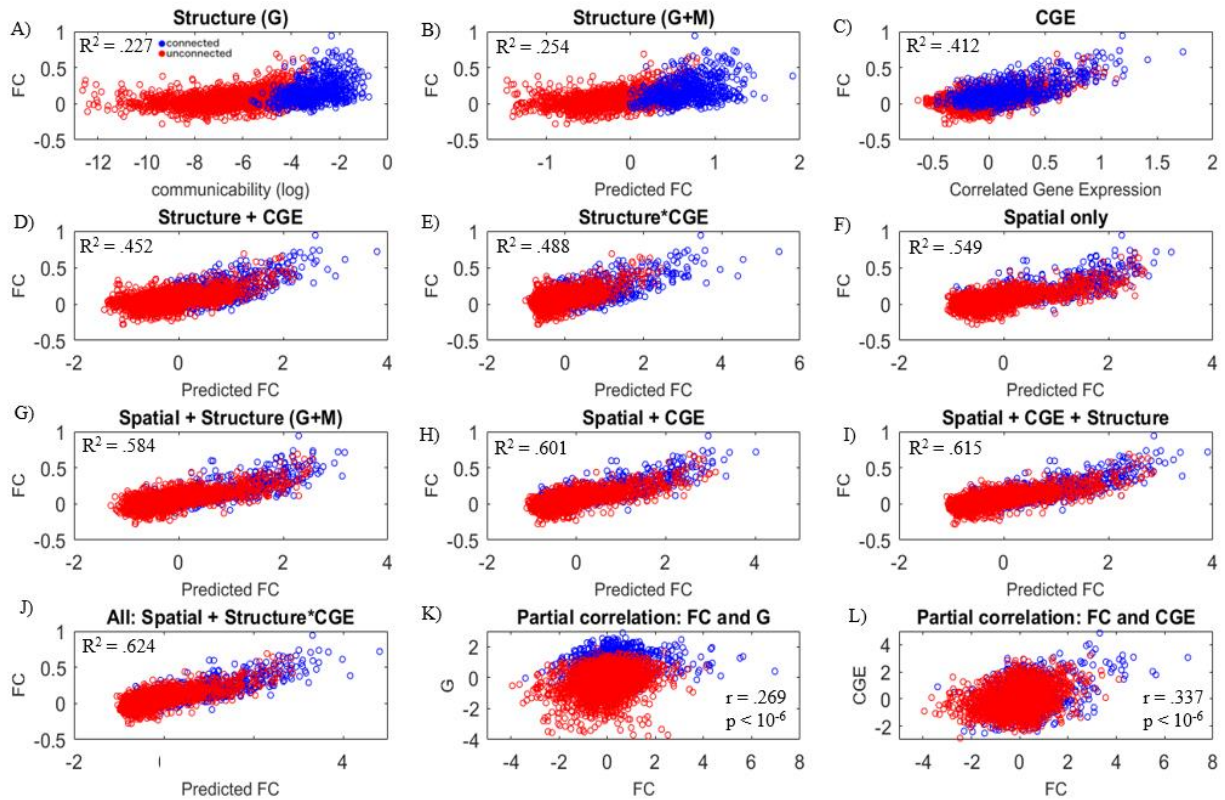
Figure 2.5. Relationships between functional connectivity (FC), anatomical connectivity measures communicability (*G*) and matching index (M), and correlated gene expression (CGE). Blue points indicate region pairs which share a direct monosynaptic anatomical connection and red points are region pairs which are anatomically unconnected. FC is illustrated as a function of A) Anatomical structure defined by only *G*, B) Anatomical structure defined by the linear regression of FC on *G* and M. C) The relationship between FC and CGE. D) FC predicted by a linear combination of structure (G+M) and CGE E) FC relationship after the inclusion the interaction between G and CGE. Next we starting with a null model predicting FC as a function of spatial topography (Euclidean distance + spatial adjacency), and show that each variable adds to the variance explained above and beyond spatial topography (G-I), ending with a final J) omnibus model including all variables and the interaction between structure and CGE, which explains the most variance in FC. Full equations for models depicted in A-J can be found in

figure 2.1 and beta weights and significance for each parameter are shown in Table 2.1. K-L) Partial correlations analyses. Relationships between G and FC, and CGE and F were computed after adjusting each metric (FC, G, and CGE) for distance and spatial adjacency (i.e., correlation between residuals after spatial topology adjustment).

Models explaining functional connectivity

1) With Spatial topology

Model	Metric	Beta	AIC	r^2	p-value
F) spatial topography only	distance	0.5036	6455	0.549	$<10^{-6}$
	SA	0.3187			$<10^{-6}$
G) spatial topography + structure	distance	0.4528			$<10^{-6}$
	SA	0.2623			$<10^{-6}$
	G	0.2219	6207.1	0.584	$<10^{-6}$
	M	0.0462			$<10^{-4}$
H) spatial topography + CGE	distance	0.3834			$<10^{-6}$
	SA	0.235	6075	0.604	$<10^{-6}$
	CGE	0.2914			$<10^{-6}$
I) spatial topography + CGE + Structure	distance	0.375			$<10^{-6}$
	SA	0.2096			$<10^{-6}$
	CGE	0.2409	5966.4	0.615	$<10^{-6}$
	G	0.1427			$<10^{-6}$
	M	0.0099			n.s.
J) Full Model: spatial topography + structure*CGE	G	0.1617			$<10^{-6}$
	CGE	0.2049			$<10^{-6}$
	M	0.0044	5886.3	0.624	n.s.
	$G*CGE$	0.1145			$<10^{-6}$
	distance	0.3654			$<10^{-6}$
	SA	0.1816			$<10^{-6}$

2) Without Spatial topology

Model	Metric	Beta	AIC	r^2	p-value
A) Structure (G)	G	0.4799	8143.2	0.227	$<10^{-6}$
B) Structure (G+M)	G	0.5433			$<10^{-6}$
	M	0.1706	8040.4	0.254	$<10^{-6}$
C) CGE	CGE	0.6421	7290.8	0.412	$<10-6$
D) Structure + CGE	G	0.2439			$<10^{-6}$
	M	0.0441	7076	0.452	0.002
	CGE	0.5231			$<10^{-6}$
E) Structure + CGE + Structure*G	G	0.2666			$<10^{-6}$
	M	0.0335			n.s.
	CGE	0.4247	6862.4	0.488	$<10^{-6}$
	$G*CGE$	0.2111			$<10^{-6}$

Model comparisons

3)

Independent Effects

	F) spatial topography only
G) spatial topography + structure	$\chi^2(2) = 379.96$, $p = 7.27^{-54}$
H) spatial topography + CGE	$\chi 2(1) = 247.93$, $p = 6.33^{-84}$

Additive Effects

	I) spatial topography + CGE + Structure
G) spatial topography + structure	$\chi 2(1) = 240.66$, $p = 1.41^{-53}$
H) spatial topography + CGE	$\chi 2(2) = 108.63$, $p = 1.29^{-23}$

Interactive Effects

	J) Full Model: spatial topography + structure*CGE
I) spatial topography + CGE + Structure	$\chi 2(1) = 80.19$, $p = 9.76^{-25}$

Table 2.1. Multivariate models of functional connectivity. The top panels show each statistical model (A-E) of functional connectivity using combinations of explanatory variables including anatomical structure, correlated gene expression, and spatial topology. Structure indicates a combination of (G) Communicability and (M) match index; two polysynaptic anatomical connectivity metrics. Correlated gene expression (CGE) measures similarity in gene expression between regions and $G*CGE$ denotes the interaction term. Spatial topology is the combination of

Euclidean distance between ROI centroids and spatial adjacency (SA), a dichotomous variable indicating whether or not two regions share a border. 1) Models are assembled without and 2) with the inclusion of spatial topology. Betas represent standardized coefficients and the variance explained for each model is represented by the R^2. AIC values denote each models goodness of fit, with lower values indicating better model fit. 3) The bottom panel takes a model comparison approach to compare models goodness of fit. Null models are shown as column headers (e.g. F) spatial topology only), and models which are compared are shown on the rows. Highlighted are the significant independent effects of structure and CGE above spatial topology, the additive effect of CGE and structure above each of their independent effects, and the interactive effect of CGE and structure above their linear combination. P-values for each model comparisons (based on a chi-square statistic based on the difference in model AICs) are Bonferroni corrected for multiple comparisons.

Distinct anatomical modules are responsible for the contribution of correlated gene expression and anatomical communicability on functional connectivity

We found that both CGE and G, independent of spatial topology, help shape/explain functional connectivity networks. As such, we then explored whether this relationship is heterogeneous or homogenous across the brain. That is, are there anatomical subdivisions in which there are distinct or overlapping relationships between FC, anatomy, and gene expression? Specifically, we examined which functional connections may be supported uniquely by CGE, G, or by a combination of CGE and G. First, in order to explore these patterns we binarized each matrix in 1% increments from the top 10%-30% connection densities. For each matrix (FC, CGE, and G) connections were considered if they survived at over half of these connection densities. In order to examine overlapping profiles, a matrix was derived indicating whether

43

there was overlap between FC and CGE, FC and G, or between all three matrices. We then calculated the statistical significance of this overlap by computing a FDR corrected chi-squared statistic for each anatomical module, which tests whether each overlap metric was more prevalent within an anatomical module than expected by chance, see methods for more details on the chi-squared approach.

Overlap between FC, G and CGE was non-uniform across the brain and depended on partial correlation adjustment based on distance. As can be seen in figure 2.6, we found that overlap between the strongest FC and CGE within and between cortical, motor, cortical to motor, striatal, and pallidal networks. After adjustment for spatial topology (adjusting metrics to correct for distance and spatial adjacency), cortical and sensory networks increase in overlap between FC and CGE, where subcortical overlap is partially dependent on distance. In regards to overlap between FC and G, with and without distance adjustment we found that overlap within hippocampal and olfactory areas. However, distance adjustment influenced the degree to with FC and G overlapped between hippocampal and olfactory to subcortical networks. With and without spatial topology adjustment), overlap between all three metrics was most robust within motor and visual networks. Distance adjustment decreased the amount of overlap between all three metrics. This was unsurprising as we know that distance dependence is real and prominent driver of all three metrics. Although these patterns are observed at the level of gross anatomical modules, a more granular view may also be informative. For instance, G, rather than CGE, may drive a subset of longer range cortical to subcortical connections. Overall this analyses suggest that FC may be both independently and cooperatively shaped by G and CGE, and that this relationship is non-uniform across the brain but depend on anatomical module.
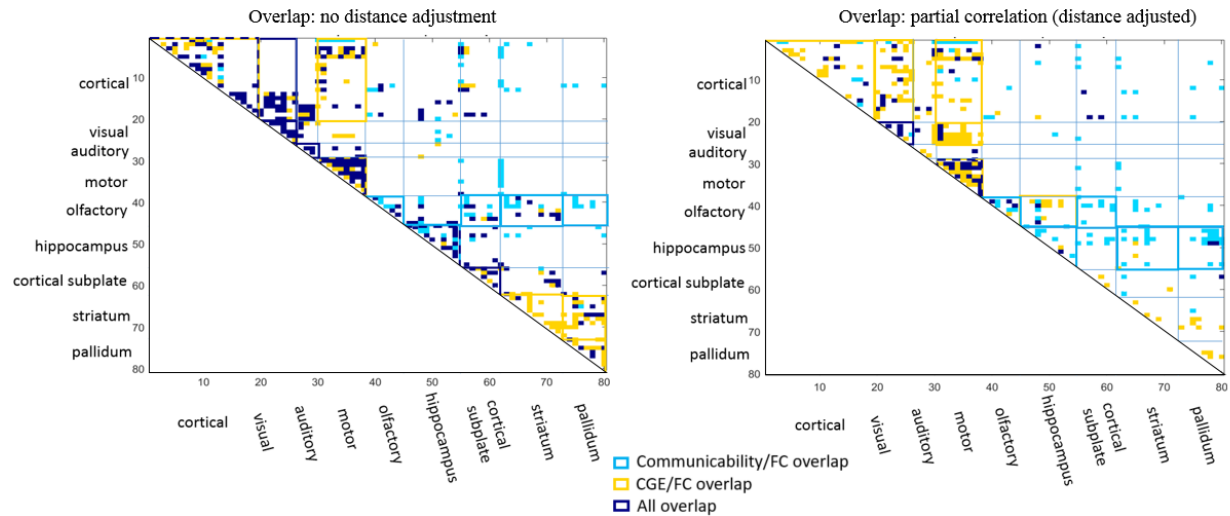
Figure 2.6. Regional distribution overlap between FC, G, and CGE. Overlap between the strongest functional connections (FC), correlated gene expression (CGE), and anatomical communicability (G) matrices was compared. Connections with shared overlap, either shared between FC and G (aqua), FC and CGE (yellow), or between all three metrics (purple) are shown. Anatomical modules that show significant overrepresentation of one category are outlined (based on an FDR corrected chi-squared test). Overlap between matrices was calculated as the consensus across 10-30% connection densities. Spatial topology adjustment indicates that metrics (FC, G, and CGE) were adjusted for distance and spatial adjacency.

A subset of genes support the relationship between correlated gene expression and functional connectivity

It is likely that not all genes contribute equally to the variations in the FC signal. Next, we asked whether all genes equally contribute to the relationship between CGE and FC, and how many genes drive this relationship. To examine this we computed the FC-CGE relationship (with and without co-varying distance). Next we removed one gene and recalculated a new CGE matrix. Then, we subtracted the variance explained in the model with all genes included in the

45

CGE matrix from the model, which was calculated on the leave one out CGE matrix, and rank

ordered each gene according to the magnitude of the difference in variance explained between

the full and leave one out CGE matrix. Next, after rank ordering each gene by most to least

related to FC, we incrementally re-introduced each gene into the CGE matrix (i.e., each time

adding back one gene before computing the CGE matrix) and re-fit each model. Figure 2.7

shows the variance in FC explained with each model, as a function of how many genes were

reintroduced into CGE matrix. The maximum amount of variance emerged after 568 genes were

included in the CGE matrix (model peak without distance R^2 = .613, with distance in model R^2 =

.726), see figure 2.7. Similar results were found when rank ordering genes without considering

distance, with a max variance at 445 genes (model peak without distance, R^2 = .671 and with

distance in model, R^2 = .702), see figure S2.1. Note the marked decline in explanatory power of

the CGE after the inclusion of additional genes beyond the peak, suggesting that a subset of

genes contribute disproportionately to the observed CGE-FC relationship.
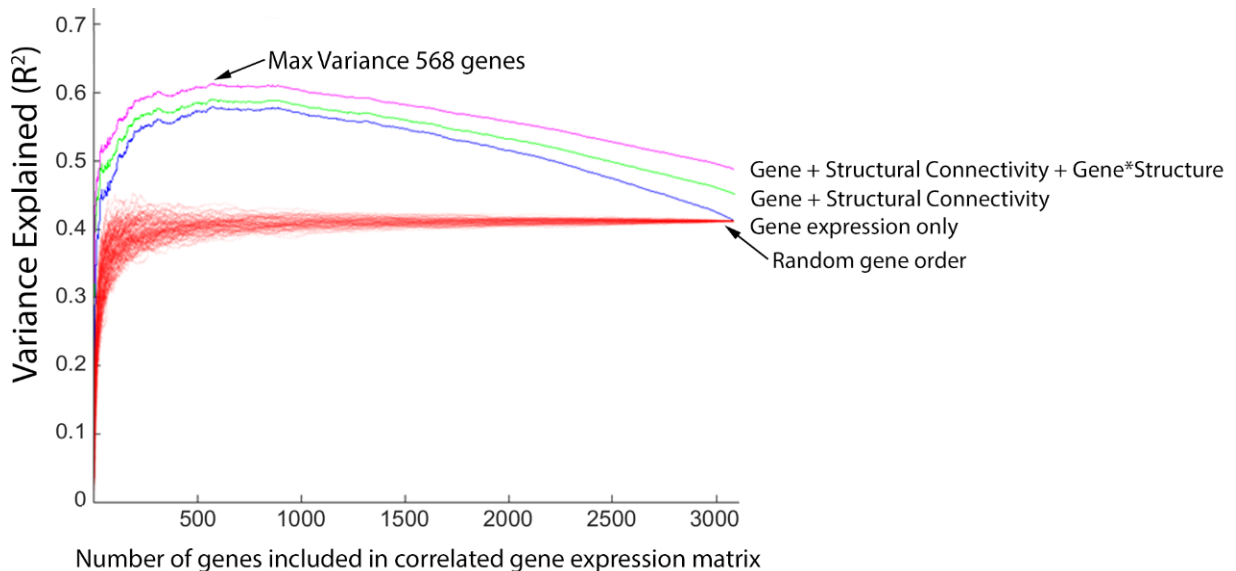
Figure 2.7. A subset of genes support the relationship between CGE and functional

connectivity. Genes were rank ordered (x-axis) based on their contribution to the CGE-FC

correlation (correcting for distance). Then, each model predicting FC was refit after incrementally adding each gene to the CGE matrix. The max variance was observed after the inclusion of 568 of the most explanatory genes to the CGE matrix, $r^2 = .6131$). Each red line indicates a different permutation for gene expression only, where gene rankings were randomized on each permutation. 100 random permutations are shown.

These results suggest that a limited number of genes contributed to the relationship between FC and CGE. In order to examine the functions of genes that most strongly contributed to the FC signal we performed an over-representation analyses (ORA) using the software ErmineJ. Top ranked genes within the max variance peak in figure 2.7 (Max variance 568 genes) were selected and compared to the background set of genes (3079 genes). This procedure identifies clusters of genes that are overrepresented within this peak, their biological and molecular processes, and cellular components. Interestingly, as opposed to some earlier work in humans (Fulcher & Fornito, 2016; Richiardi et al., 2015), no clusters passed statistical significance after FDR correction, potentially suggesting that these strongest related genes are equally related to several molecular and biological processes (see discussion). With that said, Table 2.2 shows the uncorrected results of all significant gene clusters (p<.05; peaks identified with and without covarying for Euclidian distance), which do show interesting trends that lay fodder for future study and empirical manipulation. Most notably with these findings was the over-representation of molecular processes related to voltage-gated cation channel activity, a gene cluster that was consistently over-represented regardless of distance correction.

Molecular Process

A) Distance Corrected

Functional Classification	Gene Ontology	Multifunctionality	p-value
voltage-gated cation channel activity	GO:0022843	0.168	0.04788128

B) No Distance Correction

	Gene Ontology	Multifunctionality	p-value
voltage-gated potassium channel activity	GO:0005249	0.00764	0.04815824
voltage-gated cation channel activity	GO:0022843	0.168	0.03066491
cation channel activity	GO:0005261	0.742	0.0344259

Cellular Component

A) Distance Corrected

Functional Classification	Gene Ontology	Multifunctionality	p-value
presynaptic membrane	GO:0042734	0.624	8.94E-03
synaptic membrane	GO:0097060	0.724	0.01143322
presynapse	GO:0098793	0.846	8.02E-03

B) No Distance Correction

N.S.

Biological Process

A) Distance Corrected

Functional Classification	Gene Ontology	Multifunctionality	p-value
glutamate receptor signaling pathway	GO:0007215	0.684	0.0498833
multicellular organismal homeostasis	GO:0048871	0.897	0.0464227
pallium development	GO:0021543	0.902	0.0499765
positive regulation of sequence-specific DNA binding transcription factor activity	GO:0051091	0.905	0.0315802
regulation of leukocyte migration	GO:0002685	0.909	0.0291887

B) No Distance Correction

	Gene Ontology	Multifunctionality	p-value
DNA repair	GO:0006281	0.598	0.0239477
regulation of fat cell differentiation	GO:0045598	0.806	0.0484942
response to light stimulus	GO:0009416	0.883	0.0274634
response to radiation	GO:0009314	0.897	0.0397004
multicellular organismal homeostasis	GO:0048871	0.897	0.0467673
chemical synaptic transmission	GO:0007268	0.898	0.0500627
anterograde trans-synaptic signaling	GO:0098916	0.898	0.0500627
synaptic signaling	GO:0099536	0.898	0.0500627
trans-synaptic signaling	GO:0099537	0.898	0.0500627
regulation of intracellular transport	GO:0032386	0.913	0.0488791
positive regulation of ERK1 and ERK2 cascade	GO:0070374	0.928	4.52E-03
regulation of ERK1 and ERK2 cascade	GO:0070372	0.929	7.35E-03

Table 2.2. Functions of genes that support the relationship between CGE and FC. Genes that most strongly supported the CGE-FC relationship was (top genes identified in figure 2.7) compared to the background set of all genes. Results are shown for gene rankings produced (A) with and (B) without correction for Euclidian distance between region pairs. Results are ordered by multifunctionality and were produced using the over-representation analyses in the ErmineJ software package.

Discussion
Modeling the influence of correlated gene expression and anatomical communicability across the functional connectome

This report investigates the white matter anatomy and regional similarity in gene expression influence synchronous large-scale brain activity. We found that functional connectivity is related to distinct aspects of structural communication (measured via communicability) and inter-areal similarities in gene expression. Our model accounts for a significant amount of variance in the resting state functional connectivity (FC) signal (R^2=.624) at its peak without considering improvement related to spatial proximity. The present report extends key findings from Richiardi et al., who showed in humans that correlated gene

expression (CGE) is enriched within key functional brain networks relative to between these networks (Richiardi et al., 2015). Here we show that these principles hold in rodents and that CGE predicts functional connectivity (FC) across the brain. Interestingly, CGE explains more variance in the FC signal than anatomical communication capacity (*G*), suggesting that transcriptional similarity, and presumably similarities in protein expression, may be a crucial foundation of the FC signal in addition to anatomical wiring. We also found a significant interaction between CGE and G, suggesting that a region's transcriptional profile and anatomical wiring may work in coordination to modulate functional synchrony with other regions. The addition of CGE to models of FC is significant given the abundance of literature that has been aimed at identifying the substrates that support functional connectivity via structural network analysis (reviewed in (Bassett & Sporns, 2017)). The present findings suggest that a more accurate modeling strategy requires the integration of structural connectivity with empirical measurements of areal molecular properties.

Relationships between physical proximity, functional and structural connectivity, and correlated gene expression

One area of caution, and interest, is the role of spatial proximity to the relationships across the three modalities. Areas that are close in spatial proximity are more likely to share more similar gene transcription profiles, have stronger anatomical connections, and share stronger functional connections. These distance relationships represent biologically meaningful information; however, there is nonetheless a concern that the spatial smoothness of the fMRI signal might artifactually inflate estimates of structure-function correspondences. All fMRI data were processed without any spatial blurring in order to mitigate this possibility. Further, given the relationship between CGE and Euclidian distance, with exponentially higher CGE between

49

regions pairs close in spatial proximity (Pantazatos & Li, 2017), it is important that these type of studies also take into account how these variables relate above and beyond spatial proximity. Here, we show that although highly related to distance, as expected, relationships between FC, G, and CGE, are independent of Euclidian distance and spatial adjacency. When examining relationships between FC and CGE, others have similarly corrected for Euclidian distance (but not the additional parameter of spatial adjacency (Fulcher & Fornito, 2016) or have taken alternative approaches to examine these FC/CGE relationships between spatially distributed functional networks (Richiardi et al., 2015). Given that covariation between distance and FC, G, and CGE is partly biological, we suggest that when possible the results should be compared with and without these types of correction.

The distribution of overlap between these three metrics was also of interest, as relationships with FC may be driven more prominently between some networks than others. Interestingly, we found that cortical, striatal, and sensory regions had a large degree of overlap between CGE and FC, where hippocampal and long range FC were more likely to be driven by overlap between G and FC. However, distance correction partially influenced some of these results (hippocampal) but not others (cortical and sensory). More work will need to be done to understand exactly how and between which connections, CGE and G selectively influence FC. Just as importantly, in our view, will be future experiments with a more thorough characterization of these relationships through experimental manipulation of either anatomical wiring or gene expression profiles.

Correlated expression of a subset of genes disproportionately influence functional connectivity

Given that transcriptional similarity between regions had a large effect on FC, our next aim was to understand the contributions of specific gene clusters. That is, is the regional similarity across the entire transcriptome predictive, or do some genes disproportionately influence this relationship? By ranking each gene's contribution to the CGE-FC relationship, we found that a subset of genes (568 of 3079) disproportionally drive this relationship, suggesting that covariance in particular subsets of processes may be more influential in supporting the FC signal. In this report we used gene ontology over-representation analyses (ORA) to identify the processes associated with these genes. In this section we discuss these analyses, some potential gene clusters, which may support FC, common themes, and considerations.

Although it is clear that a subset of genes disproportionately drive the relationship between CGE and FC, in contrast to previous results (Fulcher & Fornito, 2016; Richiardi et al., 2015), ORA on genes which are most likely to contribute to FC did not yield robust results, and as noted above, no gene cluster reached FDR corrected statistical significance. Such discrepancies here, relative to prior reports, may be due to methodological differences or differences in gene selection used for ORA. Alternatively, this finding could suggest that across the brain a complex mixture of genes support FC and that the contribution of the genes spreads across multiple functions (at least enough such that no clusters passed correction). This finding could also mean that different gene clusters are critical between different anatomical connections, and that a unifying genetic function cannot describe the FC to CGE relationship across the brain. Both of these considerations deserve further investigation.

That being said, when analyzing patterns at a relaxed threshold ($p < .05$, uncorrected), several interesting patterns emerged yielding somewhat convergent evidence to similar reports (Fulcher & Fornito, 2016; Richiardi et al., 2015). For instance, genes which were most related to

51

FC were more likely to be involved in molecular processes, which were specific to voltage-gated ion channel and potassium channel activity. This finding is in good accordance with Richiardi and colleagues (2014) who also found preferential enrichment for these processes within compared to between functional networks. This correspondence would suggest that similar mechanisms might underlie the FC signal across species. In our report we also identified several biological processes including glutamate receptor signaling, a putative candidate for neural bases for the functional signal (Attwell & Iadecola, 2002; Raichle, 2001), as well as cellular components related to synaptic membrane proteins and synaptic signaling.

When examining these results, it is also important to note that some gene clusters may have multiple functions that are not perfectly circumscribed to a particular process. Some genes may have many more functions than others (Gillis et al., 2011) and this can be qualified by a multifunctionality score. Genes can have many diverse biological roles and highly multifunctional genes are not necessarily incorrectly assigned to a particular role, but should be interpreted with more caution (Gillis, Pavlidis, Benson, Bryant, & Canese, 2012). In our analyses, ion channels represent a gene cluster that supports FC with relatively low multifunctionality. However, we also identify additional overrepresented biological clusters with high multifunctionality scores including genes coding for homeostatic and developmental processes. These processes might be interpreted with caution as these genes also supply a rich diversity of alternative functions that, in turn, might also be related to the FC signal.

There is a complex set of neuronal, vascular, and cellular influences on the FC signal. Any given region's activity may be modulated by neurotransmitter signaling (Attwell & Iadecola, 2002; Magistretti & Allaman, 2015), the excitatory to inhibitory ratio (Turk et al., 2016; van den Heuvel et al., 2016), local energy demands (Lu & Stein, 2014; Magistretti &

Allaman, 2015; Tomasi, Wang, & Volkow, 2013), and/or cytoarchitectural features such as synaptic density (Attwell & Iadecola, 2002; Magistretti & Allaman, 2015). Each of these contributions may be reflected in interregional variability in both gene expression and spontaneous activity. Along the same lines, molecular influences on regional activity might vary across different brain subdivisions. For example, we show that the distribution of high-CGE, high-FC links are non-uniform and occurs to a greater extent in particular types of connections (i.e. striato-pallidal). Future work should address whether the gene clusters which most contribute to the functional signal vary by connection. Overall, the specific relationships between gene transcription and FC is far from resolved and will require experimental manipulation.

Applications and conclusions

Models that explain functional brain organization are particularly useful in preclinical animal models, where genetic and pharmacological manipulation allow the exploration of both etiology and therapy in various neurological disorders. With this consideration in mind, one of the most straightforward applications of the current statistical model would be to determine the theoretical impact of experimental perturbation to specific regions, systems, or even gene clusters within specific systems. There is evidence from work in monkeys that simulated lesions can accurately predict many widespread neurophysiological changes in response to focal empirical inactivation (Grayson et al., 2016). Extending this approach to rodents, in combination with improved modeling techniques that account for transcriptional similarity, might be exceptionally useful given the time and cost associated with pharmacological screening and gene therapy testing. Recent rodent work highlights the usefulness of simulated lesions for predicting memory impairments (Vetere et al., 2017), but has yet to account for the influence of areal gene expression in the modeling framework. Our results here suggest that identifying both candidate

brain systems and candidate genes via simulated perturbation might be feasible for interrogating other cognitive deficits as well. Finally, experimental manipulation of activity and/or gene expression combined with simultaneous in vivo functional measurement might be used to assess what gene clusters (and what modeling framework) are best predictive of variation in typical or atypical brain function.

Supplementary Information:
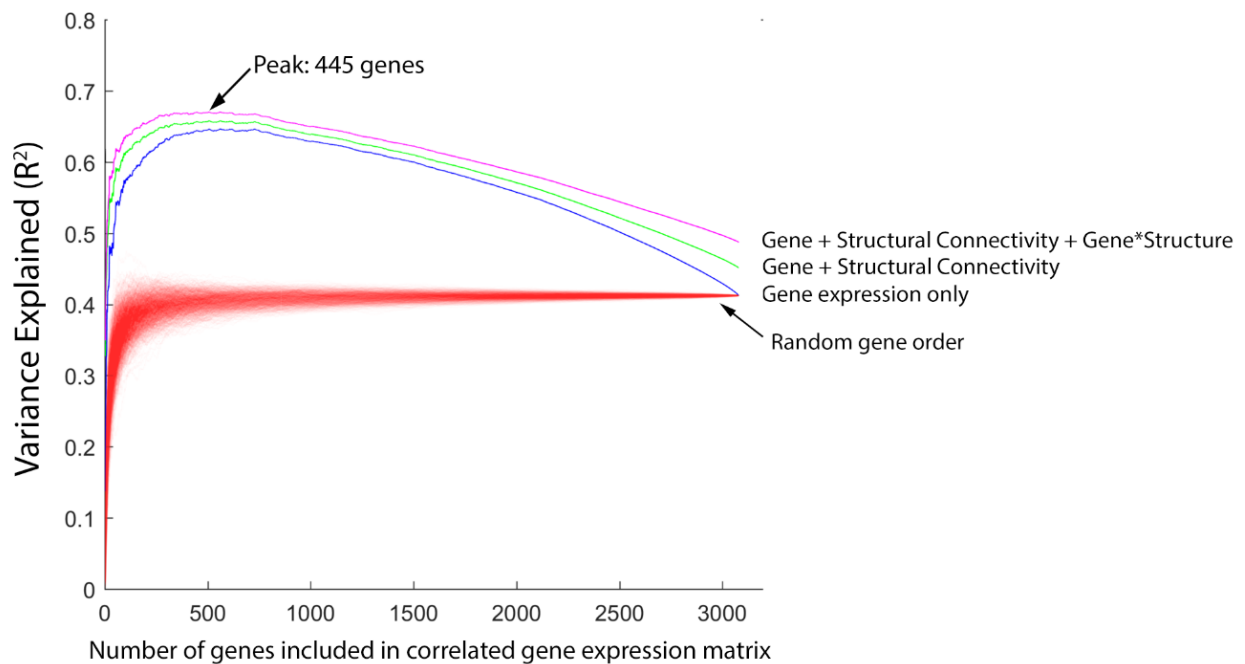
Figure S2.1. Genes that support CGE and FC, without distance correction. Incremental inclusion of genes into CGE matrix without distance correction during rank ordering of gene importance. A subset of genes support the relationship between CGE and functional connectivity. Genes were rank ordered (x-axis) based on their contribution to the CGE-FC correlation (after covarying Euclidian distance). Then, each model predicting FC was refit after incrementally adding each gene to the CGE matrix. The max variance was observed after the inclusion of 445 of the most explanatory genes to the CGE matrix, $r^2 = .702$). Each red line

indicates a different permutation for gene expression only, where gene rankings were
randomized on each permutation. 1000 permutations are shown.

ROI number	ROI name	ROI acroymn	Oh et al. 2014 Anatomical Division	Allen Anatomical Division
1	'Frontal pole, cerebral cortex'	'FRP'	'Isocortex'	Cerebral Cortex
2	'Primary motor area'	'MOp'	'Isocortex'	Cerebral Cortex
3	'Secondary motor area'	'MOs'	'Isocortex'	Cerebral Cortex
4	'Primary somatosensory area, nose'	'SSp-n'	'Isocortex'	Cerebral Cortex
5	'Primary somatosensory area, barrel field'	'SSp-bfd'	'Isocortex'	Cerebral Cortex
6	'Primary somatosensory area, lower limb'	'SSp-ll'	'Isocortex'	Cerebral Cortex
7	'Primary somatosensory area, mouth'	'SSp-m'	'Isocortex'	Cerebral Cortex
8	'Primary somatosensory area, upper limb'	'SSp-ul'	'Isocortex'	Cerebral Cortex
9	'Primary somatosensory area, trunk'	'SSp-tr'	'Isocortex'	Cerebral Cortex
10	'Supplemental somatosensory area'	'SSs'	'Isocortex'	Cerebral Cortex
11	'Infralimbic area'	'ILA'	'Isocortex'	Cerebral Cortex
12	'Gustatory areas'	'GU'	'Isocortex'	Cerebral Cortex
13	'Visceral area'	'VISC'	'Isocortex'	Cerebral Cortex
14	'Dorsal auditory area'	'AUDd'	'Isocortex'	Cerebral Cortex
15	'Primary auditory area'	'AUDp'	'Isocortex'	Cerebral Cortex
16	'Ventral auditory area'	'AUDv'	'Isocortex'	Cerebral Cortex
17	'Anterolateral visual area'	'VISal'	'Isocortex'	Cerebral Cortex
18	'Anteromedial visual area'	'VISam'	'Isocortex'	Cerebral Cortex
19	'Lateral visual area'	'VISl'	'Isocortex'	Cerebral Cortex
20	'Primary visual area'	'VISp'	'Isocortex'	Cerebral Cortex
21	'Posterolateral visual area'	'VISpl'	'Isocortex'	Cerebral Cortex
22	'posteromedial visual area'	'VISpm'	'Isocortex'	Cerebral Cortex
23	'Anterior cingulate area, dorsal part'	'ACAd'	'Isocortex'	Cerebral Cortex
24	'Anterior cingulate area, ventral part'	'ACAv'	'Isocortex'	Cerebral Cortex
25	'Prelimbic area'	'PL'	'Isocortex'	Cerebral Cortex
26	'Orbital area, lateral part'	'ORBl'	'Isocortex'	Cerebral Cortex
27	'Orbital area, medial part'	'ORBm'	'Isocortex'	Cerebral Cortex
28	'Orbital area, ventrolateral part'	'ORBvl'	'Isocortex'	Cerebral Cortex
29	'Agranular insular area, dorsal part'	'AId'	'Isocortex'	Cerebral Cortex
30	'Agranular insular area, posterior part'	'AIp'	'Isocortex'	Cerebral Cortex
31	'Agranular insular area, ventral part'	'AIv'	'Isocortex'	Cerebral Cortex
32	'Retrosplenial area, lateral agranular part'	RSPagl'	'Isocortex'	Cerebral Cortex
33	'Retrosplenial area, dorsal part'	'RSPd'	'Isocortex'	Cerebral Cortex
34	'Retrosplenial area, ventral part'	'RSPv'	'Isocortex'	Cerebral Cortex
35	'Posterior parietal association areas'	'PTLp'	'Isocortex'	Cerebral Cortex
36	'Temporal association areas'	'TEa'	'Isocortex'	Cerebral Cortex

37	'Perirhinal area'	'PERI'	'Isocortex'	Cerebral Cortex
38	'Ectorhinal area'	'ECT'	'Isocortex'	Cerebral Cortex
39	'Anterior olfactory nucleus'	'AON'	'Olfactory Areas'	Cerebral Cortex
40	'Taenia tecta'	'TT'	'Olfactory Areas'	Cerebral Cortex
41	'Piriform area'	'PIR'	'Olfactory Areas'	Cerebral Cortex
42	'Nucleus of the lateral olfactory tract'	'NLOT'	'Olfactory Areas'	Cerebral Cortex
43	'Cortical amygdalar area, anterior part'	'COAa'	'Olfactory Areas'	Cerebral Cortex
44	'Cortical amygdalar area, posterior part'	'COAp'	'Olfactory Areas'	Cerebral Cortex
45	'Field CA1'	'CA1'	'Hippocampal Formation'	Cerebral Cortex
46	'Field CA3'	'CA3'	'Hippocampal Formation'	Cerebral Cortex
47	'Dentate gyrus'	'DG'	'Hippocampal Formation'	Cerebral Cortex
48	'Entorhinal area, lateral part'	'ENTl'	'Hippocampal Formation'	Cerebral Cortex
49	'Entorhinal area, medial part, dorsal zone'	'ENTm'	'Hippocampal Formation'	Cerebral Cortex
50	'Parasubiculum'	'PAR'	'Hippocampal Formation'	Cerebral Cortex
51	'Postsubiculum'	'POST'	'Hippocampal Formation'	Cerebral Cortex
52	'Presubiculum'	'PRE'	'Hippocampal Formation'	Cerebral Cortex
53	'Subiculum, dorsal part'	'SUBd'	'Hippocampal Formation'	Cerebral Cortex
54	'Subiculum, ventral part'	'SUBv'	'Hippocampal Formation'	Cerebral Cortex
55	'Claustrum'	'CLA'	'Cortical Subplate'	Cerebral Cortex
56	'Endopiriform nucleus, dorsal part'	'EPd'	'Cortical Subplate'	Cerebral Cortex
57	'Endopiriform nucleus, ventral part'	'EPv'	'Cortical Subplate'	Cerebral Cortex
58	'Lateral amygdalar nucleus'	'LA'	'Cortical Subplate'	Cerebral Cortex
59	'Basolateral amygdalar nucleus'	'BLA'	'Cortical Subplate'	Cerebral Cortex
60	'Basomedial amygdalar nucleus'	'BMA'	'Cortical Subplate'	Cerebral Cortex
61	'Posterior amygdalar nucleus'	'PA'	'Cortical Subplate'	Cerebral Cortex
62	'Caudoputamen'	'CP'	'Striatum'	Cerebral nuclei
63	'Nucleus accumbens'	'ACB'	'Striatum'	Cerebral nuclei
64	'Fundus of striatum'	'FS'	'Striatum'	Cerebral nuclei
65	'Olfactory tubercle'	'OT'	'Striatum'	Cerebral nuclei
66	'Lateral septal nucleus, caudal (caudodorsal) part'	'LSc'	'Striatum'	Cerebral nuclei
67	'Lateral septal nucleus, rostral (rostroventral) part'	'LSr'	'Striatum'	Cerebral nuclei
68	'Lateral septal nucleus, ventral part'	'LSv'	'Striatum'	Cerebral nuclei
69	'Anterior amygdalar area'	'AAA'	'Striatum'	Cerebral nuclei
70	'Central amygdalar nucleus'	'CEA'	'Striatum'	Cerebral nuclei
71	'Intercalated amygdalar nucleus'	'IA'	'Striatum'	Cerebral nuclei
72	'Medial amygdalar nucleus'	'MEA'	'Striatum'	Cerebral nuclei
73	'Globus pallidus, external segment'	'GPe'	'Pallidum'	Cerebral nuclei
74	'Globus pallidus, internal segment'	'GPi'	'Pallidum'	Cerebral nuclei
75	'Substantia innominata'	'SI'	'Pallidum'	Cerebral nuclei
76	'Magnocellular nucleus'	'MA'	'Pallidum'	Cerebral nuclei
77	'Medial septal nucleus'	'MS'	'Pallidum'	Cerebral nuclei

78	'Diagonal band nucleus'	'NDB'	'Pallidum'	Cerebral nuclei
79	'Triangular nucleus of septum'	'TRS'	'Pallidum'	Cerebral nuclei
80	'Bed nuclei of the stria terminalis'	'BST'	'Pallidum'	Cerebral nuclei

Table S2.1. List of regions of interest, mouse connectome. These areas were obtained from the

atlas as provided by the Allen Mouse Brain Connectivity Atlas at the Allen Institute for Brain

Health (Oh et al., 2014). Regions are freely available online (Allen Brain Atlas Data Portal;

connectivity.brain-map.org).

Chapter 3: Project 2. Chronic gestational inflammation through interleukin-6 (IL-6) inflicts

persistent changes in behavior and functional connectivity network topology in rodent offspring

Introduction

The role of prenatal exposure to immune activation and prenatal inflammation has

increasingly been recognized as a critical influence on brain development. An expanding body of

epidemiological work has linked these exposures to the development of various disorders such as

ASD (Mitchell & Goldstein, 2014; Onore, Careaga, & Ashwood, 2012; Parker-Athill & Tan,

2011; Patterson, 2011). Further, prenatal exposure to maternal stress (Ronald, Pennell, &

Whitehouse, 2010) and prenatal exposure to a high fat diet (Kang, Kurti, Fair, & Fryer, 2014;

Sullivan, Nousen, & Chamlou, 2014) also result in a chronic inflammatory state that is thought to

mediate atypical neuronal development and increase risk for developmental disorders.

While other inflammatory cytokines undoubtedly play a role in CNS maturation,

interleukin-6 (IL-6) has been identified as a key cytokine mediating the link between immune

dysfunction, inflammation, and altered brain development (Estes & McAllister, 2016; Hunter &

Jones, 2015; Parker-Athill & Tan, 2011; S. Smith, Li, Garbett, Mirnics, & Patterson, 2007; Wei

et al., 2013; Wu et al., 2017). Elevations in IL-6 results in the activation of Th17 cells, which

increases downstream IL-17. This results in an inflammatory response (Estes & McAllister,

2016) and the activation of the hypothalamic-pituitary-adrenal (HPA) axis (Lenczowski et al.,

1999). IL-6 is readily capable of crossing the placental barrier, whereas other inflammatory

mediators such as IL-1β and TNF-α display only minimal transplacental transfer (Zaretsky,

Alexander, Byrd, & Bawdon, 2004). IL-6 affects early developmental processes including

regulating cell survival, proliferation, differentiation, and axonal guidance (Deverman &

Patterson, 2009; Nakanishi et al., 2007) making its regulated expression a key constituent in the brain building process.

Prenatal IL-6 exposure may also mediate risk for developmental disorders (Estes & McAllister, 2016; Onore et al., 2012; Wei et al., 2013). For example, mothers with elevated mid-gestational levels of inflammatory cytokines, such as IL-6, are more likely to have children with autism spectrum disorder (ASD) and ASD with comorbid intellectual disability (Jones et al., 2016; Wei et al., 2013). Numerous studies have shown ASD subjects have increased IL-6 in blood plasma (Ashwood et al., 2011a, 2011b; Emanuele et al., 2010; Wei et al., 2013) and brain tissue (Li et al., 2009; Onore et al., 2012), suggesting that maternal immune status can be transferred to the offspring.

Furthermore, translational research has shown that prenatal exposure to maternal immune activation (MIA) increases systemic IL-6 and results in offspring behavioral abnormalities often mirroring those of developmental disorders (Estes & McAllister, 2016), such as anxiety, social behavior, learning and memory deficits, and repetitive behaviors (Meyer, 2014; Schwartzer et al., 2013). Importantly, IL-6 has been identified as key mediator in many of these effects. The administration of recombinant IL-6 at particular periods of gestation is sufficient to induce the MIA phenotype (S. Smith et al., 2007; Wu et al., 2017), MIA challenged dams who are given the anti-IL-6 antibodies no longer show behavioral impairment (S. Smith et al., 2007), and MIA-induced behavioral impairments are prevented in placental IL-6 knockout mice (Wu et al., 2017). Taken together this suggests that a shift in the immune balance during pregnancy may lead to alterations in the neurodevelopment trajectory of affected offspring, and that IL-6 may be a key mediator in this process.

To date, the majority of research in this domain has either been focused on MIA models, which are non-specific to IL-6, or have focused on acute rather than chronic exposure to IL-6. It is important to consider the chronic inflammatory state because it is thought to mediate risk associated with chronic stress (Glaser and Kiecolt-Glaser 2005) and obesity (Monteiro & Azevedo, 2010). For these reasons the current work focuses on prenatal exposure to chronically elevated IL-6.

Although cellular abnormalities have been well-characterized in MIA models (Lin, Lin, & Wang, 2012; Lin & Wang, 2014; Meyer, 2014; Meyer, Nyffeler, Yee, Knuesel, & Feldon, 2008) and models of prenatal exposure to IL-6 specifically (S. Smith et al., 2007; Wu et al., 2017), non-invasive measurements are key to understanding how outcomes in animal studies relate to outcomes in humans. Resting state functional connectivity MRI (FC) is a powerful non-invasive *in vivo* imaging method, which measures temporal correlation of spontaneous blood oxygen level dependent (BOLD) signals among spatially distributed brain regions in the absence of an explicit task. FC is an ideal measurement for comparing physiology between humans and animal models because of its non-invasive and task-free nature and because of its wide use of characterizing brain network structure in developmental disorders.

The amygdala is a key limbic structure involved in mood regulation and anxiety. Amygdala structure and function are altered in patients with anxiety and depression (Etkin & Wager, 2007; Hamilton et al., 2012), and amygdala volume is increased in children of mothers with anxiety during pregnancy (Buss et al., 2012). Recently, studies have been relating prenatal stress to amygdala functional connectivity during infancy (Graham et al., 2015; Scheinost et al., 2016). More specifically, amygdala connectivity during infancy has been related to gestational IL-6 levels (Graham et al., 2017). Further, children with ASD show atypical patterns of FC and

abnormal amygdala growth trajectories (Nordahl et al., 2012; Shaw, Gogtay, & Rapoport, 2010; Uddin, Supekar, & Menon, 2010; Verhoeven et al., 2010). Together these studies point to a potential role for prenatal IL-6 in altering FC during infancy and highlight the amygdala as an important target for these FC impairments.

That being said, these prior studies in humans are correlational in nature and only in animal models can we test the direct effects resulting from manipulations to prenatal IL-6 levels, specifically, on offspring FC. Previously, animal models of MIA (which results in prenatal exposure to inflammation), have used non-invasive measures to show differences in ventricle size (Li et al., 2009), white and grey matter size (Short et al., 2010), and differences in white matter microstructure in frontal, striatal, and limbic regions (Li et al., 2010). One preclinical study of prenatal exposure to stress found differences in offspring FC in regions including the amygdala and caudate nucleus, and a right-lateralization of FC (Goelman, Ilinca, Zohar, & Weinstock, 2014). To our knowledge, no preclinical FC study has examined the effect of prenatal exposure to inflammation or IL-6 more specially. It is important to know how IL-6 induced FC changes relate to changes observed in humans exposed to IL-6, and to developmental disorders more generally.

The current study examines FC development and behavioral alterations in rats prenatally exposed to chronically elevated IL-6. Rat offspring were assessed during early (~PND 25) and late development (~PND 45). These ages represent periods of substantial developmental change, which correspond to a roughly 4 and 17 year old human (Semple, Blomgren, Gimlin, Ferriero, & Noble-Haeusslein, 2013). At each both early and late developmental waves, this longitudinal study examined anxiety-like, locomotor, and social behaviors as well as functional connectivity network organization. The amygdala was of particular interest due to its role in stress, anxiety,

and social behavior and due to its importance in psychiatric disorders (e.g., autism) linked to maternal inflammation during pregnancy (Meyer, Feldon, & Dammann, 2011; Nordahl et al., 2012). We hypothesized that prenatal IL-6 exposure would induce deficits in component behaviors associated with developmental disorders, cause changes in amygdala FC and its longitudinal development, and cause changes in the developmental trajectory of FC network organization across the brain.

Methods
Dam characteristics

Adult female and male Sprague-Dawley rats were obtained from Charles River Laboratory (males 350g, females 250g). Five dams were implanted with IL-6 infused osmotic mini pumps and six dams were implanted with 1% phosphate-buffered saline (PBS) infused mini-pumps. Due to practical constraints on behavioral and MRI scanning, one control and one IL-6 dam were bred in parallel.

Surgery, breeding, and weaning

Female dams were anesthetized with 3% isoflurane, then implanted with subcutaneous osmotic mini-pumps as detailed by the manufacturer (Alzet). All dams were given 5mg/kg meloxicam for pain post-surgery. Dams were allowed to recover from surgery for three days, after which they were paired with an adult male. Osmotic mini pumps (Alzet mini-pumps, model 2004, .28 ul/hr, 231.7ul, infusion duration 32.8 days) infused recombinant IL-6 (R&D systems, Recombinant Rat IL-6 protein, carrier free, Cat. No. 506-RL/CF) throughout the duration of breeding and gestation. Three dams were infused with 4.96 ug/kg IL-6 per day and two dams received 9.92 ug/kg IL-6 per day. These doses were chosen to be similar, across 24-hours, to previous research injecting IL-6 at various points in gestation (S. Smith et al., 2007). After 18

days male and female rats were separated and cages were checked daily for births. Saline and IL-6 rats were weaned 21 days after birth into same sex and condition cages, 2-3 animals per cage.

Offspring characteristics

All offspring were assessed for behavior at two ages. Once during early development, starting at PND 22 (wave 1), and again in late development, starting at PND 45 (wave 2). Offspring from each cohort were tested on the same day and test session if possible (i.e. when birth dates overlapped between groups within one day). Four of the 11 cohorts were behaviorally tested on the same day and the remaining cohorts were tested with a lag of 1-3 days between tests to match for age between groups.

Study design

As outlined in Figure 1, each set of behavioral assessments were followed by MRI scan acquisition. The behavioral tests started on PND 22 with the locomotor task, followed by the social behavior task, then the light-dark test for anxiety, with 1-2 days between tasks. After behavioral testing, the first MRI was administered, followed by an identical set of behavioral tests starting at PND 45, and a final MRI at PND 50. Groups were carefully matched on age at each behavioral and MRI assessment. Behavior and imaging dates were consistent with this timeline +/- 2 days. On locomotor and anxiety tests, roughly 45 offspring were included at each group and each developmental wave.

All rats were maintained on a 12-h light/dark cycle (lights on at 0600 h) at a room temperature of 21 °C ± 1 °C and allowed food and water *ad libitum*. All experiments were performed during the animal's light cycle.

This study was conducted in strict accordance with the National Institutes of Health Guide for the Care and Use of Laboratory Animals. The protocol was approved by the

Institutional Animal Use and Care Committee of the Oregon Health & Science University

(Protocol Number: 00319). All efforts were made to minimize the number of animals used and
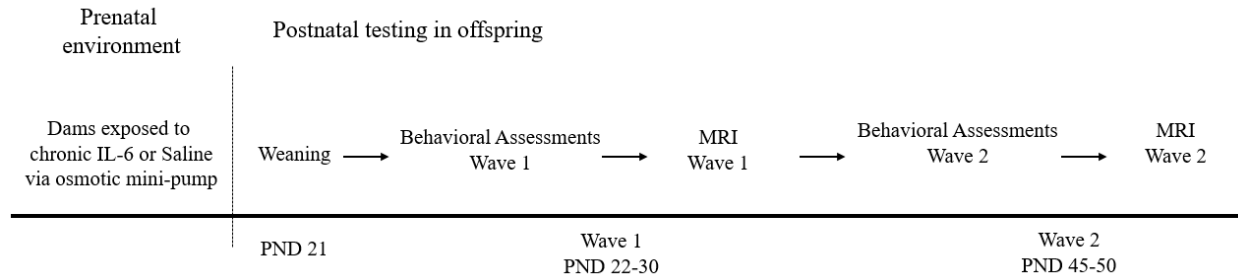
their suffering.

Figure 3.1. Study design. Dams were implanted with osmotic mini-pumps (32.8 day infusion

duration) before breeding. Offspring were prenatally exposed to PBS (control) or IL-6

throughout gestation, and were weaned at PND 21. Behavioral testing started one day after

weaning. Behavioral tests were performed over the course of the first week, with at least 24

hours between tasks, starting with locomotor behavior, the three choice social behavior task, and

followed by the light-dark box task for anxiety-like behavior. MRI scans were then performed on

a subset of animals. Beginning on PND 45 the same animals were then placed through the

identical set of behavioral experiments and MRI procedure.

Maternal IL-6 blood plasma

To confirm that IL-6 was elevated after osmotic mini-pump implantation, dams were

tested for systemic IL-6 blood plasma levels. One IL-6 and one saline dam was selected in order

to minimize stress on remaining dams. Blood serum was collected from the tail vein (while under

2% isoflurane) 6, 14, and 27 days after osmotic pump implantation, then transferred to vials

containing 0.5M ethylenediaminetetraacetic acid (EDTA). Blood was centrifuged at 8000 rpm

for 10 minutes and 200 uL of blood plasma was aliquoted and frozen at -80. Blood plasma from

each sample was analyzed with a Rat IL-6 Picokine enzyme-linked immunsorbent assay (ELISA) kit (catalogue no. EK0978; Wuhan Boster Biological Technology, Ltd., Wuhan, China, IL-6 sensitivity < 5pg/ml) according to the manufacture's protocol.

Behavioral Methods

Locomotor activity was measured in automated Accuscan activity monitors (40 cm^2; AccuScan Instruments, Inc., Columbus, OH, USA), with tests performed between 1600-1800h, during the light phase of the 12:12 h L:D cycle. Monitors were encased by sound-attenuating external chambers that were illuminated (3.3 W incandescent light bulb) and ventilated. Accuscan software translated patterns of photocell beam breaks for beams and sensors located 2 cm above the chamber floor into distance traveled in centimeters. Measurements were automatically generated by Acuvision. Total distance traveled (cm) was assessed. Duration spent in the center of the chamber was also calculated as an additional measure for anxiety, because anxious rodents generally display thigmotactic (wall-hugging) behavior (Bourin, 2015).

Our primary measure of anxiety-like behavior was assessed through the light-dark box test. This test is based on the innate aversion of rodents to the brightly illuminated and open areas (Bourin, 2015; Hascoët & Bourin, 2009). All tests were performed in the locomotor chambers allowing for automated measurements of time spent in each chamber. For this test, a custom built, infrared resistant, black opaque plastic box was used (15.75''x8''x8''). The box took up ½ of the chamber. The door to the dark box was 4'' wide and 2.5'' tall. For the experiment, after cleaning the chamber with 70% ethanol, the dark box was placed into the locomotor chamber. Next, the test rat was placed into the light side at which time the duration spent in the light and dark chambers was assessed. An increased duration of time spent in the light side of the chamber was interpreted as less anxiety-like behavior.

To measure sociability, the three choice social behavior task was employed with minor modifications (Moy et al., 2004). The apparatus consisted of a rectangular, custom built three-chambered box (30"x13.5"). This box was separated into three equal sized chambers separated by opaque black plexiglass, and a 4'' wide door allowing access to the social and non-social chambers. 24-hours prior to social behavior testing, all animals were separated from their cage mates and individually housed to increase sociability before testing. Social isolation prior to testing was performed because social isolation has been shown to increased motivated sociability in juvenile rodents (Ikemoto & Panksepp, 1992). Prior to each test, a subset of animals were selected as stimulus rats or test rats. First, the test mouse was placed in the middle chamber and allowed to explore for five minutes. After the habituation period, a rat of the same treatment group and sex was placed in one of the side chambers underneath a weighted circular cup with wire mesh (5"x4.2"). An identical empty circular cup was placed on the non-social side. The location of the stimulus rat (i.e., left vs. right side chamber) was alternated between trials. Next, both doors were unblocked allowing the test rat to explore either the social side (with the stimulus rat) and non-social chamber (empty cup). At the end of the 10 minutes, all animals were returned to their home cage.

All videos were recorded and a trained observer scored the amount of time spent in each chamber, defined as the test rat's head passing into one chamber or another, as well as time spent in direct proximity to the stimulus rat (either actively investigating or in immediate contact with the stimulus rat). Dependent measurements included the proportion of time spent in social proximity during the 10 minute test, the duration of time spent on the social side versus the total duration of the test, and the proportion of time spent on the social side vs. non-social side. Inter-

rater reliability was greater than 90% when results were compared between two trained observers scoring the same subjects.

MRI methods

This longitudinal study consisted of 86 MRI scans. W1, during early development, consisted of 41 MRIs (18 IL-6 and 23 control). W2, during late development, consisted of 45 scans (23 IL and 22 control). Across waves, there was a total of 41 IL-6 scans and 45 saline control scans. Of these scans 29 subjects retained quality MRI data between scan 1 and scan 2 (13 IL-6 and 16 controls). For the brain behavior analyses 78 scans had both imaging and behavioral data for a given wave. 38 IL-6 and 40 control scans had both MRI and behavioral data.

Animal Preparation

Imaging in rodents generally requires the use of anesthesia to limit movement of the animals in the scanner. Here, anesthesia was induced by 3% isoflurane and maintained with 1–1.5% isoflurane. The selection of anesthesia may influence FC (Grandjean et al., 2014). Of various anesthetic regimens, we selected low dose isoflurane for the present study based on the following previous findings: 1) Functional connectivity following 1% isoflurane is preserved and comparable to that of awake mice and rats (Jonckers et al., 2014; Mills et al., 2016; Shah et al., 2013; Stafford et al., 2014; K. Wang et al., 2011). 2) c-Fos activation (an immediate early gene) can be observed in isoflurane-anesthetized mice and rats (Kufahl et al., 2015, 2009; M. Smith et al., 2016). That being said, acclimated awake animals or other anesthesia regimens, such as a combination of dexmedetomidine and lower dose isoflurane (.5-.75%) (Ash et al., 2016; Brynildsen et al., 2017), may be an alternative for future studies.

During scanning, the head was kept stationary using a custom-built head holder equipped with ear bars (to limit motion) and designed with a nose cone for administration of isoflurane and for fitting the Bruker radiofrequency (RF) surface coil. Respiration (80–100 bpm) and animal temperature was monitored and controlled by a small animal monitoring system (Model 1030 Monitoring and Gating System; SA Instruments). Circulating warm air in the bore maintained animal temperature at 37 °C throughout the scan.

Imaging acquisition

The MRI was performed at 11.75 T (Bruker Corporation, Billerica MA, USA) using a system equipped with a Resonance Research, Inc. high-bandwidth shim power supply, at the Advanced Imaging Research Center. A Bruker volume coil was used for transmitting and a Bruker surface coil for receiving. All scans were performed with Paravision 5. Using MAPSHIM, a 3D Fieldmap phase image was acquired; TR = 20 ms, TE1 = 2 ms, inter echo time = 4.003 ms, FA= 20◦, FOV= 40 mm × 18 mm × 25 mm, matrix = 80 × 90 × 125 (voxel size of $0.5 \times 0.2 \times 0.2$ mm^3, matching the EPI voxel size). This was followed by a T2-weighted structural image (RARE, TR = 4590 ms, effective TE = 32 ms, RARE factor = 8, 50 contiguous slices (0.5 mm thick) with interleaved acquisition, FOV= 18 × 18 mm, matrix = 150 × 150, voxel size $0.12 \times 0.12 \times 0.5$ mm^3, 1 repetition). Global (volume) and local (brain voxel) shimming with MAPSHIM were performed to calculate first and second order shims prior to the functional MRI scan. The resting state fMRI consisted of a single shot gradient echo-planar imaging (EPI) sequence with the following parameters: two runs with 360 repetitions (total scan time = 30 min), TR = 2500 ms, TE = 10 ms, FA= 60◦, 50 contiguous slices (0.5 mm thick) with interleaved acquisition, FOV= 25.6 × 16 mm, matrix = 128 × 80, voxel size $0.2 \times 0.2 \times 0.5$ mm^3. An

identical EPI sequence with 20 repetitions was acquired in the reverse phase encoding direction

for topup distortion correction.

General fMRI BOLD preprocessing

Functional images were first processed to reduce artifacts. These steps include: (1)

removal of a central spike caused by MR signal offset; (2) correction of odd vs. even slice

intensity differences attributable to interleaved acquisition without gaps; (3) correction of field

inhomogeneities by applying topup field map correction. This required that data was collected

with reversed phase-encode blips, resulting in pairs of images with distortions going in opposite

directions. From these pairs the susceptibility-induced off-resonance field was estimated using a

method similar to that described in (Andersson et al., 2003) as implemented in FSL (S. M. Smith

et al., 2004) and the two images were combined into a single corrected one. (4) movement

correction; (5) within run intensity normalization to a whole brain mode value of 1000.

Processed functional data was registered to an anatomical atlas for each individual via the T2

scan. Each EPI run was then resampled in atlas space on an isotropic 0.2 mm grid combining

movement correction and atlas transformation in one interpolation (Lancaster et al., 1995).

Rs-fcMRI pre-processing

Additional preprocessing steps were used to reduce spurious variance unlikely to reflect

neuronal activity (e.g. heart rate and respiration). These steps included the regression of the

whole brain signal and the first order derivative of the whole brain signal, followed by a

temporal high and low band-pass filter (.008 Hz < f < 0.1 Hz).

Regions of interest (ROIs)

For ROI based analyses a rat MRI atlas developed for functional connectivity studies and

available in Analyze format (easily converted to NIfTI format) was used (Schwarz et al., 2006;

Schwarz, Gozzi, Reese, & Bifone, 2007). These ROIs correspond to brain areas are given in the

Paxinos&Watson space (Nie et al., 2013; Paxinos & Franklin, 2007). 38 bilateral ROIs were

used for these analyses (76 total). 10 regions were not used including those in white matter, or

those that were located on the extreme anterior (i.e. olfactory bulb, as opposed to olfactory

nuclei) or posterior sections of the brain (i.e. Pons). For network analyses, regions were manually

assigned an anatomical community corresponding to frontal, limbic, subcortical, motor,

olfactory, hippocampal, auditory/temporal, parietal, or visual cortex. A full list of ROIs used and

their network definitions can be seen in supplementary Table S3.1.

Connectivity matrices between these regions were constructed as follows. For each scan,

BOLD time series data was extracted post-processing for each ROI and pearsons correlations

were calculated for every region pair. Finally, ROI-ROI correlation, Fisher Z transformed r-

values were used for analysis.

Statistical Methods

Behavioral analyses

Due to the longitudinal nature of the data, linear mixed effects models were used, which

are able to model within subject, between subject variation, and is robust to missing data. These

models examined whether behavior was related to wave (early and late development), group (IL-

6 vs. control), and their interactions. Statistical models were fit using the fitlme function using

Matlab (version 16a). Post hoc analyses were performed where appropriate using t-tests. In order

to examine the prenatal dose of IL-6 influenced our results, linear mixed effects models

examined if adding the main effect of dose significantly increased the variance explained. Here,

the model including dose, was compared to the linear model without dose using the 'compare'

function in Matlab.

Functional connectivity analyses

For the main analyses, again, we used a linear mixed effects model to assess the

relationship between the connectivity between two regions, and their relationship to group status,

wave (i.e. scan was during early or late development), and their interactions (i.e. was the

connectivity differences larger for one wave than the other?). The following equation describes

this model:

$$\text{Connectivity} = \beta_0 + \beta_1 \, \text{Group} + \beta_2 \, \text{Wave} + \beta_3 \, \text{Group} * \text{Wave} + \varepsilon$$

This model was fit for each connection. When appropriate, models were compared to find

the best fit. For example, for the interaction term, the omnibus model shown above was

compared to a model including only the main effects of group and wave but no interaction.

Model fits for each connection were then compared using the 'compare' function in Matlab. For

significant models, post hoc analyses determined the direction of each t-scores for significant

parameter (e.g. IL-6 has decreased connectivity compared to controls).

Targeted and Network-wide analyses

The main analyses focused exclusively on connectivity differences from the left and right

amygdala. Amygdala connectivity significance was assessed at both a $p < .05$, uncorrected and

FDR corrected thresholds. Next, in an exploratory approach, we examined brain-wide network

connectivity patterns in regions which showed altered developmental trajectories. To assess these

network changes, a chi-squared ($\chi 2$) analyses was used to determined statistical significance of

each network or pairs of networks. This analyses essentially asks the following: "are group by

wave effects concentrated between particular networks more than expected by chance?" A benefit of this analyses is that this simplifies the interpretability of analyses, as we examine which "networks" rather than individual connections are most affected by each effect main effect or interaction of interest.

In brief, the χ2 approach (see Eggebrecht et al. 2017a for full details) compares the observed number of significant effects within a given network, with what would be expected if by chance if these effects were evenly distributed across network. The resulting statistic is large when there are more effects within a network than expected by chance. An empirical p-value are calculated by a permutation test, which is non-parametric and does not make assumptions about the population distribution (Backes et al., 2014; Eggebrecht et al., 2017). 10,000 permutations were performed, each time randomly shuffling the binary values (i.e. our statistic of interest) into other valid calls (in our case, into other cells which were not a significant negative group by wave coefficient). The reported p-values for each network reflect the observed chi-square statistic compared to the permuted chi-square statistics obtained from the given network-network pair. Significant networks for each category (p<.05) are reported in a bold red highlight around the network pair. Positive group by time coefficients were examined separately from negative group by time effects in order to examine whether trajectory differences (i.e. IL-6 has early decreased vs increased connectivity) were uniquely distributed across the brain.

Brain behavior analyses

For the brain behavior analyses, no missing data was included, that is, only scans who had both MRI data as well as behavioral data for the same wave were included. Linear mixed effects models controlled for within subject variation and fit the relationship between a given connection and behavioral performance on light dark anxiety behavior. Main analyses separately

fit each amygdala connection to anxiety behavior. Effects passing an FDR corrected p < .05 are

shown. Post hoc analyses tested whether network effects were related to behavior by averaging

each scans connectivity within a given networks significant effects and relating these measures

to behavior in one linear mixed effects model.

Results
Osmotic mini-pumps increase dams IL-6 blood plasma

As can be seen in figure 3.2, IL-6 is elevated in dams 6, 14, and 27 days after osmotic

mini-pump surgery. IL-6 levels appear to decrease with time but remain elevated throughout

gestation.
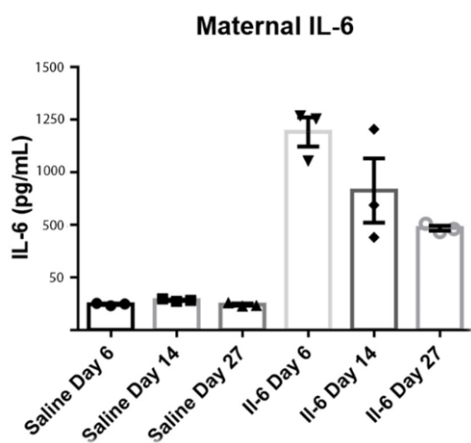
Figure 3.2. Osmotic minipumps increase maternal blood plasma levels of IL-6. Each bar represents maternal IL-6 blood plasma levels, 6, 14, and 27 days after pump implantation. Saline (control) dams do not show increases in IL-6 throughout pregnancy. However, IL-6 dams show elevated levels throughout pregnancy. These levels show some decrease with pregnancy duration. IL-6 levels were

quantified using ELISA.

Behavioral results

Linear mixed effects models tested whether each behavior changed as a function of group

status, wave (i.e., developmental wave), and their interaction, indicating that these behavioral

deficits were more prominent at one wave or the other.

On the light dark task, IL-6 animals spent significantly less time in the light (main effect,

$t(221) = -3.003$, $p = .003$) across both waves (group by wave interaction, $t(221) = 1.34$, $p = .181$).

Both groups spent more time in the light on wave 2 (W2) compared to wave 1 (W1) (main effect of wave, t(221) = 5.64, p < .0001). See figure 3.3A.

On the locomotor behavior task, IL-6 animals had significantly reduced time in the center at both W1 and W2 (main effect of group status (t(241) = -3.23, p =.001). Across groups, center time increased from W1 to W2 (main effect of wave, t(241) = 4.94, p < .0001), however the group effect was similar for both waves (no group by wave interaction p = .71). See figure 3B. Together, the light dark and center time measures indicates that IL-6 animals have persistent anxiety-like behavior in early and late development.

IL-6 animals had reduced total distance traveled compared to control animals (main effect of group, t(241) = -3.43, p = .0006), however, in this case, the effect was driven by a decrease in early development (W1), rather than the W2 (group by wave interaction, t(241) = 2.73, p = .006). Across groups, W1 animal traveled less distance compared to W2 (main effect of wave, t(241) = 3.93, p < .0001). See figure 3.3C.
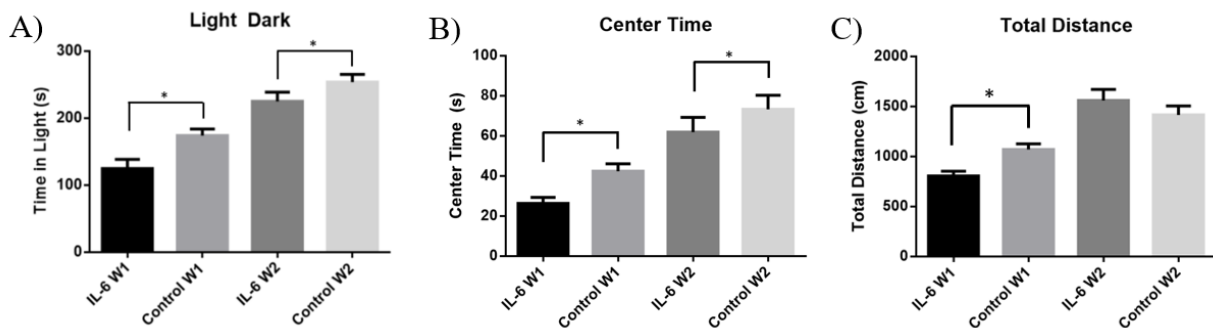

Figure 3.3. IL-6 exposure results in behavioral deficits reflecting increased anxiety. IL-6 animals spend less time in the light on the A) light dark box, B) less time in the center of during the locomotor behavior test, and C) travel less distance compared to control animals. The anxiety phenotype persists into late development as measured by A) the light dark test and B) center

time. Total distance was only impaired during early development. *p<.05. W1 = early developmental wave 1 (~PND 35), W2 = late developmental wave 2 (~PND 50). Roughly 45 offspring were used for each group at each wave.

There was a trend towards decreased social proximity in IL-6 animals during the early developmental wave (see supplementary figure 4, p = .067). Otherwise, across waves IL-6 animals performed similarly on the social behavior task to controls, both on social proximity measures as well as the proportion of time spent in the social side of the three choice chamber (all p > .05).

Dose, sex, and weight

In order to assess the effect of IL-6 dose on behavioral performance, a linear mixed effects model was run including the main effect of dose (low vs. high IL-6 dose). Anxiety-like behavior was not influenced by dose (center time (p = .74) and light dark (p = .36)). A trend was found where IL-6 subjects given a higher dose had increased locomotor distance traveled (p = .07).

Sex did not influence any of the behavioral findings (group, wave, or group by wave interactions, all p >.25). Only a trend towards a main effect of sex on center time (p = .09) was observed where females spent slightly longer in the center of the open field compared to males (males M = 49.73 seconds, females M = 50.31).

MRI results

Group and group differences in developmental trajectories

The first analyses examined differences in amygdala connectivity resulting from IL-6 exposure. We found that across developmental waves, two amygdala connections showed positive group effects, such that IL-6 animals had reduced amygdala FC (see figure 3.4D). These connections were from the left amygdala to the left caudate putamen (t = 2.87, p = .004) and ventral pallidum (t=2.23, p=.02) (see figure 3.4A).

Next, we asked whether the development of the amygdala was altered in IL-6 offspring. That is, were group differences a function of development (i.e., a group by wave interaction)? We found 9 connections indicating that IL-6 animals show under-connectivity of the amygdala during early development, but increased amygdala connectivity in late development (see figure 3.4B-D). This pattern from the amygdala spans a variety of regions including subcortical regions, and entorhinal, temporal, and cingulate cortex. The overlap between group and group by wave effects in the connection between the left amygdala and left caudate suggest that this group effects was driven in part driven by differences in this connections developmental trajectory. To illustrate these effects, figure 3.4D averages the right and left amygdala connectivity to each of their respective significant connections (figure 3.4B).
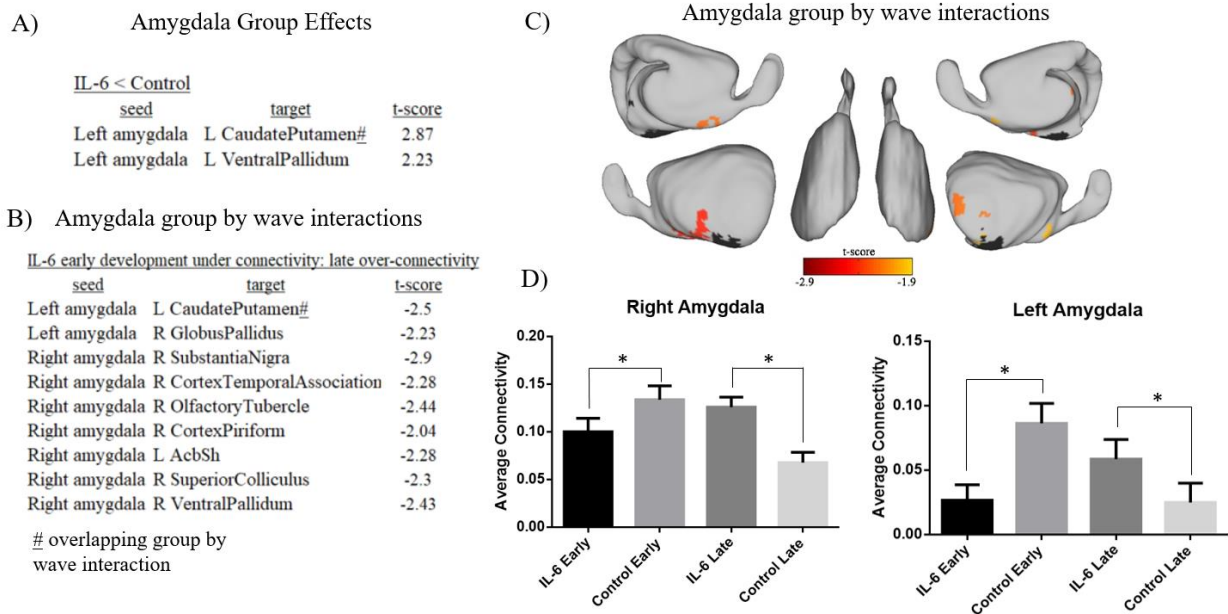
A) **Amygdala Group Effects**

IL-6 < Control

seed	target	t-score
Left amygdala	L CaudatePutamen#	2.87
Left amygdala	L VentralPallidum	2.23

B) Amygdala group by wave interactions

IL-6 early development under connectivity: late over-connectivity

seed	target	t-score
Left amygdala	L CaudatePutamen#	-2.5
Left amygdala	R GlobusPallidus	-2.23
Right amygdala	R SubstantiaNigra	-2.9
Right amygdala	R CortexTemporalAssociation	-2.28
Right amygdala	R OlfactoryTubercle	-2.44
Right amygdala	R CortexPiriform	-2.04
Right amygdala	L AcbSh	-2.28
Right amygdala	R SuperiorColliculus	-2.3
Right amygdala	R VentralPallidum	-2.43

overlapping group by wave interaction

C) Amygdala group by wave interactions

D) Right Amygdala / Left Amygdala

Figure 3.4. Amygdala connectivity changes as a function of developmental wave. A) Subtle

effects on amygdala connectivity were found across age, however, the majority of the effects

were explained by B-D) group by wave (i.e. age) interactions on connectivity. B) Regions which

show significant developmental change in the amygdala. # indicates connections with both group

by wave and group effects. C) Developmentally changing connections from the amygdala

(black) are visualized. The amygdala is broadly under-connected during early development

(PND 35), but over-connected in late development (PND 55). D) Bar graphs depict the average

connectivity between all significant amygdala connections at each developmental stage.

Four connections showed the opposite group coefficients indicating higher R values

compared to controls at W1 (see supplementary figure S3.1). Three of these connections were

driven by differences in developmental trajectories (i.e. these connections show both group and

group by wave effects), where IL-6 had higher R values at developmental W1 but lower R values

at W2 (figure 3.S2). These connections included those from the amygdala to parietal, visual, and

motor cortex. Post hoc analyses showed that these effects were driven by negative correlations. In these cases, IL-6 offspring show an increase in negative, as opposed to positive correlations compared to controls. At the first developmental wave IL-6 animals show decreased negative correlation and an increased negative correlation at W2 (see figure S3.1). See supplementary material for additional post hoc analyses and full detail on these effects.

Relationships between connectivity and anxiety-like behavior

Given the robust anxiety-like phenotype we observed, we next examined whether FC from the amygdala was related to anxiety as measured by the light dark box. Fifteen connections related to increased amygdala connectivity and increased anxiety behavior (see Figure 3.5b). For example, increased connectivity from the right amygdala to right dorsolateral thalamus (t = -7.15), right caudate putamen (t = -6.69), right posterodorsal hippocampus (t = -6.23), as well as the left amygdala to left (t = -4.8) and right (t = -4.5) retrosplenial and right cingulate cortex (t = -4.45) were all related to increased anxiety behavior. Of the 18 significant connections, 3 related to anxiety in the opposite direction, where decreased amygdala connectivity related to increased anxiety. These connections included the right amygdala to the left motor (t = 5.24) and somatosensory cortices (t = 4.98). Three of these effects overlap with group by wave effects, including connections to the temporal association cortex, ventral pallidum, and motor cortex. These overlapping effects are indicated by a # in figure 3.5.
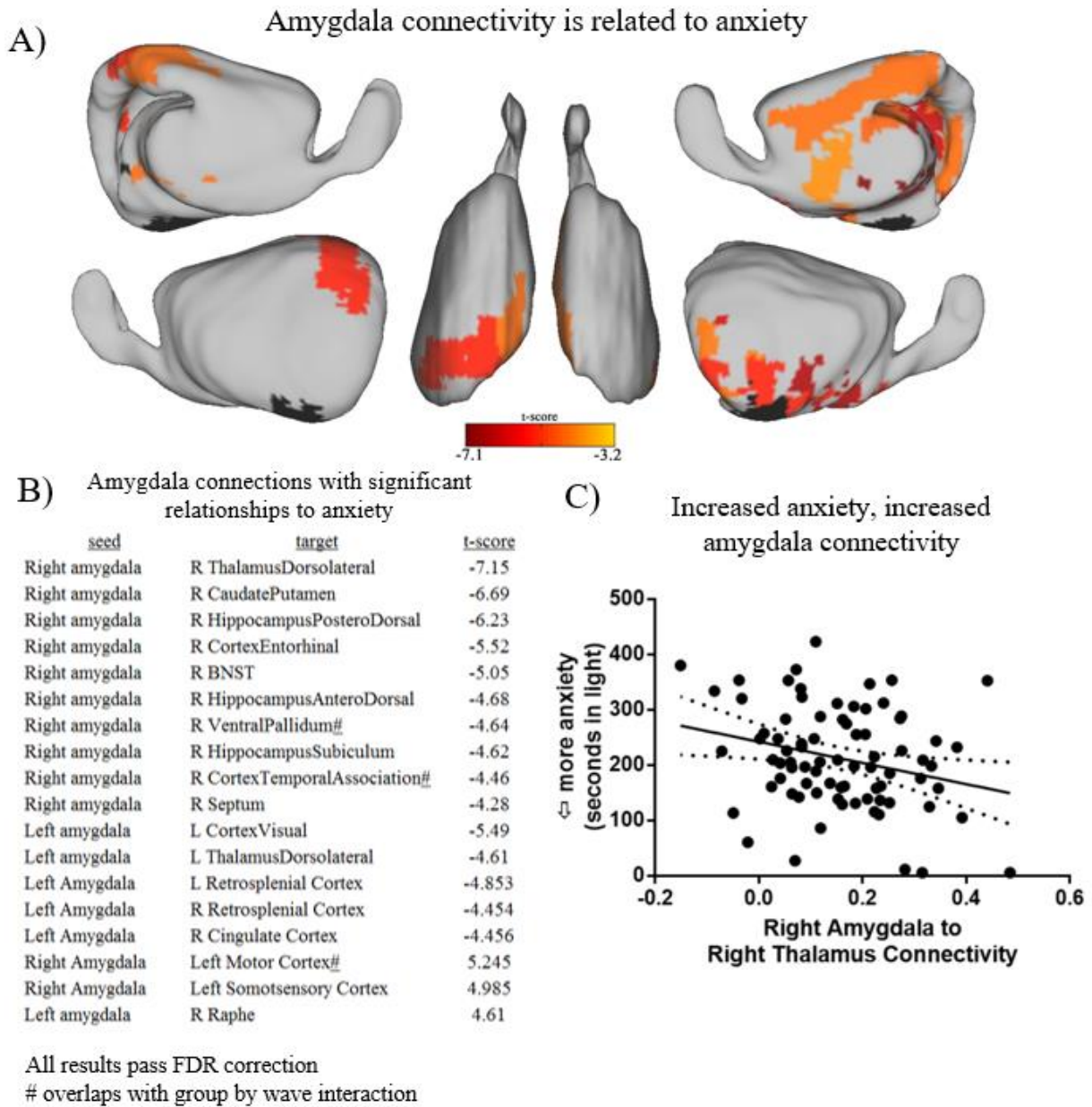
Figure 3.5. Anxiety is related to amygdala connectivity. Depicted are amygdala connections that are related to anxiety behavior. In the majority of connections, more anxiety (less time in the light during the light dark box test) is related to greater amygdala connectivity. A) Regions from the amygdala (black) showing this relationship. B) A table of all amygdala connections with a significant relationship between amygdala connectivity and anxiety behavior on the light dark task. These behavioral relationships are partially overlapping with the connections showing IL-6

related developmental change indicated by the #. Across the brain, three connections from the amygdala show the opposite effect, where increased connectivity relates to decreased anxiety. All connections shown are p < .05 (FDR corrected). C) The scatter plot highlights an example where increased connectivity between the right amygdala and right thalamus relates to greater anxiety behavior (i.e., more time spent in the dark).

Network level FC change

Next, we examined whether the observed alterations in developmental trajectories were specific to the amygdala or were also altered between large scale brain networks. For this analysis we examined the distribution of connections which showed differential developmental trajectories between groups (i.e., group by wave interactions). A chi-squared statistic was computed to examine the distribution of these effects clustered in particular networks more than expected by chance. In this way, we can observe if the pattern observed in the amygdala was also found at the network level across the brain. Figure 3.6 shows each connection with a significant group by wave interaction (negative group by wave coefficients). Each cell indicates connections that show the same pattern to that of the amygdala, that is, IL-6 offspring are under-connected early and over-connected late in development. Networks outlined by red boxes highlight significant networks which have more effects within them than expected by chance (χ^2 statistic, p < .05). On a network level, connections within subcortical regions (Figure 3.6B, χ^2, p = .0084), and connections within the parietal to frontal network (Figure 3.6C, χ^2, p = .02), had a higher proportion of group by wave effects. No other network showed significant group differences in this developmental trajectory. Note the individual amygdala connections showing this pattern, highlighted in Figure 4B. Figure 6D illustrates the group by wave effect by averaging significant subcortical connections for each group at each wave. On the network level, average connectivity

80

within significantly changing subcortical or frontal to parietal network connections were not related to anxiety behavior (p > .4).
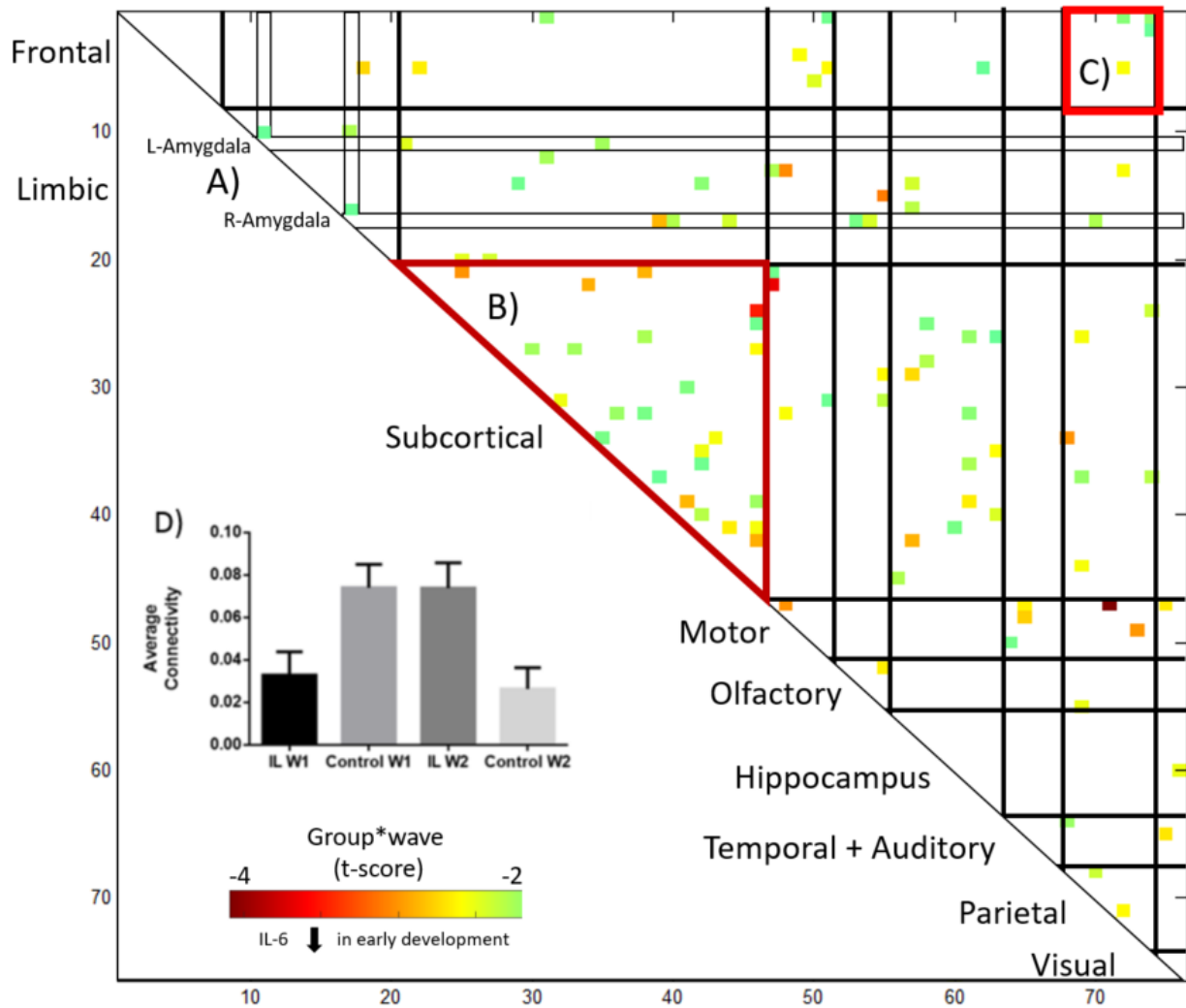
Figure 3.6. Whole brain network analyses implicate the subcortical network as the most developmentally altered network after IL-6 exposure. The region by region matrix shows connections with significant group by wave interactions (negative coefficients corresponding to positive connections). Each cell indicates a group by wave interaction where IL-6 connectivity is decreased early and increased late in development (p < .05). Typically with age, A) connections from the amygdala, B) and the subcortical network (p = .0084), tend to decrease in connectivity

from early to late development in control animals. This trajectory is reversed in IL-6 exposed offspring. C) The parietal to frontal network cortex also shows subtle group differences across development (p = .02). D) The observed differences in this developmental trajectory is illustrated by averaging FC within significantly changing subcortical connections. To identify the individual connections shown above refer to the full ROI list and their network assignments in table S1.

Chi-squared effects within positive group by wave coefficients (related to differences in negative correlations, see supplementary figure 3.2) were also examined. Here we find different developmental trajectories primarily in networks related to sensory processing and sensory integration. These networks include subcortical to visual, as well as motor to olfactory and hippocampal, and parietal to hippocampal networks (p < .05). These effects can be seen in supplementary figure 3.3. These effects mirror the main developmental trajectory findings, only now in terms of negative correlations. For instance, typically negative correlations decreased with age. IL-6 offspring show the opposite developmental pattern. That is, reduced negative correlations early in development but elevated negative correlations late in development. See supplementary figure 3 for full detail. On a network level, average connectivity within significantly changing subcortical to visual connections was related to anxiety, increased anxiety was related to more negative connectivity (p = .01, see supplementary figure S3.5). No other networks showed a relationship between connectivity and anxiety.

Discussion

This study found that prenatal exposure to chronically elevated IL-6 results in persistent behavioral abnormalities throughout development, primarily in anxiety-like behavior. IL-6 offspring show more subtle effects on locomotor and sociability tasks during early development.

FC analyses found that amygdala development was most prominently characterized by a pattern of under-connectivity then over-connectivity compared to controls during late development. Amygdala FC was related to anxiety, where increased anxiety was correlated with increased amygdala connectivity. On a network level, subcortical and parietal to frontal networks showed a similar pattern to the amygdala, but these findings were unrelated to anxiety. Interesting findings were also observed for connections that were primarily negative in nature. However, because of some of the controversy regarding these types of links (Murphy, Birn, Handwerker, Jones, & Bandettini, 2009; Murphy & Fox, 2017), we'll focus on the positive correlations here with a short discussion on negative correlations in the supplementary material.

Maternal prenatal IL-6 exposure causes a persistent anxiety-like phenotype in offspring throughout development

Anxiety is a prominent behavioral phenotype in IL-6 associated psychiatric disorders such as autism (Chalfant, Rapee, & Carroll, 2007; Lang, Regester, Lauderdale, Ashbaugh, & Haring, 2010; White, Oswald, Ollendick, & Scahill, 2009). Anxiety is also associated with prenatal exposure to stress (Davis, Glynn, Waffarn, & Sandman, 2011; Glover, 2011; Talge, Neal, & Glover, 2007) and high fat diet (Sasaki, de Vega, St-Cyr, Pan, & McGowan, 2013; Sullivan et al., 2010, 2014). Both maternal Poly-IC and LPS inflammation models have observed these anxiety-like phenotypes (Depino, 2015; Gibney, McGuinness, Prendergast, Harkin, & Connor, 2013; Le Belle et al., 2014; Meyer, 2014; Meyer & Feldon, 2012). These studies also generally find decreased sociability and less distance traveled in an open field, although results are mixed (Le Belle et al., 2014; Malkova, Yu, Hsiao, Moore, & Patterson, 2012; Samuelsson, Jennische, Hansson, & Holmäng, 2006; Schwartzer et al., 2013). To the best of our knowledge, the few studies examining the effects of prenatal IL-6 specifically have not investigated these

anxiety-like behaviors. These IL-6 induced anxiety behaviors persist throughout development; however, until now, our understanding of how they relate to anxiety related circuits using in-vivo MR imaging is largely unknown.

Maternal prenatal IL-6 exposure IL-6 exposure leads to altered amygdala connectivity in offspring, which relates to anxiety-like behavior

The amygdala is a key limbic structure involved in mood regulation and anxiety. It is associated with anxiety and depression (Etkin & Wager, 2007), is implicated autism (Haznedar et al., 2000; Stanfield et al., 2008), and its FC has been shown to be altered in infants exposed to prenatal stress (Scheinost et al., 2016), as well as prenatal IL-6 exposure more specifically (Graham et al., 2017). The amygdala may also play an important role in the central integration of afferent signals from the peripheral immune system (Engler et al., 2011). For example, low dose LPS administered to humans results in enhanced amygdala responses to threatening faces (Inagaki, Muscatell, Irwin, Cole, & Eisenberger, 2012). Further, a translational study showed that LPS induced inflammation results in a significant increase in neuronal activity within the amygdala and a substantial rise in extracellular noradrenaline levels. Importantly this study also found that amygdala activity related to an increase in anxiety-like behavior (Engler et al., 2011). According to Nusslock and colleagues, from an evolutionary perspective increased signaling, such as this, from the amygdala could be adaptive in some sense. When stimuli are perceived as threatening, cell groups in the amygdala signal hypothalamic centers that subsequently mobilize fight-or-flight responses mediated by the HPA axis. Cortico-amygdala signalling could also work to enable peripheral leukocytes to send warning signals to the brain, enhancing threat-vigilance (Nusslock & Miller, 2016). Such signaling might be maladaptive in today's environment.

Our findings are generally consistent within this framework. We find that amygdala connectivity relates to increased anxiety-like behavior. This work points to the amygdala as a critical locus for IL-6 related brain change, and suggests that its FC plays a role in mediating anxiety-like behaviors. Numerous connections from the amygdala may play a role in mediating these behaviors. Many connections we identified have also been implicated in previous work. For instance, the anterior cingulate has rich anatomical connections to amygdala (Carmichael & Price, 1995; Palomero-Gallagher, Mohlberg, Zilles, & Vogt, 2008; Palomero-Gallagher, Vogt, Schleicher, Mayberg, & Zilles, 2009), these regions are implicated in generalized anxiety disorder (Etkin, Prater, Schatzberg, Menon, & Greicius, 2009; Etkin & Wager, 2007; Tromp et al., 2012), and are thought to play a central role in emotion processing (Etkin, Egner, Peraza, Kandel, & Hirsch, 2006). FC from other amygdala connections were also related to anxiety including thalamic connections, which have been shown to mediate anxiety (Abrahamson & Moore, 2001; Shekhar, 1993; Shekhar, Hingtgen, & DiMicco, 1990). Interestingly, preclinical FC studies have also suggested that the posterior hypothalamic area, whose connectivity to the amygdala related to anxiety like behavior here, is a key hub mediating anxiety (Upadhyay et al., 2011). Furthermore, we identified connections to the nucleus accumbens, a region with integrated with the limbic system and known to be involved in emotion and anxiety regulation (Floresco, 2015). The hippocampus was also implicated here. This is in-line with previous work showing the distinct role of the hippocampus in untrained anxiety, independent of its roles in learning and memory (Engin & Treit, 2007). It should be noted that FC is not always monosynaptic (Randy L. Buckner, Krienen, & Yeo, 2013) and alterations to the amygdala can result in widespread changes to network structure across the brain, including to regions without direct anatomical projections (Grayson et al., 2016). Overall, our work suggests that increased

FC from the amygdala to a variety of regions, both those directly and indirectly connected to the amygdala, and many of which are involved in anxiety, is associated with increased anxiety-like behavior in rodents.

IL-6 exposure leads to altered developmental trajectories of the amygdala and subcortical network

Numerous studies have shown that FC changes throughout development, and that these maturation patterns are important for proper health and cognitive function in health and disease (Nordahl et al., 2012; Szatmari et al., 2015; Uddin et al., 2010). Therefore, developmental reorganization of FC is a crucial variable to consider when examining group differences in connectivity. Accordingly, we found that patterns of connectivity from the amygdala and within the subcortical network were developmentally sensitive. In our work, typical patterns within these regions were characterized by a decrease in FC with development.

Although the developmental trajectories at these ages are still incompletely understood, the decrease in connectivity of the amygdala and subcortical network with age in our control group was not unexpected. Previously it has been shown that, in humans, the amygdala decreases in connectivity with age. Although not all connections show this developmental decrease, this pattern is seen between many amygdala connections including those to temporal, insular, parahippocampal, and posterior cingulate regions (Gabard-Durnam et al., 2014). Indeed, this observed pattern also overlaps within findings from the human literature, in which subcortical connectivity is greater in children than adults. Supekar and colleagues interpreted these findings as a shift from diffuse to more focal brain activity. They suggest these FC findings could reflect a dynamic process of over-connectivity followed by pruning, which rewires connectivity at the

neuronal level, and is reflected at the systems level to reconfigure and rebalance subcortical and paralimbic connectivity in the developing brain (K Supekar, Musen, & Menon, 2009).

In our work, this developmental trajectory was reversed in IL-6, who showed early under-connectivity and a late over connectivity compared to controls. Atypical brain developmental trajectories is a common theme in autism (Courchesne, 2002). FC studies have shown that children with ASD often have increased or decreased connectivity depending on their age (Maximo, Cadena, & Kana, 2014; Uddin, Supekar, & Menon, 2013), and structural imaging studies have shown that in ASD, amygdala growth trajectories are disrupted or accelerated (Nordahl et al., 2012). Such work has suggested that cognitive developmental delay/or deficit is related to altered brain development and disrupted functional specialization and integration between brain circuits. That being said, our understanding of atypical age trajectories in developmental disorders is still incomplete. Through the use of non-invasive longitudinal imaging in preclinical animal models, we can further our understanding of how a disruption of typical connectivity trajectories may influence later developmental outcomes and atypical behavior resulting from prenatal insults. It will be important in future work to extend the developmental period longer in our animal model to determine if these overall trends reverse or are maintained over time.

Of note was that the majority of the connections from the amygdala that were altered in our study, including to the caudate/putamen, globus pallidus, thalamus, and temporal cortex, have been shown to have positive FC to the amygdala in healthy human subjects (Roy et al., 2009). This suggests that most of the amygdala connections that are impacted in IL-6 are those that are likely to be most important for amygdala FC development in humans.

Relationships to translational and human studies

The use of animal models offers the ability to understand the developmental dynamics of connectivity change in a controlled environment. However, translational studies of this nature represent a critical gap in the field. To our knowledge this is the first assessment of longitudinal developmental changes in resting state functional connectivity in rodents, and is the first FC study done on the effects of prenatal exposure to inflammatory cytokines in rodents. Therefore, we are in uncharted territory regarding how rodent connectivity changes through early and late development, and how these trajectories are impacted resulting from prenatal exposure to inflammation.

That being said, one preclinical DTI study examined white matter microstructural changes resulting from prenatal exposure to inflammation, through poly-IC. They found white matter microstructural alterations to areas including the amygdala, piriform, hippocampus, and striatum (Li et al., 2010); regions that were also implicated in the current report. One preclinical study of prenatal exposure to stress found differences in offspring FC of regions including the right amygdala, caudate, and infralimbic cortex, and found that prenatal stress disturbed FC symmetry, resulting in increased right hemisphere FC (Goelman et al., 2014). Interestingly, we similarly found more differences in FC from the right compared to left amygdala, lending converging evidence for the role of asymmetries in FC resulting from prenatal exposure to inflammation. These asymmetries should be examined further in future reports.

Comparing our results to the human literature is somewhat more complicated and offer both consistencies and inconsistencies. For instance, a recent study examined the effect of prenatal IL-6 levels on FC in infants roughly 4 weeks of age. They found that increased IL-6 correlated with greater amygdala connectivity (Graham et al., 2017). We found that the amygdala was over-connected, but only nearing late development. These inconsistencies may be

partially due to difference between the ages at which each study examined amygdala connectivity. Our first MRI occurs at approximately 35 days of age, which corresponds to about a 2.5 year old human (Semple et al., 2013). In contrast, Graham et al. examined amygdala connectivity in four week old infants. These differences in age could potentially explain the inconsistency regarding the direction of these amygdala findings between studies. Of course, differences between these studies can also likely be attributed, to a large degree, simply to the sizeable differences in human and rodent brain development in general.

With that said, our findings are generally consistent with recent studies examining infants who were prenatally exposed to stress. These studies scanned infants at 42 weeks of age, closer to our early developmental wave compared to Graham et al. Prenatal stress was associated with decreased amygdala connectivity with the thalamus, hypothalamus, and peristriatal cortex during early development (Scheinost et al., 2016).

Given that prenatal IL-6 is a risk factor for autism (Mitchell & Goldstein, 2014; Wei et al., 2013), there is reason to compare our findings with those seen in the ASD literature. Although the neurobiology of ASD is complex and no single neurobiological phenotype characterizes all children (Feczko et al., 2017; Ring, Woodbury-Smith, Watson, Wheelwright, & Baron-Cohen, 2008; Toal et al., 2010), a prominent theme is that ASD is characterized by an altered trajectory of brain development. Both cross sectional (Schumann, 2004) and longitudinal studies have identified increased rates of amygdala growth in children with ASD (Nordahl et al., 2012). These altered trajectories emerge between 2 and 4 years, roughly approximating the early developmental time in our current work.

In regards to FC measurements in ASD, amygdala FC connectivity has been assessed during very early development, at 3.5 years of age (Shen et al., 2016). Consistent with what is

observed in our study, the amygdala is under-connected at this age. In older children with ASD, a more consistent age to W2, the direction of findings are mixed. Some studies find mostly decreased amygdala FC (Guo et al., 2016; Rausch et al., 2016) and others finding increased amygdala connectivity (Nomi & Uddin, 2015), the latter being consistent with our report during late development. Overall, the trajectory of amygdala structure and FC is a dynamic process, which appears to be altered in ASD and IL-6 exposed rodents.

ASD is a heterogeneous disorder and not all presentations of ASD are likely to share mechanisms mediated by inflammatory factors. Clearly, more research will be needed to examine the degree to which inflammation mediates FC presentations in ASD and how these phenotypes compare to translational animal models of the disease.

Early Brain and Amygdala Development

IL-6 in dams was heightened for ~28 days, a period corresponding to heightened exposure during gestation and presumably into the first week of pregnancy because IL-6 can also be transferred postnatally through mothers milk (Garofalo, 2010). Brain development in the rodent, although beginning in the gestational environment does not reach comparable stages to a human term infant until about roughly PND 7. That being said, the amygdala may be particularly sensitive to even earlier insults. In the context of developmental programming the amygdala develops at an early embryonic stage compared to other structures (Buss et al., 2012; Fareri & Tottenham, 2016; Scheinost et al., 2016). Further, the amygdala is also believed to be particularly sensitive during development to elevated levels of glucocorticoids (Teicher et al., 2003), and HPA axis dysfunction (Herman, Ostrander, Mueller, & Figueiredo, 2005). Previous research has also implicated stress during the early intrauterine periods of gestation as being particularly detrimental to the amygdala. This is in part because its rapid developmental change

during this period leaves it particularly vulnerable to disorganizing influences like prenatal stress (Gluckman & Hanson, 2004; Scheinost et al., 2016). Our work further supports these arguments and highlights IL-6 exposure as a disorganizing influences on amygdala development.

Blood Plasma Levels

Blood plasma elevations observed in IL-6 dams were roughly 4-8x higher than control dams, depending on the time blood was taken. The literature is still incomplete in regards to the precise quantification of IL-6 levels in health and disease. However, there is some evidence that is useful to compare. Under normal conditions IL-6 is in relatively low abundance (Ferrucci et al., 1999). However, stress has been shown to result increases of about four times the IL-6 compared to blood plasma from non-stressed controls (Kiecolt-Glaser et al., 2003). That being said, even more subtle increases in IL-6, about 1.5x normal levels may be detrimental to long term health outcomes (Ferrucci et al., 1999). The experimental treatments described in the current work could be considered of moderate severity. Subtle increases in IL-6 are more representative to conditions like stress, in contrast, more extreme increases in IL-6 can result from direct administration of LPS (a common MIA model). LPS can cause peaks in IL-6 many thousand times greater than what are observed in the current report (Kemna, Pickkers, Nemeth, Van Der Hoeven, & Swinkels, 2005). Overall, methodological differences should be considered when comparing absolute levels of these low abundance and difficult to measure cytokines (i.e. ELISA sensitivity, mesoscale detection methods, etc.). Future work should be done to determine how both pro and anti-inflammatory cytokine expression is altered in both dams and offspring exposed to prenatal manipulations to IL-6.

Considerations and limitations

One limitation of preclinical studies is that they often require the use of anesthesia. Complicating findings regarding the typical developmental trajectory of FC is that the effect of repeated exposures to isoflurane on FC is incompletely understood. However, group differences in developmental trajectories are unlikely to be mediated by interactions between IL-6 exposure and repeated anesthesia. Future research could assess connectivity change across development using cross sectional studies, in which all animals are only given a single dose of anesthesia.

Another limitation of our study is that there were a subset of effects that we were underpowered to examine. For instance, we did not find differences in anxiety behavior between offspring exposed to low and high doses of IL-6. However, only two dams received the higher dose. The current work may have been underpowered to detect these effects. More targeted studies across more dams should be done to examine dose effects on subsequent behavior and imaging markers.

Furthermore, although anxiety is highlighted as the most prominent behavioral effect, we also identified a trend towards decreased social behavior in IL-6 exposed offspring. First, the number of behavioral tests conducted was limited in this study and more behaviors that were not examined might be altered by the maternal exposure. Second, while we know that social behavior decreases are also often reported in MIA models, in the current report technical difficulties during some social behavior tests resulted in fewer animals being assessed on this test. This may have resulted in an underpowered sample to adequately assess social behavior change. Relationships between social behaviors and connectivity could also be explored in future work with a larger sample.

Future directions

The current work represents one of the first steps in understanding the relationships between prenatal cytokine exposure and FC development, but much remains to be done. For instance, the current work examined maternal, but not offspring cytokine levels. Although likely that the mother's immune status is transferred to the offspring (Hsiao & Patterson, 2011; Patterson, 2011), it is possible that not all offspring show immune dysfunction resulting from these exposures. A few initial studies have begun to link FC directly to inflammatory states (Felger et al., 2016), and to IL-6 levels specifically (Creswell et al., 2016). Future work should investigate whether offspring cytokine levels are directly related to these FC patterns, and whether developmental change in FC tracks with changes in either plasma cytokine levels or cytokine expression in the brain. Furthermore, there is some evidence suggesting that the timing of prenatal immune insults result in variable behavioral and brain changes (Meyer et al., 2008). These complications were avoided in the current work by inducing a chronic increase in IL-6 throughout gestation. Developmental timing of these effects are critical and more research should be done to examine the timing of IL-6 exposure and resulting changes in FC through development. Furthermore, the current work examined offspring until postnatal day 55. However, developmental disorders such as autism can affect an individual across the lifespan. It remains to be tested whether IL-6 exposure causes persistent changes in FC and behavior into adulthood.

Several studies have examined histological changes resulting from prenatal exposure to MIA and IL-6 (Estes & McAllister, 2016; S. Smith et al., 2007), however, although important, it is often unclear how histological changes relate to, or are representative of changes observed in humans. One avenue for future research will be to examine how changes at this level relate to FC. With FC, new targets for subsequent histological analyses, experimental manipulation, and

further probing of causal mechanisms can be identified. For example, it has recently been shown that targeted manipulation of the amygdala using DREADDs (Urban & Roth, 2014) results in reorganization of FC networks across the brain (Grayson et al., 2016). By manipulating affected circuits (e.g. manipulating amygdala activity at given developmental windows), future research could attempt to reproduce large-scale FC profiles and behavioral phenotypes seen in IL-6, or could potentially move to reverse these phenotypes in IL-6 exposed offspring. Similarly, through these types of studies, preclinical FC could also have utility for longitudinally tracking the effects of pharmacological interventions on brain network organization in a way that could be comparable to human disease (Miranda-Domínguez et al., 2014; Stafford et al., 2014).

Supplementary Materials
Negative correlations

This work primarily focused on connectivity differences representing group and group by wave coefficients representing positive functional correlations between regions. However, we also observed interesting effects driven by differences in negative correlations. For instance, we observed similar developmental trends from the amygdala to visual, motor, and parietal regions. In these connections, IL-6 had reduced negative correlations early in development and increased negative correlation late in development; mirroring the generally trend identified in the main analyses, only with negative connectivity. Network level effects in these developmental trajectories were disproportionately identified between networks including the parietal, visual, and motor networks. These relationships may be of potential interest given that reduced negative correlations have been found in ASD (Anderson et al., 2011). Further, these networks are also of potential interest as a core component of ASD stems from difficulties in sensory processing (visual and motor cortex) and sensory integration (parietal lobe).

However, it should be noted that this manuscript used global signal regression, a MRI preprocessing technique which has been shown to reduce noise and decrease spurious correlations (Power et al., 2014), but also induce negative correlations (Murphy et al., 2009). It is highly likely that the strongest negative correlations are indeed real based on the human and non-human primate literature; however thorough examination of these effects in rodents has not yet been explored. As such, we chose to use caution when interpreting these effects not presented in the main text.

Post hoc analyses on positive and negative group and group by wave effect coefficients

Positive group and negative group by wave coefficients were reported in the main text. The following section will demonstrate that the effects reported in the main text correspond differences between positive functional correlations between regions. In contrast, coefficients in the opposite direction (negative group and positive group by wave coefficients) correspond to group differences in negative correlations between regions.

For example, negative group coefficients (that we will now term 'negative effects' herein) represented connections which show increased negative connectivity in IL-6 animals compared to controls (see figure S3.1D). Similarly, positive group by wave coefficients (that we will now term 'negative effects' herein) represented effects in which negative correlations were *decreased* in IL-6 during W1 but increased at W2. Given these unexpected findings, a series of additional post hoc analyses were performed. The purpose of these tests were to examine the relationship between the direction group and group by wave coefficients and the corresponding connectivity strength, for each connection. Two analyses were performed. First, we noticed that all positive group coefficients were between positively correlated regions (as defined by each connections R value, averaged across all scans). In contrast, negative group coefficients were

95

between connections which were on average negatively correlated across groups (see supplementary figure 3.1A&C). Next, to confirm this relationship we correlated the average connectivity strength by group coefficient term across all regions (regardless of their statistical significance). We observed a relationship between group coefficient direction (measured by positive or negative t-score) and correlation strength (R = .314, p = .0061, see supplementary figure 1E), such that increased average R was related to more positive coefficients (t-scores). Overall, these analyses suggest that positive group coefficients are likely to represent connections with positive connectivity, and show *reduced* connectivity in IL-6 animals, as was reported in the main text (Figure S3.1B). Correspondingly, negative group coefficients represent connections which are between negatively correlated regions on average, and represent connections which show *increases* in negative connectivity in IL-6 animals (figure S1D).

The same analyses were done on group by wave interactions. Here we found that negative group by wave interactions are between connections which are on average positively connected (see figure S3.2A). These coefficients are reported in the main text, and represent connections which show early decreases in connectivity in IL-6 and increased connectivity late in development compared to controls (figure S3.2B). Conversely, positive coefficients are between connections which are on average negatively correlated (supplementary figure 3.2C), and represent cases where controls show *increased* negative connectivity early in development in controls, and IL-6 offspring show *increased* negative connectivity compared to controls during late development (figure 3.2D). By correlating the average connectivity strength by coefficient, we demonstrate this relationship between connectivity strength and group by wave coefficients across amygdala connections (R = -.54, p < .0001). Based on these analyses we separate our presentation and network analyses between negative and positive coefficients and the main text
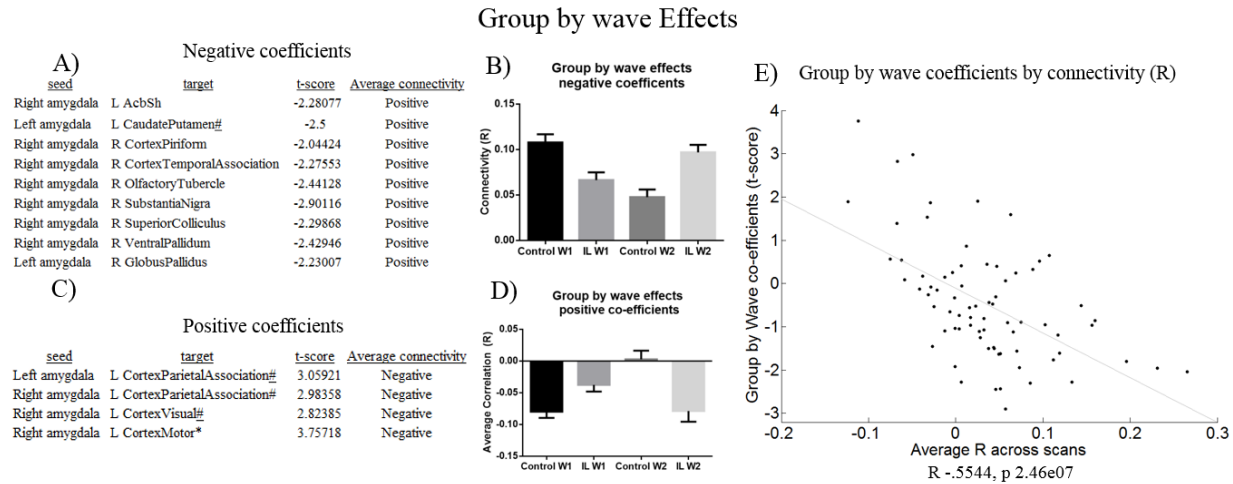
96

highlight group and group by wave coefficients indicating differences in differences in positive correlations.
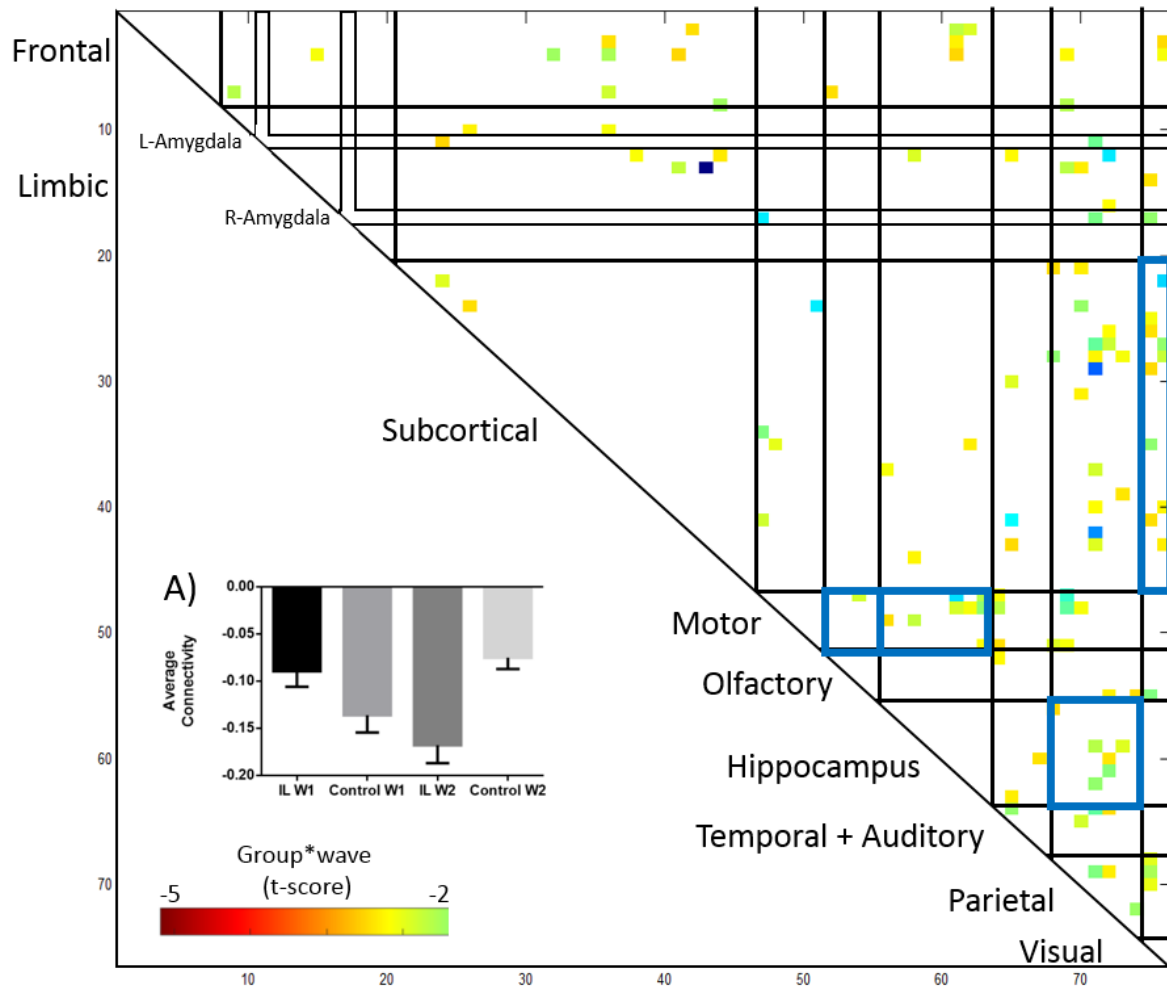
Supplementary Figures
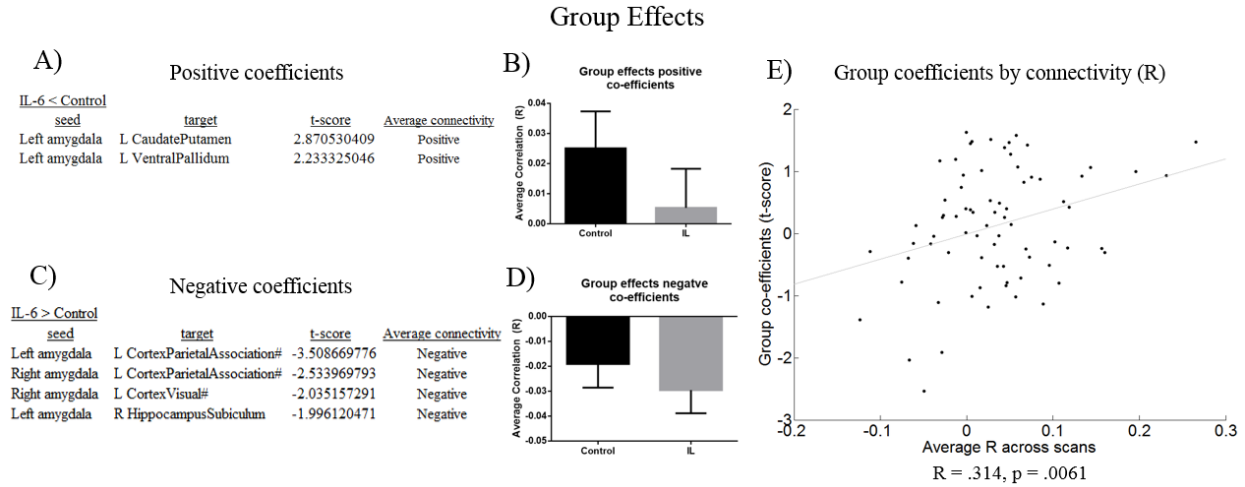
Supplementary Figure 3.1. Group effects including positive and negative coefficients. In each linear mixed effects model, group coefficients were examined, controlling for developmental wave and interactions between group and wave. A) Positive group effect coefficients were identified where B) where IL-6 is shows decreased positive functional connectivity compared to controls. Bar graphs illustrate this relationship by comparing the average R within each significant connection. C-D) Conversely, negative group coefficients represent connections in which negative correlations are increased in IL-6 animals. The Average connectivity column in A&C represent whether on average correlations are either R>0 or R<0 (computed as the grand mean in R across all scans). E) Shows the correlation between average R and the group coefficient (t-scores) across all connections from the amygdala. This relationship suggests that positive group coefficients are related to connections with positive correlations.

Group by wave Effects

A) Negative coefficients

seed	target	t-score	Average connectivity
Right amygdala	L AcbSh	-2.28077	Positive
Left amygdala	L CaudatePutamen#	-2.5	Positive
Right amygdala	R CortexPiriform	-2.04424	Positive
Right amygdala	R CortexTemporalAssociation	-2.27553	Positive
Right amygdala	R OlfactoryTubercle	-2.44128	Positive
Right amygdala	R SubstantiaNigra	-2.90116	Positive
Right amygdala	R SuperiorColliculus	-2.29868	Positive
Right amygdala	R VentralPallidum	-2.42946	Positive
Left amygdala	R GlobusPallidus	-2.23007	Positive

C) Positive coefficients

seed	target	t-score	Average connectivity
Left amygdala	L CortexParietalAssociation#	3.05921	Negative
Right amygdala	L CortexParietalAssociation#	2.98358	Negative
Right amygdala	L CortexVisual#	2.82385	Negative
Right amygdala	L CortexMotor*	3.75718	Negative

**Supplementary Figure 3.2. Group by wave effects including both positive and negative coefficients.** In each linear mixed effects model, a group by wave interaction indicated a difference in developmental trajectories between groups. A) Negative group by wave coefficients were identified B) where IL-6 is shows decreased positive correlations compared to controls at wave 1 but increased positive correlations at wave two. Bar graphs illustrate this relationship by comparing the average R within each significant connection. C-D) Conversely, positive group coefficients represent connections in which negative correlations are decreased early but increased late in development in IL-6 offspring. The Average connectivity column in A&C represent whether on average correlations are either R>0 or R<0 (computed as the grand mean in R across all scans). E) Shows the correlation between average R and the group by wave coefficient (t-scores) across all connections from the amygdala. This relationship suggests that negative group by wave coefficients are related to connections with positive correlations.

Supplementary figure 3.3. Positive group by wave coefficients corresponding to group differences in developmental trajectories within negatively correlated connections. Each cell indicates a group by wave interaction in positive coefficients, and blue outlines represent networks with a higher proportion of these effects than expected by chance. This network analyses implicate visual networks, motor, parietal, olfactory, and hippocampal networks. A) To illustrate this effect, significant connections within the motor to hippocampal network were averaged at each developmental wave. Typically with age, these connections increase in negative correlation. This pattern is reversed in IL-6 who show less negative correlation early, but increased correlation late in development.

99
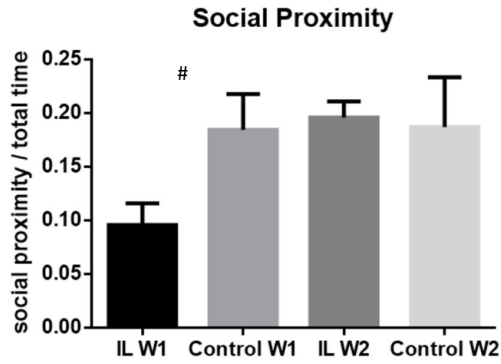
Social Proximity

Supplementary Figure 3.4. Social behavior in IL-6 exposed offspring. The proportion of time

spent in social proximity to the stimulus rat shows a trend towards being reduced in IL-6 animals

during W1. # $p = .056$.

Subcortical to visual

$p = .01$
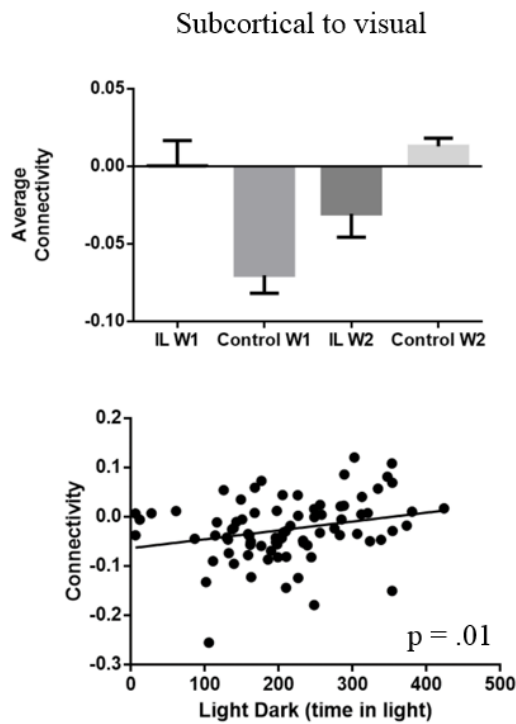
Supplementary Figure 3.5. Relationship between network level findings and anxiety

behavior. Significant network level connections (chi-squared analyses figure S3) from the

subcortical to visual network were averaged and related to anxiety behavior (in a linear mixed

effects model). As can be seen average connectivity is related to anxiety, such that increased

anxiety (as measured by less time spent in the light) is related to decreased correlation between

these networks. No other network level effects were related to anxiety.

ROI	Region Name	Network
1	L_CortexCingulate	Frontal
2	L_CortexFrontalAssociation	Frontal
3	L_CortexMedialPrefrontal	Frontal
4	L_CortexOrbitofrontal	Frontal
5	R_CortexCingulate	Frontal
6	R_CortexFrontalAssociation	Frontal
7	R_CortexMedialPrefrontal	Frontal
8	R_CortexOrbitofrontal	Frontal
9	L_AcbC	Limbic
10	L_AcbSh	Limbic
11	L_Amygdala	Limbic
12	L_BNST	Limbic
13	L_CortexInsular	Limbic
14	L_Septum	Limbic
15	R_AcbC	Limbic
16	R_AcbSh	Limbic
17	R_Amygdala	Limbic
18	R_BNST	Limbic
19	R_CortexInsular	Limbic
20	R_Septum	Limbic
21	L_CaudatePutamen	Subcortical
22	L_GlobusPallidus	Subcortical
23	L_HypothalamusLateral	Subcortical
24	L_HypothalamusMedial	Subcortical
25	L_Raphe	Subcortical
26	L_SubstantiaNigra	Subcortical
27	L_SuperiorColliculus	Subcortical
28	L_ThalamusDorsolateral	Subcortical
29	L_ThalamusMidlineDorsal	Subcortical
30	L_ThalamusVentromedial	Subcortical
31	L_VentralPallidum	Subcortical
32	L_VTA	Subcortical
33	L_ZonaIncerta	Subcortical
34	R_CaudatePutamen	Subcortical
35	R_GlobusPallidus	Subcortical
36	R_HypothalamusLateral	Subcortical
37	R_HypothalamusMedial	Subcortical

38	R_Raphe	Subcortical
39	R_SubstantiaNigra	Subcortical
40	R_SuperiorColliculus	Subcortical
41	R_ThalamusDorsolateral	Subcortical
42	R_ThalamusMidlineDorsal	Subcortical
43	R_ThalamusVentromedial	Subcortical
44	R_VentralPallidum	Subcortical
45	R_VTA	Subcortical
46	R_ZonaIncerta	Subcortical
47	L_CortexMotor	Motor
48	L_CortexSomatosensory	Motor
49	R_CortexMotor	Motor
50	R_CortexSomatosensory	Motor
51	L_CortexPiriform	Olfactory
52	L_OlfactoryTubercle	Olfactory
53	R_CortexPiriform	Olfactory
54	R_OlfactoryTubercle	Olfactory
55	L_HippocampusAnteroDorsal	Hippocampal
56	L_HippocampusPosterior	Hippocampal
57	L_HippocampusPosteroDorsal	Hippocampal
58	L_HippocampusSubiculum	Hippocampal
59	L_HippocampusVentral	Hippocampal
60	R_HippocampusAnteroDorsal	Hippocampal
61	R_HippocampusPosterior	Hippocampal
62	R_HippocampusPosteroDorsal	Hippocampal
63	R_HippocampusSubiculum	Hippocampal
64	R_HippocampusVentral	Hippocampal
65	L_CortexAuditory	Auditory/Temporal
66	L_CortexEntorhinal	Auditory/Temporal
67	L_CortexTemporalAssociation	Auditory/Temporal
68	R_CortexAuditory	Auditory/Temporal
69	R_CortexEntorhinal	Auditory/Temporal
70	R_CortexTemporalAssociation	Auditory/Temporal
71	L_CortexParietalAssociation	Parietal
72	L_CortexRetrosplenial	Parietal
73	R_CortexParietalAssociation	Parietal
74	R_CortexRetrosplenial	Parietal
75	L_CortexVisual	Visual
76	R_CortexVisual	Visual

Supplementary Table 3.1. Regions included the current study and their corresponding network definitions used in the chi-square analyses.

Chapter 4: Discussion and Future Directions

The current work helped to validate rs-fcMRI as a viable method to characterize rodent functional neuroanatomy, increased our knowledge of the biological underpinnings of this signal, and applied this method to a novel translational animal model examining the effects of prenatal exposure to IL-6.

Chapter 4 will be broken into three sections. Section 1 discusses the validation project and examines what we have learned by integrating cellular and molecular information to model FC. This section introduces the idea of using these data for targeted experimental manipulations to be used to further our knowledge of the mechanisms underlying FC organization. Section 2 discusses what we have learned by applying FC to a preclinical animal model examining prenatal exposure to IL-6 and will discuss future directions this type of research could take. Section 3 demonstrates how one can directly relate findings between human and animal models and highlights three examples of this. Example 1 qualitatively compares network organization between species; example 2 uses a quantitative approach to directly compare human and macaque connectivity; and example 3 uses graph theory to compare functional connectome topology between humans, macaques, and rodents.

Section 1: Validation and biological influences on FC

Project 1 shows how FC patterns are shaped by anatomical connectivity and genetic similarity between brain regions. Our results suggest that FC is highly related to the underlying biology. Across the brain, our model including anatomical and genetic information explained a significant amount of variance in the FC signal ($R^2 = .624$), and was explanatory above Euclidian distance and spatial adjacency.

Surprisingly, we found that models of CGE explained more variance (R^2 = .604) in FC than did models using anatomical wiring (R^2 = .584). Further, the genes that drive FC are likely to be related to voltage gated cation channels, glutamate signaling, and regulation of synaptic membrane structure. We also found that some brain areas, such as cortical, motor, and striatial regions, may have relatively more overlap between FC and CGE. This suggests that FC could be driven by distinct mechanisms depending on the connection.

Our work adds to a growing body of literature examining how anatomical connectivity influences FC (Honey et al., 2009; Miranda-Domínguez et al., 2014; Stafford et al., 2014). The addition of regional similarities in gene expression adds an important piece of the puzzle, and could be used to further improve existing models to predict functional connectivity (Hansen, Battaglia, Spiegler, Deco, & Jirsa, 2015; Honey et al., 2009; Messé et al., 2014). Although statistical models of FC are powerful, a complete understanding of their causal role in shaping FC require further validation through experimental perturbations.

Combining modeling techniques and experimental manipulation

A major goal of translational research is to leverage FC data in order to predict outcomes and pinpoint potential pathways for targeted intervention (Fornito et al., 2015; Grayson et al., 2016; Warren et al., 2014). Accordingly, through the combination of connectome level modeling techniques and experimental perturbations to specific neuronal circuits, we can make significant progress on these aims while at the same time advancing our understanding of the causal mechanisms underlying FC organization and dysfunction in disease.

This section will briefly explore the ways we can use FC to identify focal abnormalities in particular brain circuits and use experimental techniques to examine brain-wide network reorganization before and after perturbation. By examining whether these focal perturbations

result in the expected changes in large scale reorganization, we can further our knowledge and ability to treat diseases with complex presentations.

Manipulating connectivity to understand mechanisms

Recent technological advances have allowed for precise control over neuronal activity. For example, the use of designer receptors exclusively activated by designer drugs (DREADDs) (Urban & Roth, 2014), as well as optogenetics (Chow & Boyden, 2013; Deisseroth, 2011) provides a means to manipulate brain activity in vivo (Eldridge et al., 2015; Grayson et al., 2016; Michaelides et al., 2013). Through these methods one can modulate specific neuroanatomical circuits and examine the resulting global functional network reorganization. Further, through the integration of inter-regional anatomical connectivity information, modeling techniques can estimate the effects of a 'simulated lesion' on FC reorganization. These estimated effects can then be compared to FC change resulting from directional experimental lesions to these regions or connections. Such experiment would be able to experimentally assess how accurate these models of FC are or assess whether these models are more or less accurate based on the experimentally lesioned area. For example, it is possible that functional "hubs" with dense functional connections (Sporns, Honey, & Kötter, 2007) are modeled more accurately than less densely connected regions.

Accordingly, using DREADDs, Grayson and colleagues found that focal inactivation of the amygdala resulted in global FC reorganization spanning multiple brain systems. Importantly, these changes were predicted through modeling the estimated effects via 'simulated lesion' (Grayson et al., 2016). The findings indicate that FC change is partially guided by polysynaptic anatomical connectivity to the target area but also that focal alterations result in large scale but predicable change in network reorganization. This raises the possibility that complex, global

disturbances in brain function (assessed through rs-fcMRI) might quantitatively predict focal

brain pathology underlying neurological and psychiatric disorders.

Through modeling that takes into account additional variables including FC, anatomical

connectivity, and correlated gene expression data, models of FC can 1) better estimate a region's

importance and influence on global network structure, and 2) more accurately predict the way in

which network structure will be reorganized given an experimental manipulation to a particular

node. Similar to Grayson and colleagues (Grayson et al., 2016), quantitative tests of these ideas

can then be performed through temporary inactivation of one or multiple candidate regions using

DREADDs or optogenetics. The resulting topological reorganization can be assessed and

compared to predictions made from our multifactorial models of FC.

Similar applications of these methods can also advance a major aim of FC; to pinpoint

potential pathways for targeted intervention. Through the use of graph theoretical modeling

techniques (Bassett & Sporns, 2017; Golfinopoulos, Tourville, & Guenther, 2010) prominent

loci of dysfunction in particular disease states can be identified. In preclinical animal models we

can then systemically target a candidate node or sets of nodes for experimental manipulation. By

quantifying the predicted FC reorganization and determining the degree of overlap to the human

disease state (see section 3 for a discussion on how to determine this overlap), this type of

research can begin to understand the causal influences giving rise to functional brain

organization and disorganization in psychiatric disease.

Section 2: Applying validated techniques to a preclinical models

In project 2 we examined behavioral and FC change resulting from a risk factor for

developmental disorders, prenatal exposure to IL-6. We found that IL-6 induces a robust

behavioral phenotype, primarily seen as anxiety-like behavior. The most prominent imaging

finding was an altered developmental trajectory (early under-connectivity followed by later over-connectivity) of the amygdala as well as the subcortical, and parietal to frontal networks more broadly. We also found that amygdala connectivity was related to anxiety-like behavior, such that increased connectivity was associated with more anxiety.

Manipulating connectivity to further explore causal mechanisms

This project represents first steps in our understanding of the relationships between early prenatal insults, consequent network reorganization, and behavioral outcomes. One way to further our understanding and confidence in these links would be to experimentally induce the observed FC patterns and reassess their relationships to anxiety-like behavior. For example, by experimentally activating the amygdala during the rs-fcMRI experiment (e.g. through DREADDs) we would expect to identify similar FC profiles to that observed in IL-6 animals. However, given that we observed amygdala under-connectivity during early development but over-connectivity during late development, it is important to consider the timing of this manipulation. That is, silencing the amygdala (e.g. using inhibitory DREADDs) during early development and activating the amygdala during late development (e.g. excitatory DREADDs) should produce similar changes in FC downstream from the amygdala (i.e. connectivity changes to regions including the caudate and putamen, nucleus accumbens, substantia nigra, etc. (see figure 3.4)). Further, by targeting these circuits out of the scanner, we could test whether these manipulations recapitulate behavioral phenotypes observed in IL-6 exposed offspring (i.e. increased anxiety). Overall, by showing that manipulations to these circuits produce the expected downstream effects (i.e., manipulations to the amygdala result in similar changes downstream as we see in IL-6 animals), and also result in the expected behavioral alterations (i.e. anxiety), we can further the causal evidence for these targets importance in the IL-6 phenotype and anxiety.

Exploring mechanisms: microglia and pruning

As stated previously, in control animals we found increased FC during early development followed by decreased FC in late development. This pattern was inverted in IL-6 exposed offspring, who showed early under connectivity and a late over connectivity compared to controls. In the human literature, others have found similar patterns of FC through development and have suggested this could be related to the early over proliferation and later synaptic pruning (Kaustubh Supekar, Musen, & Menon, 2009). Interestingly, W1 corresponds to the age where synaptic density peaks and W2 corresponds to the developmental period at which synaptic pruning should be reducing synaptic densities towards their final adults levels (Semple et al., 2013). The use of animal models allows us to investigate whether these mechanisms are a driving factor influencing patterns of FC in control animals and if deviations in these mechanisms are responsible for the alterations seen in IL-6 exposed offspring. In preclinical animal models we can test these ideas using immunohistochemistry (IHC) to probe synaptic and neuronal density at each wave. In the amygdala, we would expect controls to have increased density during early compared to late development. Inversely, we would expect the opposite pattern in IL-6 animals (mirroring the FC findings), corresponding to decreases in densities early but increases late in development. This result would lend evidence for a synaptic overproliferation and pruning within the amygdala in control animals and deficits in these mechanisms as a result of IL-6 exposure. Importantly, through the use of preclinical animals models we can also directly compare FC and IHC based measurements to see if the IHC measurements mediate the FC patterns we see as a result of IL-6. If such an experiment confirmed these findings, we could more confidently assert that FC impairments are driven by

synaptic proliferation and pruning deficits during these periods and could identify potential

targets for biological intervention.

One such intervention could be related to the function and activation of the brains

microglia. Microglia are a promising target because they are implicated in MIA models and are

likely to be activated as a result of IL-6 exposure (Knuesel et al., 2014). Microglia also plays a

key role in eliminating synapses during normal developmental pruning (Paolicelli et al., 2011);

making it a possible mechanism that could be disturbed as a result of IL-6 exposure. Dual

labeling for synaptic and microglial markers could be used to test whether 1) microglia is indeed

activated as a result of IL-6 exposure and 2) whether increased microglia activation relates to

increased synaptic pruning and reductions in density measurements. If these processes are indeed

abnormal in IL-6 animals, it would lend experimental evidence for the role of microglia leading

to atypical pruning processes in IL-6 animals. Through these types of studies additional

mechanistic knowledge of FC impairments can be assessed, tested, and potentially reversed and

tracked in-vivo using FC measures in preclinical animal models.

Test and develop therapeutics to be used in humans

FC experiments also have the opportunity to serve as useful biomarkers for testing

various pharmacological or behavioral interventions. For instance, abnormalities to particular

systems may be playing a role in inducing FC abnormalities. Through subsequent histological

analyses *within* areas which have been identified using FC (i.e. amygdala and/or subcortical

regions), we can move to discover the likely candidate systems influencing FC change. Through

such a top-down approach we can identify areas to focus our efforts on. Several studies have

shown that MIA models result in decreases in serotonin in various areas of the brain (Fatemi et

al., 2008; S. Wang, Yan, Lo, Carvey, & Ling, 2009; Winter et al., 2008, 2009). MIA also results

in widespread changes in brain gene expression (Lombardo et al., 2017) and serotonin gene expression more specifically (Fatemi et al., 2008). Accordingly, an experiment could be designed to confirm this in IL-6 exposed animals by showing decreased serotonin receptor densities, or reduced serotonin gene expression within the amygdala, for example. Next, by targeting this system through early pharmacological intervention or experimental genetic therapies targeting the amygdala (e.g.. increase serotonin expression using CRISPR (Ran et al., 2013)), we would expect a viable therapy to result in the following. 1) Result in the expected normalization of FC and behavioral phenotypes, and 2) produce histological or genetic expression changes that track with FC change within these same regions. Should both of these criteria be satisfied in a pre-clinical animal model, the experimental therapy might also affect these phenotypes in humans. Research using rs-fcMRI in preclinical animal models can be ideal because not only can one target and track the reversal of these non-invasive measures (i.e. longitudinally track brain development at multiple times), but they can also be directly compared to human functional neuroanatomy in developmentally healthy and diseased states. Approaches to making such inter-species comparisons of FC is the topic of the next section.

Section 3: Directly comparing between human and animal models

Both rodent and nonhuman primate research provide numerous advantages detailed throughout this document, including their ability to probe the mechanisms of disease, their experimental control, and extensive histological study of brain structure and development. However, even with these benefits, it is not always clear that a given animal model is accurately reflecting the human condition for which it was designed. Performing comparisons of FC between species under normative conditions is therefore essential for future studies examining FC in typical and disease models. The following section will describe three approaches for

110

comparing FC data obtained across humans, macaques, and rodents. Approach one outlines qualitative similarities between species on measures of large scale network structure. The second approach outlines a method for making direct, quantitative comparisons between human and macaque FC, in which macaque areal atlases are mapped directly onto the human brain, using a set of homologous regions as landmarks or comparison. The final approach introduces graph theory as a method for examining and describing network structure, and will describe how these measures could be used to make comparisons between human patients and control groups, and their macaque and rodent counterparts. The following sections stem from a set of collaborative work between myself and members of the Fair Neuroimaging lab. The first project was led by Dr. Ben Jarrett and Dr. James Stafford in the previously described in work focusing on mouse functional connectivity (Stafford et al., 2014). Here I helped with analyses, data collection, and data processing. The macaque project was a joint effort between myself and Dr. Miranda-Dominguez, for which I was co-first author on the manuscript (Miranda-Domínguez et al., 2014). For this project I contributed to the analyses, data processing, and writing of the manuscript.

Qualitative comparisons of networks between humans and macaques

Comparing motor connectivity between species

Seminal work by Biswal et al. in 1995 was the first to describe the phenomena of correlations in low frequency BOLD signals between homotopic motor cortices in humans (B. Biswal, Yetkin, Haughton, & Hyde, 1995). In this paper, they describe how task-based fMRI activation maps during a finger tapping task could be recapitulated if one examined the spontaneous fluctuations in BOLD activity within the motor cortex. For example the right motor cortex BOLD activity is most strongly correlated with its activity in its homotopic region in the

111

left motor cortex; demonstrating the bilateral nature of this resting state network. Comparing these seed-based connectivity maps under various conditions and clinical presentations form the basis of many resting state FC studies. Accordingly, a logical first step in comparing human, macaque, and rodent connectivity was to examine seed-based connectivity, both in these classically described networks (i.e., motor connectivity), as well as in more complex systems such as the default network.

When examining motor network connectivity, clear qualitative similarities are seen among species. By examining the strongest functional connections from the right motor cortex (Figure 4.1), the bilateral nature of this connectivity signal can be clearly seen in a way that is conserved between species. However, we also notice that in the human, the connectivity strength is stronger; likely due to the awake versus anesthetized manipulation.
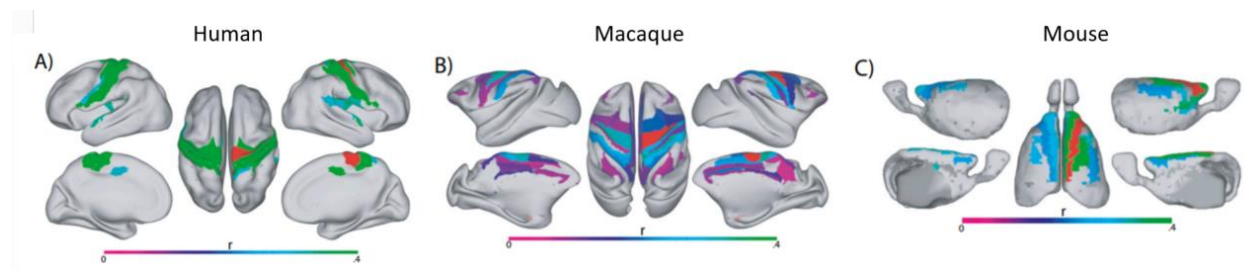

Figure 4.1. Motor network homology between species. Primary motor cortex shows homology between mouse and primate (connection density at 10%). Comparison of the primary motor cortex in (A) human, (B) macaque, and (C) mouse. The right primary motor cortex was used as the seed region (red), and areas with strong correlation are shown. Strong correspondence is seen across species. The r label refers to correlation coefficient.

Comparing default network structure between species

We can also compare more complex functional networks between species (Miranda-Domínguez et al., 2014; Stafford et al., 2014). The default mode network (DMN) is a set of functionally interconnected brain regions that were originally shown to decrease their level of activity in humans during goal-directed tasks (Raichle et al., 2001; Shulman et al., 1997). These regions have subsequently been shown, using rs-fcMRI, to be highly functionally connected in the human (M. D. Greicius, Srivastava, Reiss, & Menon, 2004). In addition, strength of functional connectivity in this system has been tied to several neurologic and psychiatric conditions, including Alzheimer's disease, Autism Spectrum Disorders, and Attention Deficit Hyperactivity Disorder (ADHD) (Broyd et al., 2009).

Comparisons of DMN functional connectivity in the human, macaque, and rodent were operationalized as follows. Macaque default mode connectivity was examined using area 30 (the retrosplenial cortex, RSP) as the seed region, as that region is highly conserved across species (Andrews-Hanna, Reidler, Sepulcre, Poulin, & Buckner, 2010; Upadhyay et al., 2011). In the macaque, the identified DMN constituted both the inferior and superior DMN subsystems, similar to that first described by Andrews-Hanna et al. (Andrews-Hanna, Reidler, Huang, & Buckner, 2010; Andrews-Hanna, Reidler, Sepulcre, et al., 2010). As can be seen in figure 4.2, the critical components of this system are the parietal cortex (pink arrow), the orbitofrontal cortex (orange arrow), and the anterior cingulate cortex (yellow arrow). Note that the superior subsystem is present in both humans and macaques and includes area 23 (posterior cingulate cortex; black arrow).

In mice, we can also identify a putative DMN in regions including the cingulate, orbitofrontal, and parietal cortices (Stafford et al., 2014). These regions overlap nicely with regions from macaques and humans (Figure 4.2). Other regions in the mouse DMN were also

113

identified that were less expected. These areas included primary visual and somatosensory areas. Although these data are consistent with work in the rat (Lu et al., 2012; Upadhyay et al., 2011), they do represent an important deviation from the primate brain. Nonetheless, these types of discrepancies highlight the difficulties in comparing functional connectivity patterns across primates and rodents and make clear the need for additional experimental conditions to solidify this potential homology.

Although the potential presence of this DMN subsystem appears intact in the mouse, there is a very important caveat. In primates, it has been proposed that the default system is split into a dorsal component and a more evolutionary distant ventral component (Andrews-Hanna, Reidler, Sepulcre, et al., 2010; Randy L Buckner & Krienen, 2013). At its core, the ventral component consists of the RSP, orbitofrontal cortex, and parietal cortices. The mouse has all of these component areas. The dorsal component of the default system consists of the posterior cingulate cortex, likely area 23, and the dorsal medial prefrontal cortex at its core (Andrews-Hanna, Reidler, Sepulcre, et al., 2010). Importantly, there is no clear correlate of area 23 in rodents (Vogt, Vogt, & Farber, 2004). In addition, similarities of the frontal cortex are minimal between the rodent and humans (Randy L Buckner & Krienen, 2013). These facts suggest that, although a small component of the default system exists in the mouse, it is not present to the fullest extent as observed in primates.

We note that examining DMN homology across species should be done with care considering the difficulty in precisely linking corresponding areas between species. Nonetheless, the findings presented here suggest that a subcomponent of the DMN is present in the mouse, enabling the use of high-throughput genetic, histological, and therapeutic manipulations that can be applied to better understand the system's function in health and disease.
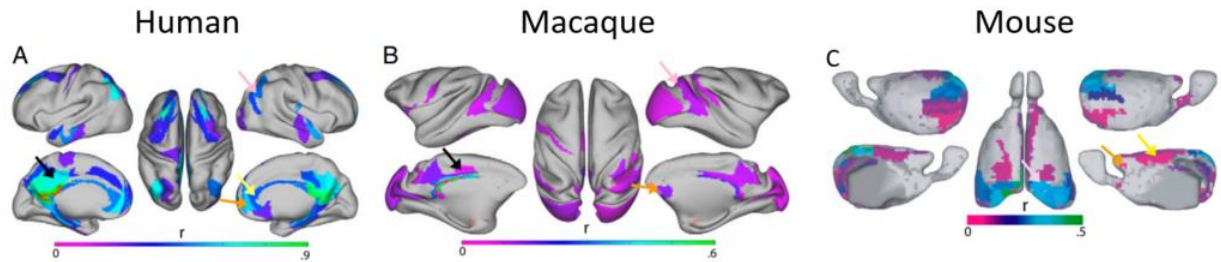
Figure 4.2. Default mode network connectivity across species. A-B) Using area 30 (RSP) as the seed region (red) reveals the presence of both the inferior (DMN) subsystem and superior DMN. The critical components of this system are the parietal cortex (pink arrow), the orbitofrontal cortex (orange arrow), and the anterior cingulate cortex (yellow arrow). Note that the superior subsystem is present in both (A) humans and (B) macaques and includes area 23 (posterior cingulate cortex; black arrow). C) The default mode network in mice. Here the inferior DMN core in mouse functional connectome is shown. The mouse seed region used was the RSPagl. The hallmarks of the inferior DMN subsystem are seen here including the parietal cortex (pink arrow), the lateral/medial orbital cortex (orange arrow), and the cingulate area (yellow arrow). The r label refers to correlation coefficients.

Quantitative comparisons between humans and macaques

As noted above, qualitative similarities as well as differences in FC network structure were observed between species. In order to make direct comparisons between species, it is beneficial to have identical region definitions. To accomplish this, we first focused on comparing humans and macaques. To identify regional homologies we use a surface-based interspecies registration technique described by Van Essen et al. (2004, 2005). This registration procedure allowed for identical areal definitions on both human and macaque data. This approach allows for both a visual (qualitative) and computational (quantitative) comparison between species.

Human macaque registration

This surface-based atlas registration uses a spherical, landmark-based registration algorithm (D C Van Essen, 2004b, 2005; D C Van Essen & Dierker, 2007b). Landmarks for registration included a standard set of regions that are likely to be homologous across species, including visual areas V1, V2, MT, and frontal eye fields; primary auditory cortex; and olfactory, gustatory, somatosensory, and primary motor cortex (Astafiev et al., 2003; D C Van Essen, 2004a). Differences in overall cortical shape are minimized by mapping each cortical surface to a standard configuration (i.e., a sphere), and then each sphere is registered to one another constrained by this set of homologous landmarks. Deformation from macaque to human cortex results in a large, non-uniform expansion of parietal, temporal, and frontal cortex and much less expansion in presumably conserved regions between species (i.e., V1, motor cortex, etc.). Landmark-based registration provides a powerful method for analyzing structural and functional brain organization between humans and macaques (Denys et al., 2004; D C Van Essen, 2005; D C Van Essen & Dierker, 2007a). Areal region of interest (ROI) deformations were done as part of the freely available CARET software package (http://brainvis.wustl.edu/wiki/index.php/Main_Page). Figure 4.3 shows a similar comparative analysis of DMN connectivity between human and macaque, as was documented in figure 2. Here, we highlight similar distributions in connectivity, particularly between anterior, posterior, and inferior temporal cortices. Importantly, qualitative comparisons of interspecies DMN connectivity can now be performed on identical cortical surfaces.
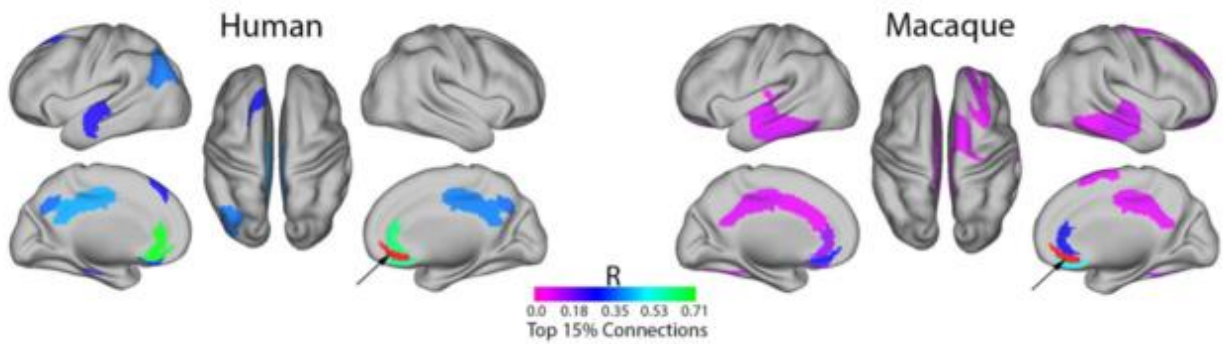
Figure 4.3. Visual comparison of DMN between humans and macaques. In this example macaque connectivity is visualized on the human brain for comparison. Areal atlases have matching labels based on their regional homologies, allowing for direct comparison between FC. FC is shown between a right anterior node of the default network, area 10 (shown in red), and the rest of the cortex in the human and the macaque. Correlation coefficients between the seed region and each other ROI are indicated by the color scale. Similar distributions in connectivity are documented between species, particular between anterior, posterior, and inferior temporal cortices.

Quantitative comparisons

We have shown how given a set of conserved landmarks between species, we can deform macaque regional definitions to project to homologous regions on the human cortical surface. Now that our areal definitions are the same between species we can make quantitative interspecies comparisons. For example, a global comparison of the similarity between human and macaque functional connectivity, across all regions, can be made using linear regression or simple correlational techniques. In figure 4.4, scatter plots and regression lines show the relationship between human and macaque FC matrices, where corresponding histograms represent the distribution of correlations in both humans and macaques after Fisher's *r* to *z*

117

transformation. Here we can see there is a modest relationship between global human and macaque connectivity across the cortex. We note that the extent of overlap between areal boundaries in the human and macaque is currently unknown and some of discrepancies may be influenced by such differences. Nonetheless, when considering only the strongest connections (i.e. top 15% of connections), the match between human and macaque connectivity dramatically improves. Therefore, this initial moderate relationship appears to correspond to a mismatch of low-probability connections and highlights the correspondence of highly probable functional connections between species.
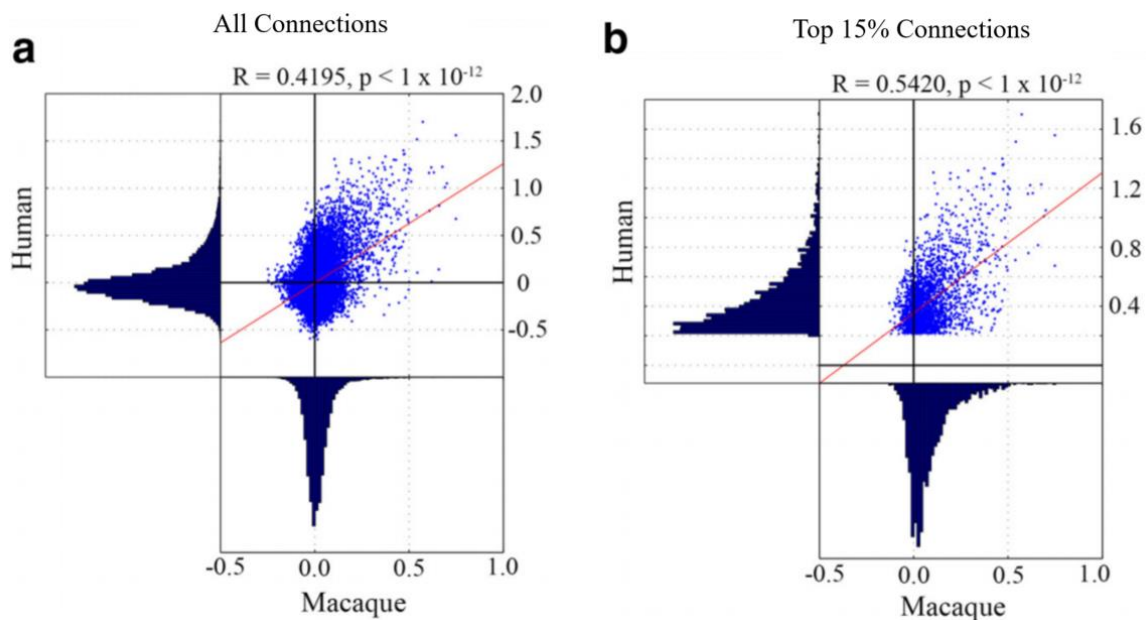

Figure 4.4. Interspecies functional connectivity match. Scatter plot and regression line show the relationship between human and macaque functional connectivity considering all functional connections in both species (a) and the top 15% human functional connections plotted against all corresponding macaque functional connections (b). All values are considered after Fisher's r to z transformation.

It should be noted that there is no method for using landmark based deformation to directly assess connectivity between humans and rodents. This possibility is unlikely to arise. That being said, outside of regression models, as described above, other methods of comparison can be used to compare and describe large scale network properties between all three species.

Using graph theory to compare between species

One way of comparing functional connectomes between species is to use graph theory. In this example we will explore the use of one such graph metric, node degree. Node degree is a cornerstone measurement of brain organization (Bullmore & Sporns, 2009). It identifies the most connected, and potentially important, nodes (or ROIs) in a network by counting the number of direct connections to all other nodes to which it is connected. A node with high degree will have strong, direct connections to many other nodes in the network (Bullmore & Sporns, 2009; Wasserman & Faust, 1994). Using node degree we can assess similarities in topological organization between species.

Using this metric we find that similar to previous studies, humans have high node degree in the posterior cingulate (Achard, Salvador, Whitcher, Suckling, & Bullmore, 2006; R L Buckner et al., 2009; P Hagmann et al., 2008). This suggests that the posterior cingulate is particularly important for integrating information across a wide range of modalities and is also an efficient route for passing information between systems. Interestingly, the posterior cingulate shows the highest node degree in the macaque, even higher than in the human. In humans, the posterior cingulate, while focal, is not the only node with relatively high node degree. Rather, these nodes are distributed in frontal-parietal systems, the anterior insula, and medial frontal areas. In humans and macaques, the degree distribution is distinct across species (Figure 4.5). In

119

the macaque, top nodes have a greater number of functional connections than do those in humans, suggesting a less scale-free and less distributed network structure in macaques.

Using a similar analysis in rodents, we find some interesting similarities but also differences from the observations in humans and macaques. For example, we see high node degree in visual, motor, and parietal cortices but weaker degree within frontal, temporal, and more dorsal regions of the cortex. This could suggest that similar to what was observed in comparisons between humans and macaques, mouse connectivity may also be less distributed (Figure 4.6).

Together, these results suggest a more scale-free network structure, perhaps more vulnerable to focal injuries in macaques and mice. In stroke patients, selective damage to network hubs with high node degree is associated with severe cognitive deficits, and damage to areas with fewer functional connections results in less severe deficits (Power, Schlaggar, Lessov-Schlaggar, & Petersen, 2013). Accordingly, a network with more distributed hubs, such as observed in the humans, may reflect a more dynamic and resilient network structure (Grayson et al., 2014). Future research could be done to assess whether focal injury to such hubs results in more severe cognitive and behavioral deficits. Testing the robustness of our findings with alternative methods of defining hub architecture (Grayson et al., 2014; Patric Hagmann, Grant, & Fair, 2012; Power et al., 2013; van den Heuvel & Sporns, 2011) or assessing "connector" and "provincial" hub architecture (Power et al., 2013; van den Heuvel & Sporns, 2011) across species is also an important avenue for future work.
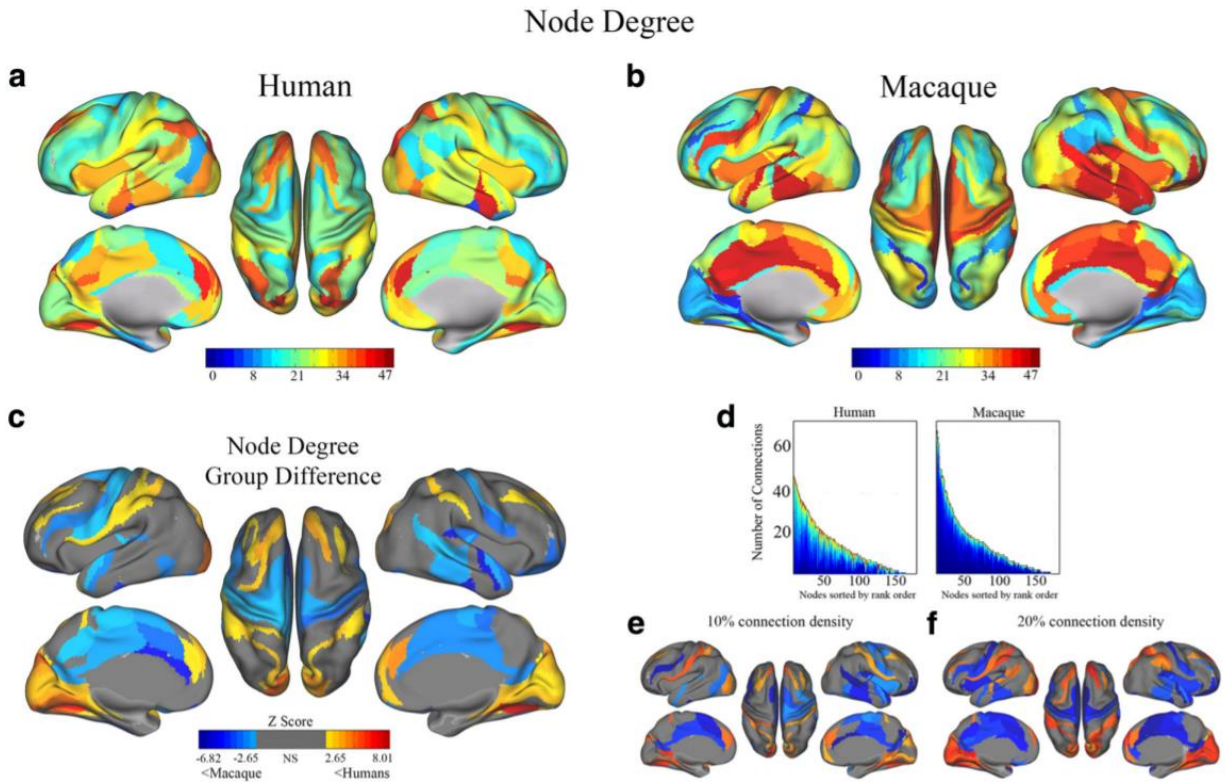
Figure 4.5. Interspecies comparison of node degree .a b. Node degree, or the number of functional connections each ROI has to all other regions, is visualized in both species. For all analyses, both human and macaque matrices were thresholded to include only the top 15% of the strongest functional connections. Macaque connectivity is visualized on the human brain and scales are identical between species, allowing for direct comparison. Statistical comparison of human and macaque node degree are based on 10,000 permutations for 15% (c), 10% (e), and 20% (f) connection density. Blue colors represent regions where macaques have higher node degree and red colors represent areas where humans have higher node degree than macaques (p < 0.05, corrected). Notice that high degree nodes are clustered in the posterior cingulate in the macaque, whereas in humans, connections are spread to other networks such as the frontoparietal system. d, Nodes have been reordered according to the number of connections to allow for comparison of degree distributions. Highly connected hubs in the macaques are clustered in only

a few select regions that also have a greater number of max connections than humans (i.e., more "scale free"). Conversely, humans show amore distributed pattern in which highly connected hubs are spread throughout the cortex (i.e., less "scale free").
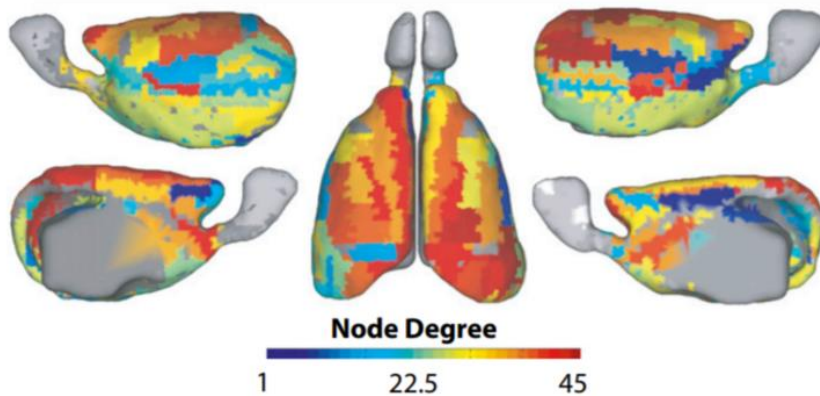

Figure 4.6. Surface map of node degree in the mouse functional connectome. Node degree, or the number of functional connections each ROI has to all other regions. Red regions indicate areas which are highly connected to the rest of the mouse connectome. Analyses were conducted on the top 16.46% connections. Note the higher node degree concentrated around motor, visual, and dorsal regions of the cortex.

Using rs-fcMRI as a tool in translational medicine

This section describes the normative baseline for comparing FC across species, and demonstrates similarities and differences that can be can be expected at both the network organization and global connectivity level. Further, we explore measurements of network organization that highlight potential areas of overlap, but also divergence, between species. Such information establishes a solid basis for using rs-fcMRI as a bridge between human and animal research. Future work could use these methods to compare between human disorders and animal

models of the respective diseases. Through these methods we might also better understand the overlap between FC change resulting from risk factors assessed in animal models and FC change resulting from the disorders themselves.

Summary and conclusion

The goal of this thesis was first, to validate and understand the biology of resting state connectivity, and next, to apply these metrics to use these methods to test a risk factor for human disease. Through the use of non-invasive imaging in preclinical animal models, we were able to obtain a greater understanding of how white matter connectivity and regional similarities in gene expression influence the functional connectome, as well as gain confidence and validation for the FC measurements we can obtain in rodents. Next by applying these FC metrics we to a preclinical rodent model we found that prenatal exposure to inflammation through IL-6 resulted in offspring behavioral abnormities that related to changes in FC network reorganization. Finally, we examined ways in which we can make interspecies comparisons between FC observed in human and preclinical animal models. Through these methods we can gain insights into the organization of the functional connectome and how it relates between humans and animal models. This is an important piece of the puzzle as we embark down a path of understanding brain structure and function and its role in psychiatric and neurological disease.

References

Abdelnour, F., Voss, H. U., & Raj, A. (2014). Network diffusion accurately models the relationship between structural and functional brain connectivity networks. *NeuroImage*, *90*, 335–347. https://doi.org/10.1016/j.neuroimage.2013.12.039

Abrahamson, E. E., & Moore, R. Y. (2001). The posterior hypothalamic area: Chemoarchitecture and afferent connections. *Brain Research*, *889*(1–2), 1–22. https://doi.org/10.1016/S0006-8993(00)03015-8

Achard, S., Salvador, R., Whitcher, B., Suckling, J., & Bullmore, E. (2006). A resilient, low-frequency, small-world human brain functional network with highly connected association cortical hubs. *Journal of Neuroscience*, *26*(1), 63–72. https://doi.org/26/1/63 [pii]10.1523/JNEUROSCI.3874-05.2006

Adachi, Y., Osada, T., Sporns, O., Watanabe, T., Matsui, T., Miyamoto, K., & Miyashita, Y. (2012). Functional Connectivity between Anatomically Unconnected Areas Is Shaped by Collective Network-Level Effects in the Macaque Cortex. *Cerebral Cortex*, *22*(7), 1586–1592. https://doi.org/10.1093/cercor/bhr234

Alzheimer's Association. (2014). Alzheimer Latest Facts & Figures Report. Retrieved from http://www.alz.org/alzheimers_disease_facts_and_figures.asp

Anderson, J. S., Nielsen, J. A., Froehlich, A. L., DuBray, M. B., Druzgal, T. J., Cariello, A. N., … Lainhart, J. E. (2011). Functional connectivity magnetic resonance imaging classification of autism. *Brain*, *134*(Pt 12), 3742–3754. https://doi.org/10.1093/brain/awr263

Andersson, J. L. R., Skare, S., & Ashburner, J. (2003). How to correct susceptibility distortions in spin-echo echo-planar images: application to diffusion tensor imaging. *NeuroImage*, *20*(2), 870–888. https://doi.org/10.1016/S1053-8119(03)00336-7

Andrews-Hanna, J. R., Reidler, J. S., Huang, C., & Buckner, R. L. (2010). Evidence for the

default network's role in spontaneous cognition. *Journal of Neurophysiology*, *104*(1), 322–35. https://doi.org/10.1152/jn.00830.2009

Andrews-Hanna, J. R., Reidler, J. S., Sepulcre, J., Poulin, R., & Buckner, R. L. (2010). Functional-anatomic fractionation of the brain's default network. *Neuron*, *65*(4), 550–62. https://doi.org/10.1016/j.neuron.2010.02.005

Ash, J. A., Lu, H., Taxier, L. R., Long, J. M., Yang, Y., Stein, E. A., & Rapp, P. R. (2016). Functional connectivity with the retrosplenial cortex predicts cognitive aging in rats. *Proceedings of the National Academy of Sciences of the United States of America*, *113*(43), 12286–12291. https://doi.org/10.1073/pnas.1525309113

Ashburner, M., Ball, C. A., Blake, J. A., Botstein, D., Butler, H., Cherry, J. M., … Sherlock, G. (2000). Gene Ontology: tool for the unification of biology. *Nature Genetics*, *25*(1), 25–29. https://doi.org/10.1038/75556

Ashwood, P., Krakowiak, P., Hertz-Picciotto, I., Hansen, R., Pessah, I. N., & Van de Water, J. (2011a). Altered T cell responses in children with autism. *Brain, Behavior, and Immunity*, *25*(5), 840–849. https://doi.org/10.1016/j.bbi.2010.09.002

Ashwood, P., Krakowiak, P., Hertz-Picciotto, I., Hansen, R., Pessah, I., & Van de Water, J. (2011b). Elevated plasma cytokines in autism spectrum disorders provide evidence of immune dysfunction and are associated with impaired behavioral outcome. *Brain, Behavior, and Immunity*, *25*(1), 40–5. https://doi.org/10.1016/j.bbi.2010.08.003

Astafiev, S. V, Shulman, G. L., Stanley, C. M., Snyder, A. Z., Van Essen, D. C., & Corbetta, M. (2003). Functional organization of human intraparietal and frontal cortex for attending, looking, and pointing. *J Neurosci*, *23*(11), 4689–4699. Retrieved from http://www.ncbi.nlm.nih.gov/entrez/query.fcgi?cmd=Retrieve&db=PubMed&dopt=Citation

&list_uids=12805308

Attwell, D., & Iadecola, C. (2002). The neural basis of functional brain imaging signals. *Trends in Neurosciences*, *25*(12), 621–625. https://doi.org/10.1016/S0166-2236(02)02264-6

Backes, C., Rühle, F., Stoll, M., Haas, J., Frese, K., Franke, A., … Keller, A. (2014). Systematic permutation testing in GWAS pathway analyses: identification of genetic networks in dilated cardiomyopathy and ulcerative colitis. *BMC Genomics*, *15*(1), 622. https://doi.org/10.1186/1471-2164-15-622

Bassett, D. S., & Sporns, O. (2017). Network Neuroscience. *Nature Neuroscience*, *20*(3), 353–364. https://doi.org/10.1038/nn.4502

Becerra, L., Pendse, G., Chang, P. C., Bishop, J., & Borsook, D. (2011). Robust reproducible resting state networks in the awake rodent brain. *PLoS One*, *6*(10), e25701. https://doi.org/10.1371/journal.pone.0025701

Biswal, B. B., & Kannurpatti, S. S. (2009). Resting-state functional connectivity in animal models: Modulations by exsanguination. *Methods in Molecular Biology*, *489*, 255–274. https://doi.org/10.1007/978-1-59745-543-5_12

Biswal, B., Yetkin, F. Z., Haughton, V. M., & Hyde, J. S. (1995). Functional connectivity in the motor cortex of resting human brain using echo-planar MRI. *Magnetic Resonance in Medicine*, *34*(4), 537–541. Retrieved from http://www.ncbi.nlm.nih.gov/entrez/query.fcgi?cmd=Retrieve&db=PubMed&dopt=Citation &list_uids=8524021

Blondel, V. D., Guillaume, J.-L., Lambiotte, R., & Lefebvre, E. (2008). Fast unfolding of communities in large networks. https://doi.org/10.1088/1742-5468/2008/10/P10008

Bourin, M. (2015). Animal models for screening anxiolytic-like drugs: A perspective. *Dialogues*

in Clinical Neuroscience, *17*(3), 295–303.

Broyd, S. J., Demanuele, C., Debener, S., Helps, S. K., James, C. J., & Sonuga-Barke, E. J. S.

(2009). Default-mode brain dysfunction in mental disorders: a systematic review.

Neuroscience and Biobehavioral Reviews, *33*(3), 279–96.

https://doi.org/10.1016/j.neubiorev.2008.09.002

Brynildsen, J. K., Hsu, L.-M., Ross, T. J., Stein, E. A., Yang, Y., & Lu, H. (2017). Physiological

characterization of a robust survival rodent fMRI method. *Magnetic Resonance Imaging*,

35, 54–60. https://doi.org/10.1016/j.mri.2016.08.010

Buckner, R. L., & Krienen, F. M. (2013). The evolution of distributed association networks in

the human brain. *Trends in Cognitive Sciences*, *17*(12), 648–665.

https://doi.org/10.1016/j.tics.2013.09.017

Buckner, R. L., Krienen, F. M., & Yeo, B. T. T. (2013). Opportunities and limitations of intrinsic

functional connectivity MRI. *Nature Neuroscience*, *16*(7), 832–837.

https://doi.org/10.1038/nn.3423

Buckner, R. L., Sepulcre, J., Talukdar, T., Krienen, F. M., Liu, H., Hedden, T., … Johnson, K. A.

(2009). Cortical hubs revealed by intrinsic functional connectivity: mapping, assessment of

stability, and relation to Alzheimer's disease. *Journal of Neuroscience*, *29*(6), 1860–1873.

https://doi.org/10.1523/JNEUROSCI.5062-08.2009

Bullmore, E., & Sporns, O. (2009). Complex brain networks: graph theoretical analysis of

structural and functional systems. *Nature Reviews. Neuroscience*, *10*(3), 186–98.

https://doi.org/10.1038/nrn2575

Buss, C., Davis, E. P., Shahbaba, B., Pruessner, J. C., Head, K., & Sandman, C. A. (2012).

Maternal cortisol over the course of pregnancy and subsequent child amygdala and

hippocampus volumes and affective problems. *Proceedings of the National Academy of Sciences*, *109*(20), E1312–E1319. https://doi.org/10.1073/pnas.1201295109

Carmichael, S. T., & Price, J. L. (1995). Limbic connections of the orbital and medial prefrontal cortex of macaque monkeys. *Journal of Comparative Neurology*, *368*(4), 642–664.

Chalfant, A. M., Rapee, R., & Carroll, L. (2007). Treating anxiety disorders in children with high functioning autism spectrum disorders: A controlled trial. *Journal of Autism and Developmental Disorders*, *37*(10), 1842–1857. https://doi.org/10.1007/s10803-006-0318-4

Chavhan, G. B., Babyn, P. S., Thomas, B., Shroff, M. M., & Haacke, E. M. (2009). Principles, techniques, and applications of T2*-based MR imaging and its special applications. *Radiographics : A Review Publication of the Radiological Society of North America, Inc*, *29*(62983), 1433–1449. https://doi.org/10.1148/rg.295095034

Chow, B. Y., & Boyden, E. S. (2013). Optogenetics and translational medicine. *Science Translational Medicine*. https://doi.org/10.1126/scitranslmed.3003101

Chuang, K. H., & Nasrallah, F. A. (2017). Functional networks and network perturbations in rodents. *NeuroImage*. https://doi.org/10.1016/j.neuroimage.2017.09.038

Churchland, P. S., & Sejnowski, T. J. (1992). *The computational brain*. Cambridge, MA: MIT Press.

Cohen, A. L., Fair, D. A., Dosenbach, N. U., Miezin, F. M., Dierker, D., Van Essen, D. C., … Petersen, S. E. (2008). DUPLICATE-Defining functional areas in individual human brains using resting functional connectivity MRI. *Neuroimage*, *41*(1), 45–57. https://doi.org/10.1016/j.neuroimage.2008.01.066S1053-8119(08)00117-1 [pii]10.1016/j.neuroimage.2008.01.066

Cole, M. W., Pathak, S., & Schneider, W. (2010). Identifying the brain's most globally

connected regions. *NeuroImage*, *49*(4), 3132–48.

https://doi.org/10.1016/j.neuroimage.2009.11.001

Courchesne, E. (2002). Abnormal early brain development in autism. *Molecular Psychiatry*, *7*,

21–23. https://doi.org/10.1038/sj.mp.4001169

Craddock, R. C., Hu, X. P., Mayberg, H. S., & Holtzheimer, P. E. (2009). Disease state

prediction from resting state functional connectivity. *Magnetic Resonance in Medicine*,

62(6), 1619–1628. https://doi.org/10.1002/mrm.22159

Creswell, J. D., Taren, A. A., Lindsay, E. K., Greco, C. M., Gianaros, P. J., Fairgrieve, A., …

Ferris, J. L. (2016). Alterations in resting-state functional connectivity link mindfulness

meditation with reduced interleukin-6: A randomized controlled trial. *Biological Psychiatry*,

80(1), 53–61. https://doi.org/10.1016/j.biopsych.2016.01.008

Crofts, J. J., & Higham, D. J. (2009). A weighted communicability measure applied to complex

brain networks. *Journal of The Royal Society Interface*. Retrieved from

http://rsif.royalsocietypublishing.org/content/early/2009/02/09/rsif.2008.0484.short

Davis, E. P., Glynn, L. M., Waffarn, F., & Sandman, C. A. (2011). Prenatal maternal stress

programs infant stress regulation. *Journal of Child Psychology and Psychiatry and Allied

Disciplines*, *52*(2), 119–129. https://doi.org/10.1111/j.1469-7610.2010.02314.x

Deisseroth, K. (2011). Optogenetics. *Nature Methods*. https://doi.org/10.1038/nmeth.f.324

Denys, K., Vanduffel, W., Fize, D., Nelissen, K., Sawamura, H., Georgieva, S., … Orban, G. A.

(2004). Visual activation in prefrontal cortex is stronger in monkeys than in humans. *J Cogn

Neurosci*, *16*(9), 1505–1516. Retrieved from

http://www.ncbi.nlm.nih.gov/entrez/query.fcgi?cmd=Retrieve&db=PubMed&dopt=Citation

&list_uids=15601515

Depino, A. M. (2015). Early prenatal exposure to LPS results in anxiety- and depression-related behaviors in adulthood. *Neuroscience*, *299*, 56–65. https://doi.org/10.1016/j.neuroscience.2015.04.065

Deverman, B. E., & Patterson, P. H. (2009). Cytokines and CNS development. *Neuron*, *64*(1), 61–78. https://doi.org/10.1016/j.neuron.2009.09.002

Di Martino, a, Yan, C.-G., Li, Q., Denio, E., Castellanos, F. X., Alaerts, K., … Milham, M. P. (2014). The autism brain imaging data exchange: towards a large-scale evaluation of the intrinsic brain architecture in autism. *Molecular Psychiatry*, *19*(6), 659–67. https://doi.org/10.1038/mp.2013.78

Eggebrecht, A. T., Elison, J. T., Feczko, E., Todorov, A., Wolff, J. J., Kandala, S., … Pruett, J. R. (2017). Joint Attention and Brain Functional Connectivity in Infants and Toddlers. *Cerebral Cortex*. https://doi.org/10.1093/cercor/bhw403

Eldridge, M. A. G., Lerchner, W., Saunders, R. C., Kaneko, H., Krausz, K. W., Gonzalez, F. J., … Richmond, B. J. (2015). Chemogenetic disconnection of monkey orbitofrontal and rhinal cortex reversibly disrupts reward value. *Nature Neuroscience*, *19*(1), 37–39. https://doi.org/10.1038/nn.4192

Emanuele, E., Orsi, P., Boso, M., Broglia, D., Brondino, N., Barale, F., … Politi, P. (2010). Low-grade endotoxemia in patients with severe autism. *Neuroscience Letters*, *471*(3), 162–165. https://doi.org/10.1016/j.neulet.2010.01.033

Engin, E., & Treit, D. (2007). The role of hippocampus in anxiety: Intracerebral infusion studies. *Behavioural Pharmacology*. https://doi.org/10.1097/FBP.0b013e3282de7929

Engler, H., Doenlen, R., Engler, A., Riether, C., Prager, G., Niemi, M. B., … Schedlowski, M. (2011). Acute amygdaloid response to systemic inflammation. *Brain, Behavior, and*

Immunity, *25*(7), 1384–1392. https://doi.org/10.1016/j.bbi.2011.04.005

Estes, M. L., & McAllister, A. K. (2016). Maternal immune activation: Implications for
neuropsychiatric disorders. *Science*, *353*(6301), 772 LP-777.
https://doi.org/10.1126/science.aag3194

Estrada, E., & Hatano, N. (2008). Communicability in complex networks. *Physical Review E*,
77(3), 36111. https://doi.org/10.1103/PhysRevE.77.036111

Etkin, A., Egner, T., Peraza, D. M., Kandel, E. R., & Hirsch, J. (2006). Resolving emotional
conflict: a role for the rostral anterior cingulate cortex in modulating activity in the
amygdala. *Neuron*, *51*(6), 871–882. Retrieved from
http://www.ncbi.nlm.nih.gov/entrez/query.fcgi?cmd=Retrieve&db=PubMed&dopt=Citation
&list_uids=16982430

Etkin, A., Prater, K. E., Schatzberg, A. F., Menon, V., & Greicius, M. D. (2009). Disrupted
amygdalar subregion functional connectivity and evidence of a compensatory network in
generalized anxiety disorder. *Archives of General Psychiatry*, *66*(12), 1361–1372.
https://doi.org/10.1001/archgenpsychiatry.2009.104

Etkin, A., & Wager, T. D. (2007). Functional neuroimaging of anxiety: a meta-analysis of
emotional processing in PTSD, social anxiety disorder, and specific phobia. *The American
Journal of Psychiatry*, *164*(10), 1476–1488. https://doi.org/10.1176/appi.ajp.2007.07030504

Fareri, D. S., & Tottenham, N. (2016). Effects of early life stress on amygdala and striatal
development. *Developmental Cognitive Neuroscience*, *19*, 233–247.
https://doi.org/10.1016/j.dcn.2016.04.005

Fatemi, S. H., Reutiman, T. J., Folsom, T. D., Huang, H., Oishi, K., Mori, S., … Juckel, G.
(2008). Maternal infection leads to abnormal gene regulation and brain atrophy in mouse

offspring: implications for genesis of neurodevelopmental disorders. *Schizophrenia Research*, *99*(1–3), 56–70. https://doi.org/10.1016/j.schres.2007.11.018

Feczko, E., Balba, N., Miranda-Dominguez, O., Cordova, M., Karalunas, S. L., Irwin, L., … Fair, D. A. (2017). Subtyping cognitive profiles in Autism Spectrum Disorder using a random forest algorithm. *NeuroImage*. https://doi.org/10.1016/j.neuroimage.2017.12.044

Felger, J. C., Li, Z., Haroon, E., Woolwine, B. J., Jung, M. Y., Hu, X., & Miller, A. H. (2016). Inflammation is associated with decreased functional connectivity within corticostriatal reward circuitry in depression. *Molecular Psychiatry*, *21*(10), 1358–1365. https://doi.org/10.1038/mp.2015.168

Ferrucci, L., Harris, T. B., Guralnik, J. M., Tracy, R. P., Corti, M. C., Cohen, H. J., … Havlik, R. J. (1999). Serum IL-6 level and the development of disability in older persons. *Journal of the American Geriatrics Society*, *47*(6), 639–646. https://doi.org/10.1111/j.1532-5415.1999.tb01583.x

Floresco, S. B. (2015). The Nucleus Accumbens: An Interface Between Cognition, Emotion, and Action. *Annual Review of Psychology*, *66*(1), 25–52. https://doi.org/10.1146/annurev-psych-010213-115159

Fornito, A., Zalesky, A., & Breakspear, M. (2015). The connectomics of brain disorders. *Nature Reviews Neuroscience*, *16*(3), 159–172. https://doi.org/10.1038/nrn3901

Fox, M. D., Snyder, A. Z., Vincent, J. L., Corbetta, M., Van Essen, D. C., & Raichle, M. E. (2005). The human brain is intrinsically organized into dynamic, anticorrelated functional networks. *Proceedings of the National Academy of Sciences*, *102*(27), 9673–8. https://doi.org/10.1073/pnas.0504136102

Fruchterman, T. M. J., & Reingold, E. M. (1991). Graph drawing by force-directed placement.

Software: Practice and Experience, *21*(11), 1129–1164.

https://doi.org/10.1002/spe.4380211102

Fulcher, B. D., & Fornito, A. (2016). A transcriptional signature of hub connectivity in the
mouse connectome. *Proceedings of the National Academy of Sciences of the United States
of America*, *113*(5), 1435–40. https://doi.org/10.1073/pnas.1513302113

Gabard-Durnam, L. J., Flannery, J., Goff, B., Gee, D. G., Humphreys, K. L., Telzer, E., …
Tottenham, N. (2014). The development of human amygdala functional connectivity at rest
from 4 to 23 years: A cross-sectional study. *NeuroImage*, *95*(310), 193–207.
https://doi.org/10.1016/j.neuroimage.2014.03.038

Gao, Y. R., Ma, Y., Zhang, Q., Winder, A. T., Liang, Z., Antinori, L., … Zhang, N. (2017). Time
to wake up: Studying neurovascular coupling and brain-wide circuit function in the un-
anesthetized animal. *NeuroImage*. https://doi.org/10.1016/j.neuroimage.2016.11.069

Garofalo, R. (2010). Cytokines in Human Milk. *The Journal of Pediatrics*, *156*(2), S36–S40.
https://doi.org/10.1016/j.jpeds.2009.11.019

Gibney, S. M., McGuinness, B., Prendergast, C., Harkin, A., & Connor, T. J. (2013). Poly I: C-
induced activation of the immune response is accompanied by depression and anxiety-like
behaviours, kynurenine pathway activation and reduced BDNF expression. *Brain, Behavior,
and Immunity*, *28*, 170–181. https://doi.org/10.1016/j.bbi.2012.11.010

Gillis, J., Mistry, M., & Pavlidis, P. (2010). Gene function analysis in complex data sets using
ErmineJ. *Nature Protocols*, *5*(6), 1148–1159. https://doi.org/10.1038/nprot.2010.78

Gillis, J., Pavlidis, P., Benson, D., Bryant, S., & Canese, K. (2012). "Guilt by Association" Is the
Exception Rather Than the Rule in Gene Networks. *PLoS Computational Biology*, *8*(3),
e1002444. https://doi.org/10.1371/journal.pcbi.1002444

Gillis, J., Pavlidis, P., Chan, C., Richard, N., Laird, M., Allen, N., … Bertram, L. (2011). The

    Impact of Multifunctional Genes on "Guilt by Association" Analysis. *PLoS*

    ONE, *6*(2), e17258. https://doi.org/10.1371/journal.pone.0017258

Glover, V. (2011). Annual Research Review: Prenatal stress and the origins of psychopathology:

    an evolutionary perspective. *Journal of Child Psychology and Psychiatry, and Allied*

    Disciplines, *52*(4), 356–67. https://doi.org/10.1111/j.1469-7610.2011.02371.x

Gluckman, P. D., & Hanson, M. a. (2004). Living with the past: evolution, development, and

    patterns of disease. *Science (New York, N.Y.)*, *305*(5691), 1733–1736.

    https://doi.org/10.1126/science.1095292

Goelman, G., Ilinca, R., Zohar, I., & Weinstock, M. (2014). Functional connectivity in prenatally

    stressed rats with and without maternal treatment with ladostigil, a brain-selective

    monoamine oxidase inhibitor. *The European Journal of Neuroscience*, *40*(5), 2734–43.

    https://doi.org/10.1111/ejn.12621

Golfinopoulos, E., Tourville, J. a, & Guenther, F. H. (2010). The integration of large-scale neural

    network modeling and functional brain imaging in speech motor control. *NeuroImage*,

    52(3), 862–74. https://doi.org/10.1016/j.neuroimage.2009.10.023

Goñi, J., van den Heuvel, M. P., Avena-Koenigsberger, A., Velez de Mendizabal, N., Betzel, R.

    F., Griffa, A., … Sporns, O. (2014). Resting-brain functional connectivity predicted by

    analytic measures of network communication. *Proceedings of the National Academy of*

    Sciences of the United States of America, *111*(2), 833–8.

    https://doi.org/10.1073/pnas.1315529111

Gordon, E. M., Laumann, T. O., Adeyemo, B., Huckins, J. F., Kelley, W. M., & Petersen, S. E.

    (2014). Generation and Evaluation of a Cortical Area Parcellation from Resting-State

Correlations. *Cerebral Cortex*. https://doi.org/10.1093/cercor/bhu239

Graham, A. M., Pfeifer, J. H., Fisher, P. A., Lin, W., Gao, W., & Fair, D. A. (2015). The

potential of infant fMRI research and the study of early life stress as a promising exemplar.

Developmental Cognitive Neuroscience, *12*, 12–39.

https://doi.org/10.1016/j.dcn.2014.09.005

Graham, A. M., Rasmussen, J. M., Rudolph, M. D., Heim, C. M., Gilmore, J. H., Styner, M., …

Buss, C. (2017). Maternal Systemic Interleukin-6 During Pregnancy Is Associated With

Newborn Amygdala Phenotypes and Subsequent Behavior at 2 Years of Age. *Biological*

Psychiatry. https://doi.org/10.1016/j.biopsych.2017.05.027

Grandjean, J., Schroeter, A., Batata, I., & Rudin, M. (2014). Optimization of anesthesia protocol

for resting-state fMRI in mice based on differential effects of anesthetics on functional

connectivity patterns. *NeuroImage*, *102*(P2), 838–847.

https://doi.org/10.1016/j.neuroimage.2014.08.043

Grayson, D. S., Bliss-Moreau, E., Machado, C. J., Bennett, J., Shen, K., Grant, K. A., … Amaral,

D. G. (2016). The Rhesus Monkey Connectome Predicts Disrupted Functional Networks

Resulting from Pharmacogenetic Inactivation of the Amygdala. *Neuron*, *91*(2), 453–66.

https://doi.org/10.1016/j.neuron.2016.06.005

Grayson, D. S., & Fair, D. A. (2017). Development of large-scale functional networks from birth

to adulthood: A guide to the neuroimaging literature. *NeuroImage*.

https://doi.org/10.1016/j.neuroimage.2017.01.079

Grayson, D. S., Ray, S., Carpenter, S., Iyer, S., Dias, T. G. C., Stevens, C., … Fair, D. A. (2014).

Structural and functional rich club organization of the brain in children and adults. *PloS*

One, *9*(2), e88297. https://doi.org/10.1371/journal.pone.0088297

Greicius, M. (2008). Resting-state functional connectivity in neuropsychiatric disorders. *Current Opinion in Neurology*, *21*(4), 424–30. https://doi.org/10.1097/WCO.0b013e328306f2c5

Greicius, M. D., Srivastava, G., Reiss, A. L., & Menon, V. (2004). Default-mode network activity distinguishes Alzheimer's disease from healthy aging: evidence from functional MRI. *Proceedings of the National Academy of Sciences of the United States of America*, *101*(13), 4637–42. https://doi.org/10.1073/pnas.0308627101

Guilfoyle, D. N., Gerum, S. V, Sanchez, J. L., Balla, A., Sershen, H., Javitt, D. C., & Hoptman, M. J. (2013). Functional connectivity fMRI in mouse brain at 7T using isoflurane. *Journal of Neuroscience Methods*, *214*(2), 144–8. https://doi.org/10.1016/j.jneumeth.2013.01.019

Guo, X., Duan, X., Long, Z., Chen, H., Wang, Y., Zheng, J., … Chen, H. (2016). Decreased amygdala functional connectivity in adolescents with autism: A resting-state fMRI study. *Psychiatry Research - Neuroimaging*, *257*, 47–56. https://doi.org/10.1016/j.pscychresns.2016.10.005

Hagmann, P., Cammoun, L., Gigandet, X., Meuli, R., Honey, C. J., Wedeen, V. J., & Sporns, O. (2008). Mapping the structural core of human cerebral cortex. *PLoS Biol*, *6*(7), e159. Retrieved from http://www.ncbi.nlm.nih.gov/entrez/query.fcgi?cmd=Retrieve&db=PubMed&dopt=Citation&list_uids=18597554

Hagmann, P., Grant, P. E., & Fair, D. A. (2012). MR connectomics: a conceptual framework for studying the developing brain. *Front Syst Neurosci*, *6*, 43. https://doi.org/10.3389/fnsys.2012.00043

Hamilton, J. P., Etkin, A., Furman, D. J., Lemus, M. G., Johnson, R. F., & Gotlib, I. H. (2012). Functional neuroimaging of major depressive disorder: a meta-analysis and new integration

of base line activation and neural response data. *The American Journal of Psychiatry*, *169*(7), 693–703. https://doi.org/10.1176/appi.ajp.2012.11071105

Hansen, E. C. A., Battaglia, D., Spiegler, A., Deco, G., & Jirsa, V. K. (2015). Functional connectivity dynamics: Modeling the switching behavior of the resting state. *NeuroImage*, *105*, 525–535. https://doi.org/10.1016/j.neuroimage.2014.11.001

Hascoët, M., & Bourin, M. (2009). The mouse light-dark box test. *Neuromethods*. https://doi.org/10.1007/978-1-60761-303-9-11

Haznedar, M. M., Buchsbaum, M. S., Wei, T. C., Hof, P. R., Cartwright, C., Bienstock, C. A., & Hollander, E. (2000). Limbic circuitry in patients with autism spectrum disorders studied with positron emission tomography and magnetic resonance imaging. *Am J Psychiatry*, *157*(12), 1994–2001.

Henckens, M. J. A. G., van der Marel, K., van der Toorn, A., Pillai, A. G., Fernández, G., Dijkhuizen, R. M., & Joëls, M. (2015). Stress-induced alterations in large-scale functional networks of the rodent brain. *NeuroImage*, *105*, 312–322. https://doi.org/10.1016/j.neuroimage.2014.10.037

Herman, J. P., Ostrander, M. M., Mueller, N. K., & Figueiredo, H. (2005). Limbic system mechanisms of stress regulation: Hypothalamo-pituitary- adrenocortical axis. *Progress in Neuro-Psychopharmacology and Biological Psychiatry*. https://doi.org/10.1016/j.pnpbp.2005.08.006

Hilgetag, C. C., Burns, G. A., O'Neill, M. A., Scannell, J. W., & Young, M. P. (2000). Anatomical connectivity defines the organization of clusters of cortical areas in the macaque monkey and the cat. *Philos Trans R Soc Lond B Biol Sci*, *355*(1393), 91–110. Retrieved from

http://www.ncbi.nlm.nih.gov/entrez/query.fcgi?cmd=Retrieve&db=PubMed&dopt=Citation

&list_uids=10703046

Honey, C. J., Sporns, O., Cammoun, L., Gigandet, X., Thiran, J. P., Meuli, R., & Hagmann, P.

(2009). Predicting human resting-state functional connectivity from structural connectivity.

Proc Natl Acad Sci USA, *106*(6), 2035–2040. https://doi.org/10.1073/pnas.0811168106

Hsiao, E. Y., & Patterson, P. H. (2011). Activation of the maternal immune system induces

endocrine changes in the placenta via IL-6. *Brain, Behavior, and Immunity*, *25*(4), 604–615.

https://doi.org/10.1016/j.bbi.2010.12.017

Hunter, C. A., & Jones, S. A. (2015). IL-6 as a keystone cytokine in health and disease. *Nature*

Immunology. https://doi.org/10.1038/ni.3153

Hutchison, R. M., Mirsattari, S. M., Jones, C. K., Gati, J. S., & Leung, L. S. (2010). Functional

networks in the anesthetized rat brain revealed by independent component analysis of

resting-state FMRI. *Journal of Neurophysiology*, *103*(6), 3398–406.

https://doi.org/10.1152/jn.00141.2010

Ikemoto, S., & Panksepp, J. (1992). The effects of early social isolation on the motivation for

social play in juvenile rats. *Developmental Psychobiology*, *25*(4), 261–74.

https://doi.org/10.1002/dev.420250404

Inagaki, T. K., Muscatell, K. A., Irwin, M. R., Cole, S. W., & Eisenberger, N. I. (2012).

Inflammation selectively enhances amygdala activity to socially threatening images.

NeuroImage, *59*(4), 3222–3226. https://doi.org/10.1016/j.neuroimage.2011.10.090

Jonckers, E., Delgado y Palacios, R., Shah, D., Guglielmetti, C., Verhoye, M., & Van der

Linden, A. (2014). Different anesthesia regimes modulate the functional connectivity

outcome in mice. *Magnetic Resonance in Medicine*, *72*(4), 1103–1112.

https://doi.org/10.1002/mrm.24990

Jonckers, E., Van Audekerke, J., De Visscher, G., Van der Linden, A., & Verhoye, M. (2011). Functional connectivity fMRI of the rodent brain: comparison of functional connectivity networks in rat and mouse. *PLoS One*, *6*(4), e18876. https://doi.org/10.1371/journal.pone.0018876

Jones, K. L., Croen, L. A., Yoshida, C. K., Heuer, L., Hansen, R., Zerbo, O., … Van de Water, J. (2016). Autism with intellectual disability is associated with increased levels of maternal cytokines and chemokines during gestation. *Molecular Psychiatry*, (January), 1–7. https://doi.org/10.1038/mp.2016.77

Kang, S. S., Kurti, A., Fair, D. A., & Fryer, J. D. (2014). Dietary intervention rescues maternal obesity induced behavior deficits and neuroinflammation in offspring. *Journal of Neuroinflammation*, *11*(1), 156. https://doi.org/10.1186/PREACCEPT-1047692381265837

Kemna, E., Pickkers, P., Nemeth, E., Van Der Hoeven, H., & Swinkels, D. (2005). Time-course analysis of hepcidin, serum iron, and plasma cytokine levels in humans injected with LPS. *Blood*, *106*(5), 1864–1866. https://doi.org/10.1182/blood-2005-03-1159

Kiecolt-Glaser, J. K., Preacher, K. J., MacCallum, R. C., Atkinson, C., Malarkey, W. B., & Glaser, R. (2003). Chronic stress and age-related increases in the proinflammatory cytokine IL-6. *Proceedings of the National Academy of Sciences*, *100*(15), 9090–9095. https://doi.org/10.1073/pnas.1531903100

Knuesel, I., Chicha, L., Britschgi, M., Schobel, S. A., Bodmer, M., Hellings, J. A., … Prinssen, E. P. (2014). Maternal immune activation and abnormal brain development across CNS disorders. *Nature Reviews Neurology*, *10*(11), 643–660. https://doi.org/10.1038/nrneurol.2014.187

Kufahl, P. R., Peartree, N. A., Heintzelman, K. L., Chung, M., & Neisewander, J. L. (2015). Region-specific effects of isoflurane anesthesia on Fos immunoreactivity in response to intravenous cocaine challenge in rats with a history of repeated cocaine administration. *Brain Research*, *1594*, 256–66. https://doi.org/10.1016/j.brainres.2014.10.027

Kufahl, P. R., Pentkowski, N. S., Heintzelman, K., & Neisewander, J. L. (2009). Cocaine-induced Fos expression is detectable in the frontal cortex and striatum of rats under isoflurane but not α-chloralose anesthesia: Implications for FMRI. *Journal of Neuroscience Methods*, *181*(2), 241–248. https://doi.org/10.1016/j.jneumeth.2009.05.012

Lancaster, J. L., Glass, T. G., Lankipalli, B. R., Downs, H., Mayberg, H., & Fox, P. T. (1995). A Modality-Independent Approach to Spatial Normalization of Tomographic Images of the Human Brain. *Human Brain Mapping*, *3*, 209–223.

Lang, R., Regester, A., Lauderdale, S., Ashbaugh, K., & Haring, A. (2010). Treatment of anxiety in autism spectrum disorders using cognitive behaviour therapy: A systematic review. *Developmental Neurorehabilitation*. https://doi.org/10.3109/17518420903236288

Le Belle, J. E., Sperry, J., Ngo, A., Ghochani, Y., Laks, D. R., López-Aranda, M., … Kornblum, H. I. (2014). Maternal inflammation contributes to brain overgrowth and autism-associated behaviors through altered redox signaling in stem and progenitor cells. *Stem Cell Reports*, *3*(5), 725–734. https://doi.org/10.1016/j.stemcr.2014.09.004

Lee, J. H., Gradinaru, V., Zhang, F., Goshen, I., Kim, D., Fenno, L. E., … Deisseroth, K. (2010). Global and local fMRI signals driven by neurons defined optogenetically by type and wiring. *Nature*, *465*(10), 788–792.

Lein, E. S., Hawrylycz, M. J., Ao, N., Ayres, M., Bensinger, A., Bernard, A., … Jones, A. R. (2007). Genome-wide atlas of gene expression in the adult mouse brain. *Nature*, *445*(7124),

168–176. https://doi.org/10.1038/nature05453

Lenczowski, M. J. P., Bluthé, R. M., Roth, J., Rees, G. S., Rushforth, D. A., van Dam, A.-M. M., … Luheshi, G. N. (1999). Central administration of rat IL-6 induces HPA activation and fever but not sickness behavior in rats. *The American Journal of Physiology. Regulatory, Integrative and Comparative Physiology*, *276*, R652–R658. Retrieved from http://ajpregu.physiology.org/content/276/3/R652

Li, Q., Cheung, C., Wei, R., Cheung, V., Hui, E. S., You, Y., … Wu, E. X. (2010). Voxel-based analysis of postnatal white matter microstructure in mice exposed to immune challenge in early or late pregnancy. *NeuroImage*, *52*(1), 1–8. https://doi.org/10.1016/j.neuroimage.2010.04.015

Li, Q., Cheung, C., Wei, R., Hui, E. S., Feldon, J., Meyer, U., … McAlonan, G. M. (2009). Prenatal immune challenge is an environmental risk factor for brain and behavior change relevant to schizophrenia: Evidence from MRI in a mouse model. *PLoS ONE*, *4*(7). https://doi.org/10.1371/journal.pone.0006354

Liang, Z., King, J., & Zhang, N. (2011). Uncovering intrinsic connectional architecture of functional networks in awake rat brain. *The Journal of Neuroscience : The Official Journal of the Society for Neuroscience*, *31*(10), 3776–83. https://doi.org/10.1523/JNEUROSCI.4557-10.2011

Lin, Y. L., Lin, S. Y., & Wang, S. (2012). Prenatal lipopolysaccharide exposure increases anxiety-like behaviors and enhances stress-induced corticosterone responses in adult rats. *Brain, Behavior, and Immunity*, *26*(3), 459–468. https://doi.org/10.1016/j.bbi.2011.12.003

Lin, Y. L., & Wang, S. (2014). Prenatal lipopolysaccharide exposure increases depression-like behaviors and reduces hippocampal neurogenesis in adult rats. *Behavioural Brain Research*,

259, 24–34. https://doi.org/10.1016/j.bbr.2013.10.034

Logothetis, N. K., Pauls, J., Augath, M., Trinath, T., & Oeltermann, A. (2001).

Neurophysiological investigation of the basis of the fMRI signal. *Nature*, *412*, 150–157.

Lombardo, M. V., Moon, H. M., Su, J., Palmer, T. D., Courchesne, E., & Pramparo, T. (2017).

Maternal immune activation dysregulation of the fetal brain transcriptome and relevance to

the pathophysiology of autism spectrum disorder. *Molecular Psychiatry*.

https://doi.org/10.1038/mp.2017.15

Lu, H., & Stein, E. A. (2014). Resting state functional connectivity: Its physiological basis and

application in neuropharmacology. *Neuropharmacology*, *84*, 79–89.

https://doi.org/10.1016/j.neuropharm.2013.08.023

Lu, H., Zou, Q., Gu, H., Raichle, M. E., Stein, E. A., & Yang, Y. (2012). Rat brains also have a

default mode network. *Proceedings of the National Academy of Sciences of the United

States of America*, *109*(10), 3979–84. https://doi.org/10.1073/pnas.1200506109

Magistretti, P. J., & Allaman, I. (2015). A Cellular Perspective on Brain Energy Metabolism and

Functional Imaging. *Neuron*, *86*(4), 883–901. https://doi.org/10.1016/j.neuron.2015.03.035

Majeed, W., Magnuson, M., Hasenkamp, W., Schwarb, H., Schumacher, E. H., Barsalou, L., &

Keilholz, S. D. (2011). Spatiotemporal dynamics of low frequency BOLD fluctuations in

rats and humans. *NeuroImage*, *54*(2), 1140–50.

https://doi.org/10.1016/j.neuroimage.2010.08.030

Malkova, N. V., Yu, C. Z., Hsiao, E. Y., Moore, M. J., & Patterson, P. H. (2012). Maternal

immune activation yields offspring displaying mouse versions of the three core symptoms

of autism. *Brain, Behavior, and Immunity*, *26*(4), 607–616.

https://doi.org/10.1016/j.bbi.2012.01.011

Malonek, D., Dirnagl, U., Lindauer, U., Yamada, K., Kanno, I., & Grinvald, A. (1997). Vascular

imprints of neuronal activity: Relationships between the dynamics of cortical blood flow,

oxygenation, and volume changes following sensory stimulation. *Proceedings of the*

National Academy of Sciences of the United States of America, *94*(26), 14826–14831.

https://doi.org/10.1073/pnas.94.26.14826

Markov, N. T., Ercsey-Ravasz, M. M., Ribeiro Gomes, a R., Lamy, C., Magrou, L., Vezoli, J.,

… Kennedy, H. (2014). A weighted and directed interareal connectivity matrix for macaque

cerebral cortex. *Cerebral Cortex (New York, N.Y. : 1991)*, *24*(1), 17–36.

https://doi.org/10.1093/cercor/bhs270

Masamoto, K., & Kanno, I. (2012). Anesthesia and the quantitative evaluation of neurovascular

coupling. *Journal of Cerebral Blood Flow and Metabolism*.

https://doi.org/10.1038/jcbfm.2012.50

Maximo, J. O., Cadena, E. J., & Kana, R. K. (2014). The implications of brain connectivity in

the neuropsychology of autism. *Neuropsychology Review*. https://doi.org/10.1007/s11065-

014-9250-0

Meila, M. (2007). Comparing clusterings - an information based distance. *Journal of*

Multivariate Analysis, (5), 873–895.

Messé, A., Rudrauf, D., Benali, H., Marrelec, G., & Honey, C. (2014). Relating Structure and

Function in the Human Brain: Relative Contributions of Anatomy, Stationary Dynamics,

and Non-stationarities. *PLoS Computational Biology*, *10*(3), e1003530.

https://doi.org/10.1371/journal.pcbi.1003530

Meyer, U. (2014). Prenatal Poly(I:C) exposure and other developmental immune activation

models in rodent systems. *Biological Psychiatry*, *75*(4), 307–315.

https://doi.org/10.1016/j.biopsych.2013.07.011

Meyer, U., & Feldon, J. (2012). To poly(I:C) or not to poly(I:C): Advancing preclinical
schizophrenia research through the use of prenatal immune activation models.
Neuropharmacology, *62*(3), 1308–1321. https://doi.org/10.1016/j.neuropharm.2011.01.009

Meyer, U., Feldon, J., & Dammann, O. (2011). Schizophrenia and autism: Both shared and
disorder-specific pathogenesis via perinatal inflammation? *Pediatric Research*, *69*(5 PART
2). https://doi.org/10.1203/PDR.0b013e318212c196

Meyer, U., Nyffeler, M., Yee, B. K., Knuesel, I., & Feldon, J. (2008). Adult brain and behavioral
pathological markers of prenatal immune challenge during early/middle and late fetal
development in mice. *Brain, Behavior, and Immunity*, *22*(4), 469–486.
https://doi.org/10.1016/j.bbi.2007.09.012

Michaelides, M., Anderson, S. A. R., Ananth, M., Smirnov, D., Thanos, P. K., Neumaier, J. F.,
… Hurd, Y. L. (2013). Whole-brain circuit dissection in free-moving animals reveals cell-
specific mesocorticolimbic networks. *Journal of Clinical Investigation*, *123*(12), 5342–
5350. https://doi.org/10.1172/JCI72117

Mills, B. D., Pearce, H. L., Khan, O., Jarrett, B. R., Fair, D. A., & Lahvis, G. P. (2016). Prenatal
domoic acid exposure disrupts mouse pro-social behavior and functional connectivity MRI.
Behavioural Brain Research, *308*, 14–23. https://doi.org/10.1016/j.bbr.2016.03.039

Miranda-Domínguez, Ó., Mills, B. D., Grayson, D., Woodall, A., Grant, K. A., Kroenke, C. D.,
& Fair, D. A. (2014). Bridging the gap between the human and macaque connectome: a
quantitative comparison of global interspecies structure-function relationships and network
topology. *The Journal of Neuroscience : The Official Journal of the Society for
Neuroscience*, *34*(16), 5552–5563. https://doi.org/10.1523/JNEUROSCI.4229-13.2014

Mitchell, R. H. B., & Goldstein, B. I. (2014). Inflammation in Children and Adolescents With

    Neuropsychiatric Disorders: A Systematic Review. *Journal of the American Academy of*

    Child & Adolescent Psychiatry, *53*(3), 274–296. https://doi.org/10.1016/j.jaac.2013.11.013

Monk, C. S. (2008). The development of emotion-related neural circuitry in health and

    psychopathology. *Dev Psychopathol*, *20*(4), 1231–1250.

    https://doi.org/S095457940800059X [pii]10.1017/S095457940800059X

Monteiro, R., & Azevedo, I. (2010). Chronic inflammation in obesity and the metabolic

    syndrome. *Mediators of Inflammation*. https://doi.org/10.1155/2010/289645

Moy, S. S., Nadler, J. J., Perez, A., Barbaro, R. P., Johns, J. M., Magnuson, T. R., … Crawley, J.

    N. (2004). Sociability and preference for social novelty in five inbred strains: An approach

    to assess autistic-like behavior in mice. *Genes, Brain and Behavior*, *3*(5), 287–302.

    https://doi.org/10.1111/j.1601-1848.2004.00076.x

Murphy, K., Birn, R. M., Handwerker, D. a, Jones, T. B., & Bandettini, P. a. (2009). The impact

    of global signal regression on resting state correlations: are anti-correlated networks

    introduced? *NeuroImage*, *44*(3), 893–905.

    https://doi.org/10.1016/j.neuroimage.2008.09.036

Murphy, K., & Fox, M. D. (2017). Towards a consensus regarding global signal regression for

    resting state functional connectivity MRI. *NeuroImage*, *154*, 169–173.

    https://doi.org/10.1016/j.neuroimage.2016.11.052

Nakanishi, M., Niidome, T., Matsuda, S., Akaike, A., Kihara, T., & Sugimoto, H. (2007).

    Microglia-derived interleukin-6 and leukaemia inhibitory factor promote astrocytic

    differentiation of neural stem/progenitor cells. *European Journal of Neuroscience*, *25*(3),

    649–658. https://doi.org/10.1111/j.1460-9568.2007.05309.x

Nasrallah, F. A., Tay, H.-C., & Chuang, K.-H. (2014). Detection of functional connectivity in the

    resting mouse brain. *NeuroImage*, *86*, 417–24.

    https://doi.org/10.1016/j.neuroimage.2013.10.025

Nie, B., Chen, K., Zhao, S., Liu, J., Gu, X., Yao, Q., … Shan, B. (2013). A rat brain MRI

    template with digital stereotaxic atlas of fine anatomical delineations in paxinos space and

    its automated application in voxel-wise analysis. *Human Brain Mapping*, *34*(6), 1306–18.

    https://doi.org/10.1002/hbm.21511

Nomi, J. S., & Uddin, L. Q. (2015). Developmental changes in large-scale network connectivity

    in autism. *NeuroImage: Clinical*, *7*, 732–741. https://doi.org/10.1016/j.nicl.2015.02.024

Nordahl, C. W., Scholz, R., Yang, X., Buonocore, M. H., Simon, T., Rogers, S., & Amaral, D. G.

    (2012). Increased rate of amygdala growth in children aged 2 to 4 years with autism

    spectrum disorders: a longitudinal study. *Archives of General Psychiatry*, *69*(1), 53–61.

    https://doi.org/10.1001/archgenpsychiatry.2011.145

Nusslock, R., & Miller, G. E. (2016). Early-life adversity and physical and emotional health

    across the lifespan: A neuroimmune network hypothesis. *Biological Psychiatry*.

    https://doi.org/10.1016/j.biopsych.2015.05.017

Ogawa, S., Lee, T. M., Kay, A. R., & Tank, D. W. (1990). Brain magnetic resonance imaging

    with contrast dependent on blood oxygenation. *Proceedings of the National Academy of

    Sciences*, *87*, 9868–9872.

Oh, S. W., Harris, J. A., Ng, L., Winslow, B., Cain, N., Mihalas, S., … Zeng, H. (2014). A

    mesoscale connectome of the mouse brain. *Nature*, *508*(7495), 207–214.

    https://doi.org/10.1038/nature13186

Onore, C., Careaga, M., & Ashwood, P. (2012). The role of immune dysfunction in the

pathophysiology of autism. *Brain, Behavior, and Immunity*.

https://doi.org/10.1016/j.bbi.2011.08.007

Palmer, H. S. (2010). Optogenetic fMRI Sheds Light on the Neural Basis of the BOLD Signal.

Journal of Neurophysiology, *104*(4), 1838–1840. https://doi.org/10.1152/jn.00535.2010

Palomero-Gallagher, N., Mohlberg, H., Zilles, K., & Vogt, B. (2008). Cytology and receptor

architecture of human anterior cingulate cortex. *Journal of Comparative Neurology*, *508*(6),

906–926. https://doi.org/10.1002/cne.21684

Palomero-Gallagher, N., Vogt, B. A., Schleicher, A., Mayberg, H. S., & Zilles, K. (2009).

Receptor architecture of human cingulate cortex: Evaluation of the four-region

neurobiological model. *Human Brain Mapping*, *30*(8), 2336–2355.

https://doi.org/10.1002/hbm.20667

Pantazatos, S. P., & Li, X. (2017). Commentary: Brain networks. Correlated gene expression

supports synchronous activity in brain networks. Science 348, 1241-4. *Frontiers in

Neuroscience*, *11*(JUL). https://doi.org/10.3389/fnins.2017.00412

Paolicelli, R. C., Bolasco, G., Pagani, F., Maggi, L., Scianni, M., Panzanelli, P., … Gross, C. T.

(2011). Synaptic pruning by microglia is necessary for normal brain development. *Science*,

333(6048), 1456–1458. https://doi.org/10.1126/science.1202529

Parker-Athill, E. C., & Tan, J. (2011). Maternal immune activation and autism spectrum

disorder: Interleukin-6 signaling as a key mechanistic pathway. *NeuroSignals*, *18*(2), 113–

128. https://doi.org/10.1159/000319828

Patterson, P. H. (2011). Maternal infection and immune involvement in autism. *Trends in

Molecular Medicine*, *17*(7), 389–94. https://doi.org/10.1016/j.molmed.2011.03.001

Pawela, C. P., Biswal, B. B., Cho, Y. R., Kao, D. S., Li, R., Jones, S. R., … Hyde, J. S. (2008).

Resting-state functional connectivity of the rat brain. *Magnetic Resonance in Medicine : Official Journal of the Society of Magnetic Resonance in Medicine / Society of Magnetic Resonance in Medicine*, *59*(5), 1021–9. https://doi.org/10.1002/mrm.21524

Paxinos, G., & Franklin, K. B. J. (2007). *The Mouse Brain in Stereotaxic Coordinates, Third Edition* (3rd ed.). Academic Press.

Petersen, S. E., & Sporns, O. (2015). Brain Networks and Cognitive Architectures. *Neuron*, *88*(1), 207–219. https://doi.org/10.1016/j.neuron.2015.09.027

Power, J., Cohen, A., Nelson, S., Wig, G., Barnes, K., Church, J., … Petersen, S. (2011). Functional network organization of the human brain. *Neuron*, *72*(4), 665–678. https://doi.org/10.1016/j.neuron.2011.09.006

Power, J., Mitra, A., Laumann, T., Snyder, A., Schlaggar, B., & Petersen, S. (2014). Methods to detect, characterize, and remove motion artifact in resting state fMRI. *Neuroimage*, *84*, 320–341. https://doi.org/10.1016/j.neuroimage.2013.08.048

Power, J., Schlaggar, B., Lessov-Schlaggar, C., & Petersen, S. (2013). Evidence for hubs in human functional brain networks. *Neuron*, *79*(4), 798–813. https://doi.org/10.1016/j.neuron.2013.07.035

Qiu, A., Anh, T. T., Li, Y., Chen, H., Rifkin-Graboi, A., Broekman, B. F. P., … Meaney, M. J. (2015). Prenatal maternal depression alters amygdala functional connectivity in 6-month-old infants. *Translational Psychiatry*, *5*(2). https://doi.org/10.1038/tp.2015.3

Raichle, M. E. (2001). Cognitive neuroscience. Bold insights. *Nature*, *412*(6843), 128–130. Retrieved from http://www.ncbi.nlm.nih.gov/entrez/query.fcgi?cmd=Retrieve&db=PubMed&dopt=Citation&list_uids=11449247

Raichle, M. E. (2015). The brain's default mode network. *Annual Review of Neuroscience*, *38*(April), 433–447. https://doi.org/10.1146/annurev-neuro-071013-014030

Raichle, M. E., MacLeod, A. M., Snyder, A. Z., Powers, W. J., Gusnard, D. A., & Shulman, G. L. (2001). Inaugural Article: A default mode of brain function. *Proceedings of National Academy of Sciences, USA*, *98*(2), 676–682. Retrieved from http://www.ncbi.nlm.nih.gov/htbin-post/Entrez/query?db=m&form=6&dopt=r&uid=11209064

Ran, F. A., Hsu, P. D., Wright, J., Agarwala, V., Scott, D. A., & Zhang, F. (2013). Genome engineering using the CRISPR-Cas9 system. *Nature Protocols*, *8*(11), 2281–2308. https://doi.org/10.1038/nprot.2013.143

Rausch, A., Zhang, W., Haak, K. V., Mennes, M., Hermans, E. J., Van Oort, E., … Groen, W. B. (2016). Altered functional connectivity of the amygdaloid input nuclei in adolescents and young adults with autism spectrum disorder: A resting state fMRI study. *Molecular Autism*, *7*(1). https://doi.org/10.1186/s13229-015-0060-x

Richiardi, J., Altmann, A., & Greicius, M. (2017). Distance Is Not Everything In Imaging Genomics Of Functional Networks: Reply To A Commentary On Correlated Gene Expression Supports Synchronous Activity In Brain Networks *bioRxiv*, 1–10. https://doi.org/10.1101/132746

Richiardi, J., Altmann, A., Milazzo, A.-C., Chang, C., Chakravarty, M. M., Banaschewski, T., … consortium, I. (2015). BRAIN NETWORKS. Correlated gene expression supports synchronous activity in brain networks. *Science (New York, N.Y.)*, *348*(6240), 1241–1244. https://doi.org/10.1126/science.1255905

Ring, H., Woodbury-Smith, M., Watson, P., Wheelwright, S., & Baron-Cohen, S. (2008).

Clinical heterogeneity among people with high functioning autism spectrum conditions: evidence favouring a continuous severity gradient. *Behavioral and Brain Functions*, *4*(11).

Ronald, A., Pennell, C. E., & Whitehouse, A. J. O. (2010). Prenatal Maternal Stress Associated with ADHD and Autistic Traits in early Childhood. *Frontiers in Psychology*, *1*, 223. https://doi.org/10.3389/fpsyg.2010.00223

Rosvall, M., & Bergstrom, C. T. (2008). Maps of random walks on complex networks reveal community structure. *Proceedings of the National Academy of Sciences of the United States of America*, *105*(4), 1118–1123 %U http://www.ncbi.nlm.nih.gov.beckerpro.

Roy, A. K., Shehzad, Z., Margulies, D. S., Kelly, a M. C., Uddin, L. Q., Gotimer, K., … Milham, M. P. (2009). Functional connectivity of the human amygdala using resting state fMRI. *NeuroImage*, *45*(2), 614–26. https://doi.org/10.1016/j.neuroimage.2008.11.030

Rubinov, M., & Sporns, O. (2011). Weight-conserving characterization of complex functional brain networks. *Neuroimage*, *56*(4), 2068–2079. https://doi.org/10.1016/j.neuroimage.2011.03.069

Samuelsson, A.-M., Jennische, E., Hansson, H.-A., & Holmäng, A. (2006). Prenatal exposure to interleukin-6 results in inflammatory neurodegeneration in hippocampus with NMDA/GABA(A) dysregulation and impaired spatial learning. *American Journal of Physiology. Regulatory, Integrative and Comparative Physiology*, *290*(5), R1345-56. https://doi.org/10.1152/ajpregu.00268.2005

Sanz-Leon, P., Knock, S. A., Spiegler, A., & Jirsa, V. K. (2015). Mathematical framework for large-scale brain network modeling in The Virtual Brain. *NeuroImage*, *111*, 385–430. https://doi.org/10.1016/j.neuroimage.2015.01.002

Sasaki, A., de Vega, W. C., St-Cyr, S., Pan, P., & McGowan, P. O. (2013). Perinatal high fat diet

alters glucocorticoid signaling and anxiety behavior in adulthood. *Neuroscience*, *240*, 1–12. https://doi.org/10.1016/j.neuroscience.2013.02.044

Scheinost, D., Kwon, S. H., Lacadie, C., Sze, G., Sinha, R., Constable, R. T., & Ment, L. R. (2016). Prenatal stress alters amygdala functional connectivity in preterm neonates. *NeuroImage: Clinical*, *12*, 381–388. https://doi.org/10.1016/j.nicl.2016.08.010

Scholvinck, M. L., Maier, A., Ye, F. Q., Duyn, J. H., & Leopold, D. A. (2010). Neural basis of global resting-state fMRI activity. *Proc Natl Acad Sci U S A*, *107*(22), 10238–10243. https://doi.org/10.1073/pnas.0913110107

Schumann, C. M. (2004). The Amygdala Is Enlarged in Children But Not Adolescents with Autism; the Hippocampus Is Enlarged at All Ages. *Journal of Neuroscience*, *24*(28), 6392–6401. https://doi.org/10.1523/JNEUROSCI.1297-04.2004

Schwartzer, J. J., Careaga, M., Onore, C. E., Rushakoff, J. A., Berman, R. F., & Ashwood, P. (2013). Maternal immune activation and strain specific interactions in the development of autism-like behaviors in mice. *Translational Psychiatry*, *3*. https://doi.org/10.1038/tp.2013.16

Schwarz, A. J., Danckaert, A., Reese, T., Gozzi, A., Paxinos, G., Watson, C., … Bifone, A. (2006). A stereotaxic MRI template set for the rat brain with tissue class distribution maps and co-registered anatomical atlas: Application to pharmacological MRI. *NeuroImage*, *32*(2), 538–550. https://doi.org/10.1016/j.neuroimage.2006.04.214

Schwarz, A. J., Gozzi, A., Reese, T., & Bifone, A. (2007). In vivo mapping of functional connectivity in neurotransmitter systems using pharmacological MRI. *NeuroImage*, *34*(4), 1627–1636. https://doi.org/10.1016/j.neuroimage.2006.11.010

Scott A. Huettel; Allen W. Song; Gregory McCarthy, Huettel, Scott; Song, A., Beckmann, C. F.,

Smith, S. M., Huettel, S. a., Song, A. W., & McCarthy, G. (2004). *Functional Magnetic Resonance Imaging*. *Book* (Vol. 23).

Seeley, W. W., Crawford, R. K., Zhou, J., Miller, B. L., & Greicius, M. D. (2009). Neurodegenerative diseases target large-scale human brain networks. *Neuron*, *62*(1), 42–52 %U http://www.ncbi.nlm.nih.gov.beckerproxy.w.

Semple, B. D., Blomgren, K., Gimlin, K., Ferriero, D. M., & Noble-Haeusslein, L. J. (2013). Brain development in rodents and humans: Identifying benchmarks of maturation and vulnerability to injury across species. *Progress in Neurobiology*. https://doi.org/10.1016/j.pneurobio.2013.04.001

Sforazzini, F., Schwarz, A. J., Galbusera, A., Bifone, A., & Gozzi, A. (2014). Distributed BOLD and CBV-weighted resting-state networks in the mouse brain. *NeuroImage*, *87*, 403–15. https://doi.org/10.1016/j.neuroimage.2013.09.050

Shah, D., Jonckers, E., Praet, J., Vanhoutte, G., Delgado y Palacios, R., Bigot, C., … Van der Linden, A. (2013). Resting State fMRI Reveals Diminished Functional Connectivity in a Mouse Model of Amyloidosis. *PLoS ONE*, *8*(12), e84241. https://doi.org/10.1371/journal.pone.0084241

Shaw, P., Gogtay, N., & Rapoport, J. (2010). Childhood psychiatric disorders as anomalies in neurodevelopmental trajectories. *Human Brain Mapping*, *31*(6), 917–25. https://doi.org/10.1002/hbm.21028

Shekhar, A. (1993). GABA receptors in the region of the dorsomedial hypothalamus of rats regulate anxiety in the elevated plus-maze test. I. Behavioral measures. *Brain Research*, *627*(1), 9–16. https://doi.org/10.1016/0006-8993(93)90742-6

Shekhar, A., Hingtgen, J. N., & DiMicco, J. A. (1990). GABA receptors in the posterior

hypothalamus regulate experimental anxiety in rats. *Brain Research*, *512*(1), 81–88. https://doi.org/10.1016/0006-8993(90)91173-E

Shen, M. D., Li, D. D., Keown, C. L., Lee, A., Johnson, R. T., Angkustsiri, K., … Nordahl, C. W. (2016). Functional Connectivity of the Amygdala Is Disrupted in Preschool-Aged Children With Autism Spectrum Disorder. *Journal of the American Academy of Child & Adolescent Psychiatry*, *55*(9), 817–824. https://doi.org/10.1016/j.jaac.2016.05.020

Short, S. J., Lubach, G. R., Karasin, A. I., Olsen, C. W., Styner, M., Knickmeyer, R. C., … Coe, C. L. (2010). Maternal Influenza Infection During Pregnancy Impacts Postnatal Brain Development in the Rhesus Monkey. *Biological Psychiatry*, *67*(10), 965–973. https://doi.org/10.1016/j.biopsych.2009.11.026

Shulman, G. L., Fiez, J. A., Corbetta, M., Buckner, R. L., Miezin, F. M., Raichle, M. E., & Petersen, S. E. (1997). Common blood flow changes across visual tasks: II. Decreases in cerebral cortex. *J Cogn Neurosci*, *9*, 648–663.

Smith, M., Li, J., Cote, D., & Ryabinin, A. (2016). Effects of isoflurane and ethanol administration on c-Fos immunoreactivity in mice. *Neuroscience*, *316*, 337–343. https://doi.org/10.1016/j.neuroscience.2015.12.047

Smith, S., Li, J., Garbett, K., Mirnics, K., & Patterson, P. (2007). Maternal immune activation alters fetal brain development through interleukin-6. *Journal of Neuroscience*, *27*(40), 10695–10702. https://doi.org/10.1523/JNEUROSCI.2178-07.2007

Smith, S. M., Jenkinson, M., Woolrich, M. W., Beckmann, C. F., Behrens, T. E. J., Johansen-Berg, H., … Matthews, P. M. (2004). Advances in functional and structural MR image analysis and implementation as FSL. *NeuroImage*, *23 Suppl 1*, S208--19. https://doi.org/10.1016/j.neuroimage.2004.07.051

Sporns, O. (2011). The human connectome: a complex network. *Annals of the New York Academy of Sciences*, *1224*, 109–25. https://doi.org/10.1111/j.1749-6632.2010.05888.x

Sporns, O. (2013). Structure and function of complex brain networks. *Dialogues in Clinical Neuroscience*, *15*(3), 247–262. https://doi.org/10.1137/S003614450342480

Sporns, O., Honey, C. J., & Kötter, R. (2007). Identification and classification of hubs in brain networks. *PloS One*, *2*(10), e1049. https://doi.org/10.1371/journal.pone.0001049

Stafford, J. M., Jarrett, B. R., Miranda-Dominguez, O., Mills, B. D., Cain, N., Mihalas, S., … Fair, D. A. (2014). Large-scale topology and the default mode network in the mouse connectome. *Proceedings of the National Academy of Sciences*, *111*(52), 18745–18750. https://doi.org/10.1073/pnas.1404346111

Stanfield, A. C., McIntosh, A. M., Spencer, M. D., Philip, R., Gaur, S., & Lawrie, S. M. (2008). Towards a neuroanatomy of autism: a systematic review and meta-analysis of structural magnetic resonance imaging studies. *Eur Psychiatry*, *23*(4), 289–299. https://doi.org/10.1016/j.eurpsy.2007.05.006

Sullivan, E. L., Grayson, B., Takahashi, D., Robertson, N., Maier, A., Bethea, C. L., … Grove, K. L. (2010). Chronic consumption of a high-fat diet during pregnancy causes perturbations in the serotonergic system and increased anxiety-like behavior in nonhuman primate offspring. *The Journal of Neuroscience : The Official Journal of the Society for Neuroscience*, *30*(10), 3826–30. https://doi.org/10.1523/JNEUROSCI.5560-09.2010

Sullivan, E. L., Nousen, E. K., & Chamlou, K. A. (2014). Maternal high fat diet consumption during the perinatal period programs offspring behavior. *Physiology & Behavior*, *123*, 236–42. https://doi.org/10.1016/j.physbeh.2012.07.014

Supekar, K., Musen, M., & Menon, V. (2009). Development of large-scale functional brain

networks in children. *PLoS Biol*, *7*(7), e1000157.

https://doi.org/10.1371/journal.pbio.1000157

Supekar, K., Musen, M., & Menon, V. (2009). Development of large-scale functional brain

networks in children. *PLoS Biol*, *7*(7), e1000157.

https://doi.org/10.1371/journal.pbio.1000157

Szatmari, P., Georgiades, S., Duku, E., Bennett, T. A., Bryson, S., Fombonne, E., … Pathways in

ASD Study Team. (2015). Developmental trajectories of symptom severity and adaptive

functioning in an inception cohort of preschool children with autism spectrum disorder.

JAMA Psychiatry, *72*(3), 276–83. https://doi.org/10.1001/jamapsychiatry.2014.2463

Talge, N. M., Neal, C., & Glover, V. (2007). Antenatal maternal stress and long-term effects on

child neurodevelopment: how and why? *Journal of Child Psychology and Psychiatry*, *48*(3–

4), 245–261. https://doi.org/10.1111/j.1469-7610.2006.01714.x

Teicher, M. H., Andersen, S. L., Polcari, A., Anderson, C. M., Navalta, C. P., & Kim, D. M.

(2003). The neurobiological consequences of early stress and childhood maltreatment. In

Neuroscience and Biobehavioral Reviews (Vol. 27, pp. 33–44).

https://doi.org/10.1016/S0149-7634(03)00007-1

Toal, F., Daly, E. M., Page, L., Deeley, Q., Hallahan, B., Bloemen, O., … Murphy, D. G. (2010).

Clinical and anatomical heterogeneity in autistic spectrum disorder: a structural MRI study.

Psychol Med, *40*(7), 1171–1181. https://doi.org/10.1017/s0033291709991541

Tomasi, D., Wang, G. J., & Volkow, N. D. (2013). Energetic cost of brain functional

connectivity. *Proc Natl Acad Sci U S A*, *110*(33), 13642–13647.

https://doi.org/10.1073/pnas.1303346110

Tromp, D. P. M., Grupe, D. W., Oathes, D. J., McFarlin, D. R., Hernandez, P. J., Kral, T. R. a,

… Nitschke, J. B. (2012). Reduced structural connectivity of a major frontolimbic pathway in generalized anxiety disorder. *Archives of General Psychiatry*, *69*(9), 925–34. https://doi.org/10.1001/archgenpsychiatry.2011.2178

Turk, E., Scholtens, L. H., & van den Heuvel, M. P. (2016). Cortical chemoarchitecture shapes macroscale effective functional connectivity patterns in macaque cerebral cortex. *Human Brain Mapping*, *37*(5), 1856–1865. https://doi.org/10.1002/hbm.23141

Uddin, L. Q., Supekar, K., & Menon, V. (2010). Typical and atypical development of functional human brain networks: insights from resting-state FMRI. *Front Syst Neurosci*, *4*(May), 21. https://doi.org/10.3389/fnsys.2010.00021

Uddin, L. Q., Supekar, K., & Menon, V. (2013). Reconceptualizing functional brain connectivity in autism from a developmental perspective. *Frontiers in Human Neuroscience*, *7*. https://doi.org/10.3389/fnhum.2013.00458

Upadhyay, J., Baker, S. J., Chandran, P., Miller, L., Lee, Y., Marek, G. J., … Day, M. (2011). Default-Mode-Like Network Activation in Awake Rodents. *PLoS ONE*, *6*(11). https://doi.org/10.1371/journal.pone.0027839

Urban, D. J., & Roth, B. L. (2014). DREADDs (Designer Receptors Exclusively Activated by Designer Drugs): Chemogenetic Tools with Therapeutic Utility. *Annual Review of Pharmacology and Toxicology*, *55*, 399–417. https://doi.org/10.1146/annurev-pharmtox-010814-124803

van den Heuvel, M. P., Scholtens, L. H., Turk, E., Mantini, D., Vanduffel, W., & Feldman Barrett, L. (2016). Multimodal analysis of cortical chemoarchitecture and macroscale fMRI resting-state functional connectivity. *Human Brain Mapping*, *37*(9), 3103–13. https://doi.org/10.1002/hbm.23229

van den Heuvel, M. P., & Sporns, O. (2011). Rich-club organization of the human connectome. *J Neurosci*, *31*(44), 15775–15786. https://doi.org/10.1523/JNEUROSCI.3539-11.2011

Van Dijk, K. R., Hedden, T., Venkataraman, A., Evans, K. C., Lazar, S. W., & Buckner, R. L. (2010). Intrinsic functional connectivity as a tool for human connectomics: theory, properties, and optimization. *J Neurophysiol*, *103*(1), 297–321. https://doi.org/10.1152/jn.00783.2009

Van Essen, D. C. (2004a). Organization of visual areas in macaque and human cerebral cortex. In L. M. Chalupa & J. S. Werner (Eds.), *The visual neurosciences* (pp. 507–521). MIT Press.

Van Essen, D. C. (2004b). Surface-based approaches to spatial localization and registration in primate cerebral cortex. *Neuroimage*, *23 Suppl 1*, S97-107. Retrieved from http://www.ncbi.nlm.nih.gov/entrez/query.fcgi?cmd=Retrieve&db=PubMed&dopt=Citation &list_uids=15501104

Van Essen, D. C. (2005). A Population-Average, Landmark- and Surface-based (PALS) Atlas of Human Cerebral Cortex. *Neuroimage*, *28*(3), 635–662. Retrieved from http://www.ncbi.nlm.nih.gov/entrez/query.fcgi?cmd=Retrieve&db=PubMed&dopt=Citation &list_uids=16172003

Van Essen, D. C. (2012). Cortical cartography and Caret software. *NeuroImage*, *62*(2), 757–764. https://doi.org/10.1016/j.neuroimage.2011.10.077

Van Essen, D. C., Dickson, J., Harwell, J., Hanlon, D., Anderson, C. H., & Drury, H. A. (2001). An integrated software suite for surface-based analyses of cerebral cortex. *J Am Med Inform Assoc*, *41*, 1359–1378. See also http://brainmap.wustl.edu/car. Retrieved from http://www.ncbi.nlm.nih.gov/entrez/query.fcgi?cmd=Retrieve&db=PubMed&dopt=Citation

&list_uids=11522765

Van Essen, D. C., & Dierker, D. (2007a). On navigating the human cerebral cortex: Response to "in praise of tedious anatomy." *Neuroimage*, *37*(4), 1050–1054. Retrieved from http://www.ncbi.nlm.nih.gov/entrez/query.fcgi?cmd=Retrieve&db=PubMed&dopt=Citation &list_uids=17766148

Van Essen, D. C., & Dierker, D. L. (2007b). Surface-based and probabilistic atlases of primate cerebral cortex. *Neuron*, *56*(2), 209–225. Retrieved from http://www.ncbi.nlm.nih.gov/entrez/query.fcgi?cmd=Retrieve&db=PubMed&dopt=Citation &list_uids=17964241

Verhoeven, J. S., De Cock, P., Lagae, L., & Sunaert, S. (2010). Neuroimaging of autism. *Neuroradiology*, *52*(1), 3–14. https://doi.org/10.1007/s00234-009-0619-3

Vértes, P. E., & Bullmore, E. T. (2015). Annual research review: Growth connectomics--the organization and reorganization of brain networks during normal and abnormal development. *Journal of Child Psychology and Psychiatry, and Allied Disciplines*, *56*(3), 299–320. https://doi.org/10.1111/jcpp.12365

Vetere, G., Kenney, J. W., Tran, L. M., Xia, F., Steadman, P. E., Parkinson, J., … al., et. (2017). Chemogenetic Interrogation of a Brain-wide Fear Memory Network in Mice. *Neuron*, *94*(2), 363–374.e4. https://doi.org/10.1016/j.neuron.2017.03.037

Vogt, B. A., Vogt, L., & Farber, N. B. (2004). Cingulate Cortex and Disease Models. In *The Rat Nervous System* (pp. 705–727). https://doi.org/10.1016/B978-012547638-6/50023-7

Wang, D., Buckner, R. L., Fox, M. D., Holt, D. J., Holmes, A. J., Stoecklein, S., … Liu, H. (2015). Parcellating cortical functional networks in individuals. *Nature Neuroscience*, *18*(12), 1853–60. https://doi.org/10.1038/nn.4164

Wang, K., van Meer, M. P. A., van der Marel, K., van der Toorn, A., Xu, L., Liu, Y., …
Dijkhuizen, R. M. (2011). Temporal scaling properties and spatial synchronization of
spontaneous blood oxygenation level-dependent (BOLD) signal fluctuations in rat
sensorimotor network at different levels of isoflurane anesthesia. *NMR in Biomedicine*,
24(1), 61–67. https://doi.org/10.1002/nbm.1556

Wang, S., Yan, J. Y., Lo, Y. K., Carvey, P. M., & Ling, Z. (2009). Dopaminergic and
serotoninergic deficiencies in young adult rats prenatally exposed to the bacterial
lipopolysaccharide. *Brain Research*, *1265*, 196–204.
https://doi.org/10.1016/j.brainres.2009.02.022

Warren, D. E., Power, J. D., Bruss, J., Denburg, N. L., Waldron, E. J., Sun, H., … Tranel, D.
(2014). Network measures predict neuropsychological outcome after brain injury.
Proceedings of the National Academy of Sciences, *111*(39), 14247–14252.
https://doi.org/10.1073/pnas.1322173111

Wasserman, S., & Faust, K. (1994). *Social network analysis: Methods and applications*.
Cambridge: Cambridge University Press.

Wei, H., Alberts, I., & Li, X. (2013). Brain IL-6 and autism. *Neuroscience*.
https://doi.org/10.1016/j.neuroscience.2013.08.025

White, S. W., Oswald, D., Ollendick, T., & Scahill, L. (2009). Anxiety in children and
adolescents with autism spectrum disorders. *Clinical Psychology Review*.
https://doi.org/10.1016/j.cpr.2009.01.003

WHO. (2014). Neurological Disorders: public health challenges. *Neurological Disorders: Public
Health Challenges*, 26–39. https://doi.org/10.1037/e521482010-002

Winter, C., Djodari-Irani, A., Sohr, R., Morgenstern, R., Feldon, J., Juckel, G., & Meyer, U.

(2009). Prenatal immune activation leads to multiple changes in basal neurotransmitter levels in the adult brain: Implications for brain disorders of neurodevelopmental origin such as schizophrenia. *International Journal of Neuropsychopharmacology*, *12*(4), 513–524. https://doi.org/10.1017/S1461145708009206

Winter, C., Reutiman, T. J., Folsom, T. D., Sohr, R., Wolf, R. J., Juckel, G., & Fatemi, S. H. (2008). Dopamine and serotonin levels following prenatal viral infection in mouse--implications for psychiatric disorders such as schizophrenia and autism. *European Neuropsychopharmacology : The Journal of the European College of Neuropsychopharmacology*, *18*(10), 712–6. https://doi.org/10.1016/j.euroneuro.2008.06.001

Wu, W.-L., Hsiao, E. Y., Yan, Z., Mazmanian, S. K., & Patterson, P. H. (2017). The placental interleukin-6 signaling controls fetal brain development and behavior. *Brain, Behavior, and Immunity*, *62*, 11–23. https://doi.org/10.1016/j.bbi.2016.11.007

Zaretsky, M. V., Alexander, J. M., Byrd, W., & Bawdon, R. E. (2004). Transfer of Inflammatory Cytokines Across the Placenta. *Obstetrics & Gynecology*, *103*(3), 546–550. https://doi.org/10.1097/01.AOG.0000114980.40445.83

Zhao, F., Zhao, T., Zhou, L., Wu, Q., & Hu, X. (2008). BOLD study of stimulation-induced neural activity and resting-state connectivity in medetomidine-sedated rat. *NeuroImage*, *39*(1), 248–60. https://doi.org/10.1016/j.neuroimage.2007.07.063

Zoubarev, A., Hamer, K. M., Keshav, K. D., McCarthy, E. L., Santos, J. R. C., Van Rossum, T., … Pavlidis, P. (2012). Gemma: a resource for the reuse, sharing and meta-analysis of expression profiling data. *Bioinformatics*, *28*(17), 2272–2273. https://doi.org/10.1093/bioinformatics/bts430